

Safi-Ur-Rehman Qamar

Biomedical application of green synthesized nanoparticles as anti-cancer agents and nanoparticle incorporated nanofibers as potential coating for drug coated balloons

Doctoral dissertation



Safi-Ur-Rehman Qamar

Biomedical application of green synthesized nanoparticles as anti-cancer agents and nanoparticle incorporated nanofibers as potential coating for drug coated balloons

Doctoral dissertation



Универзитета у Крагујевцу Факултет инжењерских наука

Сафи-Ур-Рехман Камар

Биомедицинска примена зелених синтетизованих наночестица као агенса против карцинома и нановлакна уграђених у наночестице као потенцијалног премаза за балоне обложене лековима

докторска дисертација

Identification page of the Doctoral dissertation

Author

Name and surname: Safi-Ur-Rehman Qamar

Date and place of birth: 12.04.1996., Faisalabad, Pakistan

Current employment: Bioengineering Research and Development Center (BioIRC) Doo. Kragujevac, Serbia.

Ph.D. Thesis

Title: Biomedical application of green synthesized nanoparticles as anti-cancer agents and nanoparticle incorporated nanofibers as potential coating for drug coated balloons

No. of pages: 95

No. of figures: 34

No. of references: 193

Institution and place of thesis preparation: Faculty of Engineering, University of Kragujevac, Kragujevac, Serbia

Scientific area (UDK): Biomedical science

Mentor: Professor Dr Nenad Filipović, Full Professor, Faculty of Engineering, University of Kragujevac, Kragujevac, Serbia

Co-mentor: Dr Marko Živanović, Senior Research Associate, Institute for Information Technologies, University of Kragujevac, Kragujevac, Serbia.

Grade and Dissertation Defense

Topic Application Date: 17.10.2023

Decision number and date of acceptance of the doctoral dissertation topic:

01-1/4368-3 (13.11.2023)

Acknowledgement

Firstly, I would like to thank my wife Eman Saqib for her support during my Ph.D. studies. She stood by my side during the ups and downs of my PhD journey. During this time, she gave birth to a wonderful human being, my daughter Hezlin Qamar. In addition to that, I would like to thank my parents Bashir Ahmad (father) and Naveed Akhtar (mother) who provided every facility that they could to make me get educated. I want to thank my brother Wasi-Ur-Rehman Qamar for sending me countless memes to cheer me up when I felt low during my Ph.D. journey.

Secondly, I would like to thank my advisor Prof. Dr. Nenad Filipović for giving me the opportunity to work independently on this project, in a close collaboration with co-advisor Dr. Marko Živanović from Institute for Information Technologies Kragujevac, University of Kragujevac, Serbia. I would like to especially mention Katarina Virijević, who was always there for me whenever I faced difficulties in my experiments. Moreover, I would like to thank Dr. Jelena Košarić, Dejan Arsenijević, and Edina Avdović from the Institute for Information Technologies Kragujevac, University of Kragujevac, Serbia for providing technical assistance during my analytical experiments. Moreover, I would like to thank Dr. Andrija Ćirić from Faculty of Natural Sciences and Mathematics, University of Kragujevac, Serbia for immense support during nanoparticles characterization.

Thirdly, I would like to mention that this study was made possible by the DECODE project (https://www.decodeitn.eu/) that has received funding from the European Union's Horizon 2020 research and innovation program under the Marie Skłodowska-Curie grant agreement No 956470.

Kragujevac, 2024

Safi-Ur-Rehman Qamar

Abstract

Green nanotechnology enables the conversion of biological systems into environmentally friendly methods for synthesizing nanomaterials. Green approaches utilize biological sources as an alternative to the physicochemical creation of nanoparticles, which involves the use of harmful chemicals and severe settings. By combining the principles of green chemistry, green nanotechnology, and chemical engineering may create metal nanoparticles that are both environmentally beneficial and cost effective, without the need for harmful chemicals during their production. Therefore, in this study, we used the extract of the traditional Serbian tea Bosiljak (Ocimum basilicum L.) and Borovnica (Vaccinium myrtillus) extracts to create silver nanoparticles (AgNPs) in a single step without the use of hazardous chemicals. This eco-friendly, easy-to-use, and reasonably priced approach uses an aqueous plant extract as a reducing and stabilizing agent for AgNPs. The NPs synthesized from Bosiljak and Borovnica were termed as OBTe-AgNPs and VMTe-AgNPs, respectively. UV-Vis spectroscopy, energy dispersive spectroscopy (EDS), transmission electron microscopy (TEM), field emission scanning electron microscopy (FESEM), and dynamic light spectroscopy (DLS) were all used to examine the AgNPs. UV-Vis spectroscopy displayed surface plasmon resonance (SPR) at 344 nm and 305 nm, respectively for OBTe-AgNPs and VMTe-AgNPs. The FESEM analysis of OBTe-AgNPs and VMTe-AgNPs revealed that both processes oval shape with average size of 55 and 52 nm, respectively. While and TEM analysis revealed that the average size of OBTe-AgNPs and VMTe-AgNPs was 35 nm and 80 nm, respectively. The anti-cancer ability of OBTe-AgNPs against human cervical immortalized (HeLa) cancer cells was tested. While on the other hand, VMTe-AgNPs were used as double action tool as anti-cancer and anti-atherosclerosis against breast adenocarcinoma epithelial cells (MDA-MB-231) and human umbilical vein endothelial cells (HUVEC). The results showed that both AgNPs possess cytotoxic effect in a dose dependent manner. OBTe-AgNPs showed IC₅₀ value of $21.78 \pm 0.68 \,\mu\text{g/ml}$ against HeLa cells. While VMTe-AgNPs showed IC₅₀ value of $29.69 \pm 1.47 \,\mu\text{g/ml}$ and $17.72 \pm 1.25 \,\mu\text{g/ml}$ against MDA-MB-231 and HUVEC cells, respectively. Furthermore, the potential of OBTe-AgNPs were incorporated into nanofibers (NFs) as anti-atherosclerosis agent as well as a new coating material for drug coated balloons (DCBs). The Ag release study reveals that there is sustainable release over time from various variations of OBTe-AgNPs-NF. Due to this we saw antiatherosclerosis potential of these OBTe-AgNPs-NFs when exposed to HUVEC cells. In conclusion, AgNPs and AgNPs-NF produced via green nanotechnology have the potential to be used as anti-cancer and anti-atherosclerosis agents. Moreover, AgNPs-NF acts as a newer coating material for DCBs to treat atherosclerosis and peripheral artery disease.

Keywords: Green nanotechnology, silver nanoparticles, anti-cancer, anti-atherosclerosis, nanofibers, drug coated balloons.

Serbian language abstract

Зелена нанотехнологија омогућава претварање биолошких система у еколошки прихватљиве методе за синтезу наноматеријала. Зелени приступи користе биолошке изворе као алтернативу физичко-хемијском креирању наночестица, што укључује употребу штетних хемикалија и тешке услове. Комбиновањем принципа зелене хемије, зелене нанотехнологије и хемијског инжењеринга могу се створити металне наночестице које су и еколошки корисне и исплативе, без потребе за штетним хемикалијама током њихове производње. Због тога смо у овој студији користили екстракт традиционалног српског чаја Босиљак (Ocimum basilicum L.) и екстракте Боровнице (Vaccinium myrtillus) за стварање наночестица сребра (AgNPs) у једном кораку без употребе опасних хемикалија. Овај еколошки прихватљив приступ, једноставан за употребу и приступачне цене, користи водени биљни екстракт као средство за редукцију и стабилизацију наночестица сребра. Нано честице синтетисане из Босиљака и Боровнице названи су као OBTe-AgNPs и VMTe-AgNPs, респективно. УВ-Вис спектроскопија, спектроскопија дисперзије енергије (ЕДС), трансмисиона електронска микроскопија скенирајућа (TEM), емисиона електронска микроскопија (ФЕСЕМ) и динамичка светлосна спектроскопија (ДЛС) су коришћени за испитивање AgNPs. УВ-Вис спектроскопија је показала површинску плазмонску резонанцу (СПР) на 344 nm и 305 nm, респективно за OBTe-AgNPs и VMTe-AgNPs. ФЕСЕМ анализа OBTe-AgNPs и VMTe-AgNPs открила је да оба процеса овалног облика са просечном величином од 55 и 52 nm. Док и TEM анализа је открила да је просечна величина OBTe-AgNPs и VMTe-AgNPs била 35 nm и 80 nm, респективно. Тестирана је ефикасност OBTe-AgNPs у односу на ћелије канцера и људских имортализованих ћелија канцера грлића материце (HeLa). Док су, с друге стране, VMTe-AgNPs коришћене као средство двоструког дејства као анти-канцер и анти-атеросклероза против епителних ћелија аденокарцинома дојке (MDA-MB-231) и ендотелних ћелија хумане пупчане вене (HUVEC). Резултати су показали да обе AgNPs поседују цитотоксични ефекат у зависности од дозе. OBTe-AgNPs су показали ИЦ50 вредност од 21,78 ± 0,68 µg/ml према HeLa ћелијама. Док су VMTe-AgNPs показали ИЦ50 вредност од $29,69 \pm 1,47$ µg/ml и $17,72 \pm 1,25$ µg/ml у односу на MDA-MB-231 и HUVEC ћелије, респективно. Штавише, потенцијал OBTe-AgNPs је уграђен у нановлакна (НФ) као агенс против атеросклерозе, као и нови материјал за облагање балона обложених лековима (ДЦБ). Студија ослобађања Ад открива да постоји одрживо ослобађање током времена из различитих варијација OBTe-AgNPs-NFs. Због тога смо видели антиатеросклерозни потенцијал ових ОБТе-АгНПс-НФ када су били изложени HUVEC ћелијама. У закључку, AgNPs и AgNPs-NFs произведени преко зелене нанотехнологије имају потенцијал да се користе као агенси против рака и атеросклерозе. Штавише, AgNPs-NFs делују као новији материјал за облагање за ДЦБ за лечење атеросклерозе и болести периферних артерија.

Serbian language keywords: Зелена нанотехнологија, наночестице сребра, антиканцер, анти-атеросклероза, нановлакна, балони обложени лековима.

Table of Contents

Ackno	wledgement	i		
Abstra	ct	ii		
Serbia	n language abstract	iii		
Table o	of Contents	iv		
List of	Figures	vi		
List of	Tables	vii		
List of	Abbrivations	viii		
Chapte	er 1 Introduction	1		
1.1	Introduction	1		
1.2	Aim of the dissertation	6		
1.3	Objective of the dissertation	9		
Chapte	er 2 Review of literature	10		
2.1	Prevalence of cancer	10		
2.2	Current cancer treatment	12		
2.3	Challenges in cancer treatment	13		
2	Difficulty in targeting cancer stem cells (CSC)	13		
2	3.2 Drug resistivity towards anti-cancer drugs	14		
2	Constraints of traditional chemotherapeutic drugs	14		
2.4	AgNPs as possible anti-cancer agents	14		
2.5	Global prevalence of peripheral artery disease (PAD)	23		
2.6	Prevalence of peripheral artery disease (PAD) in Serbia	25		
2.7	Application of NPs for the treatment of PAD	26		
2.8	Drug Coated Balloons (DCBs) for the treatment of PAD	31		
2.9	Electrospinning technique for coating material	33		
Chapte	er 3 Material and Method	36		
3.1	Selection of plant	36		
3.2	Extraction and preparation of O. basilicum and V. myrtillus tea extract.	36		
3.3	Synthesis of AgNPs using O. basilicum and V. myrtillus tea extract	36		
3.4	Preparation of polymer solution for electrospinning	37		
3.5	Electrospinning of OBTe AgNPs incorporated polymer	37		
3.6	3.6 Characterization of AgNPs, and tea extracts			
3.7	Characterization of OBTe-AgNPs incorporated NFs			
3.8	Anticancer and antiatherosclerosis properties of green synthesized AgN	Ps39		
3.8.1 Cell culture		39		
3.	8.2 Cell viability analysis in cell lines	39		

3.9	Reactive oxygen species production in AgNPs exposed cells	40
3.9.1	Glutathione (GSH) concentration analysis in cell lines	40
3.9.2	Nitrite (NO ₂ ⁻) concentration analysis in cell lines	40
3.9.3	Super oxide anion radical $(O_2^{\bullet-})$ concentration analysis in cell line	es . 40
3.10	Gene expression analysis of apoptotic genes in HeLa cells	41
3.10.	1 RNA isolation from HeLa cells	41
3.10.	2 Reverse transcription polymerase chain reaction (RT-PCR)	42
3.10. PCR		`-
3.11	Apoptosis and necrosis analysis using Annexin FITC Assay in HeLa co	ells 42
3.12	Silver ion release study	43
3.13	Statistical analysis	43
Chapter	4 Results	44
4.1	Characterization and toxicological studies of OBTe-AgNPs	44
4.1.1	Characterization of OBTe-AgNPs and O. basilicum tea extract	44
4.1.2	OBTe-AgNPs stability against Temperature and pH	46
4.1.3	Influence of OBTe-AgNPs on cell viability	47
4.1.4	ROS production in HeLa cells upon exposure to OBTe-AgNPs	48
4.1.5	Apoptotic gene expression in HeLa cells	49
4.1.6	Annexin FITC assay for apoptosis analysis in HeLa cells	50
4.2	Characterization and toxicological studies of VMTe-AgNPs	52
4.2.1	Characterization of VMTe-AgNPs and V. myrtillus tea extract	52
4.2.2	VMTe-AgNPs stability against Temperature and pH	53
4.2.3	Influence of VMTe-AgNPs on cell viability	55
4.2.4	ROS production in cells after VMTe-AgNPs exposure	56
4.3 ballons	OBTe-AgNPs incorporated nanofibers as a coating material for drug co	oated
4.3.1	Characterization of OBTe-AgNPs incorporated nanofibers	60
4.3.2	Ag ion release from nanofibers	62
4.3.3	Application of nanofibers to remove atherosclerosis	63
Chapter :	5 Discussion	64
Chapter	6 Conclusion	76
Referenc	es	77

List of Figures

Figure 1.1. Illustration of NPs application in various fields	
Figure 1.2. Illustration of NPs synthesis process	
Figure 1.3. Application of NMs for the treatment of CVDs	3
Figure 2.1. Cancer's ranking as a cause of death for individuals under the age of 70 in	
2019	
Figure 2.2. Most prevalent types of cancer categorized by gender	1
Figure 2.3. Top ten cancer types for the predictable total of new cancer cases and	
deaths in USA	2
Figure 2.4. Forecasted cancer survivorship rate in the United States in 2021	3
Figure 2.5. Illustration of how cancer cells survive therapy	3
Figure 2.6. Diagram of cancer cell killing mechanism of AgNPs	3
Figure 2.7. Demonstration of PAD presence in leg	4
Figure 2.8. Geographic dispersion of age-adjusted rates of PAD in the year 2019 25	5
Figure 2.9. Schematic illustration of NPs application towards PAD2	7
Figure 2.10. Illustration of drug release from (A) DCBs and (B) DESs	2
Figure 2.11. Illustration of electrospinning equipment	4
Figure 3.1. Illustration of AgNPs synthesis process	5
Figure 3.2. Electrospinning set up	3
Figure 4.1. Characterization of OBTe-AgNPs	5
Figure 4.2. (A) EDS analysis revealing Ag-presence (B) TEM micrograph of OBTe-	
AgNPs with crystal shape and size distribution	5
Figure 4.3. Effect of (A) pH and (B) temperature on the stability OBTe-AgNPs 4"	
Figure 4.4. Cytotoxicity of OBTe-AgNPs against HeLa cells	3
Figure 4.5. ROS production upon exposure to OBTe-AgNPs in HeLa cells)
Figure 4.6. Relative gene expression of the Cas 3, 8, 9; pro-apoptotic Bax; and anti-	
apoptotic Bcl-250)
Figure 4.7. Flow cytometry analysis	1
Figure 4.8. Characterization of VMTe-AgNPs	3
Figure 4.9. Impact of (A) Temperature (B) pH on VMTe-AgNPs stability 54	4
Figure 4.10. Cytotoxic efficacy of VMTe-AgNPs against (A) MDA-MB-231 and (B)	
HUVEC cell lines	5
Figure 4.11. ROS production upon exposure to VMTe-AgNPs in MDA-MB-231 cells	3
	7
Figure 4.12. ROS production upon exposure to VMTe-AgNPs in HUVEC cells 59)
Figure 4.13. FTIR spectra of OBTe-AgNPs-NFs and biogenic OBTe-AgNPs 60)
Figure 4.14. FESEM images of produced NFs	
Figure 4.15. Surface roughness analysis using AFM of OBTe-AgNPs-NFs	2
Figure 4.16. Silver ion cumulative release over time from NFs	3
Figure 4.17. HUVEC viability after exposure to various variations of NFs	
Figure 5.1. Potential mechanisms behind cellular apoptosis	3

List of Tables

List of Abbrivations

NPs Nanoparticles **NMs** Nanomaterials **MNPs** Metal nanoparticles **AgNPs** Silver nanoparticles AuNPs Gold nanoparticles **PAD** Peripheral artery disease Drug coated balloons **DCBs** Coronary heart disease **CAD** World health organization **WHO** ATP-binding cassette **ABC** Breast cancer resistance protein **BCRP**

Acute myelogenous leukemia **AML**

Cancer stem cells **CSC**

ROS Reactive oxygen species Scanning electron microscope **SEM** Peripheral arterial disease **PAD**

Years of life lost **YLLs**

YLDs Years lived with disability Disability-adjusted life years **DALYs** CVI Chronic venous insufficiency **BMI** Elevated body mass index Carotid artery disease **CAD BMS** Bare metal stents Drug-eluting stents DES

PTX Paclitaxel

Biomedical substances **BMS DESs** Drug eluting stents Green nanotechnology **GNT**

NFs Nanofibers

Chapter 1

Introduction

1.1 Introduction

The question "What is the allure of green processes?" can be asked. The answer can be found in our environment. The advent of the industrial uprising in the 1760s brought out an accumulation of environmental challenges. We are currently on the verge of a 'nano-revolution' that will profoundly shape all aspects of life on Earth (Thipe et al., 2022). Nanoparticles (NPs) are minute molecular structures, fluctuating in size from 1 to 100nm, that have the prospective to revolutionize different divisions of modern society, such as health, transportation, electronics, and telecommunications (Qamar, 2021). Nevertheless, nanomaterials (NMs) have the potential to cause significant alterations to our surroundings due to their prolonged usage, exposure, and accumulation in the atmosphere and water (Ramzan et al., 2022). We are currently faced with a decision between selecting distinct NPs/NMs embedded products that will contribute to a secure and sustainable future, or opting for a future that is marred by environmental contamination resulting from the usage of various forms of NMs, both in the short and long term (Thipe et al., 2022). Given the circumstances, it is crucial to have environmentally friendly techniques that can reduce or eliminate the harmful impact on our environment while producing and using products with embedded NPs in many industries.

Green methods, such as green chemistry and green nanotechnology, employ non-toxic starting materials and environmentally-friendly solvents throughout the entire synthesis process (Qamar & Ahmad, 2021). These techniques strive to fully eradicate harmful compounds in the reaction media and also try to eradicate toxic derivatives that harm our environment (M. Gupta & Seema, 2021). Green nanotechnology (GNT) seeks to completely eradicate all harmful compounds across the entirety of manufacturing processes (Ahmed et al., 2022). GNT is portrayed by the use of phyto-chemicals obtained from various plants species to act as stabilizing-reducing mediators in the conversion of metal ions (M⁺) into metallic nanoparticles (MNPs) (Qamar & Ahmad, 2021). Green chemistry is guided by a set of 12 widely recognized principles. These principles serve as a grounds for the development and enhancement of materials, processes, products, and systems (DeVierno Kreuder et al., 2017). The objectives are as follows: (i) preventing the generation of toxic waste, (ii) maximizing the amount of final product by ensuring efficient use of atoms in the synthetic route, (iii) avoiding the use of harmful chemicals in the synthetic pathways, (iv) designing of materials that are compatible with living organisms and pose no harm, (v) using environmentally-friendly solvents such as water, (vi) minimizing energy usage while achieving high yields to minimize environmental as well as economic influences, (vii) using renewable feedstock or raw materials to promote sustainability, (vii) reducing the number of byproducts to limit extra steps, and (ix) utilizing catalysts instead of less effectual stoichiometric reactions, (x) the design leads to the formation of harmless byproducts, (xi) the life cycle analysis aims to minimize and prevent environmental damage, and (xii) there is improved efficiency in the manufacturing, storing, and transportation operations.

Nanotechnology is now in its early stages of development, although it is seeing significant growth with far-reaching consequences in the fields of energy, electronics,

food, medical, and related industries (Shafique et al., 2023). The global market for nanomachines and nano-devices is predicted to grow from \$736.1 million in 2018 to approximately \$2.7 billion in 2028, according to a prediction (McWilliams, 2018b). The worldwide nanocomposites market is predicted to reach above \$7 billion by 2022, with a combined annual growth rate of about 29.5% during the period from 2017 to 2022 (McWilliams, 2018a). Hence, it is crucial that we foster the progression of GNT in a way that is both sustainable and environmentally benign, in order to facilitate its expansion and effectively mitigate the present and forthcoming consequences of the nano-revolution on our surroundings. The notion of GNT encompasses the notion of environmentally-friendly and sustainable-technology (Verma et al., 2019).

Over the previous few years, there has been significant interest and extensive research persistence seen on the biomedical assessment and reassessment of MNPs obtained from noble metals, such as silver (Ag) and gold (Au). This is due to their distinct chemical, biological, and physical properties (Nadaf et al., 2022). Significant focus was directed towards the evaluation of silver nanoparticles (AgNPs) in the discipline of biomedicine, since they gained global recognition as non-traditional antibacterial agents (Simon et al., 2022). Despite the limited knowledge about the *invivo* toxicokinetic behavior of AgNPs, these NPs have extensively been utilized as antibacterial agents in the healthcare industry (Rodríguez-Félix et al., 2022), cosmetics (Gajbhiye & Sakharwade, 2016), food storage (Taha et al., 2022), textile coatings (Lange et al., 2022), and various environmental applications (González-Pedroza et al., 2023) (see Figure 1.1).

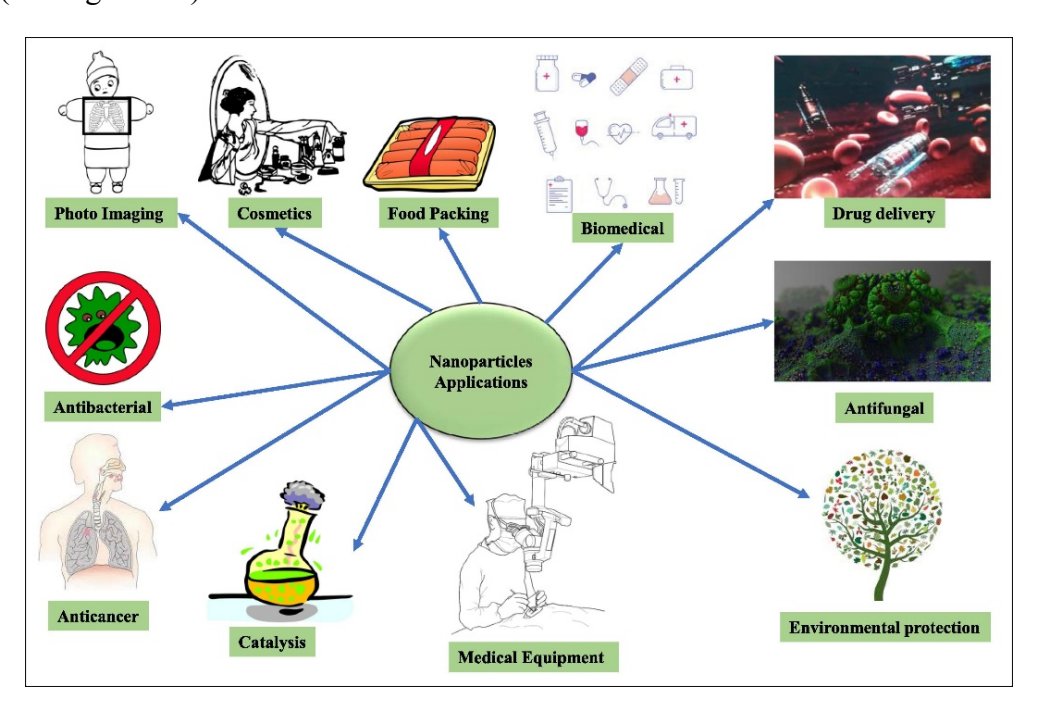


Figure 1.1. Illustration of NPs application in various fields (Adapted with permission from (Qamar & Ahmad, 2021))

The inherent therapeutic effects of medicines in the field of medicine are equally significant as their pharmacokinetics and pharmacodynamics (Xie et al., 2019). Due to its potential to improve present healthcare practices, the targeted distribution and effectiveness of therapeutic agents have become a highly researched area. As a result, AgNPs have gained significant interest for their role in designing and developing

advanced drug-delivery systems (Nikolova et al., 2023). AgNPs based nano-systems were assessed as effective carriers for a range of therapeutic compounds, such as anti-inflammatory (Steckiewicz et al., 2022), anti-oxidant (Alsareii et al., 2022), antibacterial (Ha et al., 2023), and anticancer (Dutt et al., 2023) agents.

Due to their inherent ability to fight cancer, AgNPs have received significant interest in this field and have been proven to be effective in delivering anti-tumor medications (Ebtesam S Al-Sheddi et al., 2023; Benyettou et al., 2015). They can operate as either passive (Patra et al., 2015) or active (Poudel et al., 2018) carriers for anticancer treatments. To prepare biocompatible AgNPs, many methods were employed, including radiolysis, organic-water 2-phase synthesis, micro-emulsion, and the most often used method, reduction in aqueous mixture (Qamar & Ahmad, 2021). Due to its unique properties, AgNPs have lately attracted a lot of interest as a potential drug-delivery platform (Hussein & Abdullah, 2022). These encompass its versatile organic molecule-binding capabilities, potent and modifiable absorption characteristics, and minimal toxicity. Considerable attention, scientific expertise, and financial support have been devoted to this (Qamar, 2021). Recent studies have demonstrated the potential application of AgNPs as carriers for vaccines and drugs, allowing for directed delivery to specific tissues and cells (A. Yusuf et al., 2023).

Sanchez-Guzman et al. did a study, where they demonstrated that via the use of a mouse model, that the incorporation of silver nanoparticles (AgNPs) into a virus-inactivated influenza vaccination led to a decrease in viral loads and the prevention of severe lung inflammation that occurred after influenza infection. Concurrently, AgNPs caused an increase in the number of particular IgA secreting plasma cells as well as antibody titers, which is a characteristic of effective mucosal immunity. In addition, vaccination with silver nanoparticles, but not with gold nanoparticles, protected mice from the fatal influenza virus. As opposed to other commercial adjuvants (squalene/oil-based emulsion) or silver salts, silver nanoparticles (AgNPs) performed as a genuine mucosal adjuvant and encouraged higher antigen-specific IgA production with reduced toxicity. This was accomplished by boosting bronchus-associated lymphoid tissue (BALT) neogenesis (Sanchez-Guzman et al., 2019).

Asgary et al. performed experiment in which AgNPs were created by reducing aqueous silver nitrate with Eucalyptus procera leaf extract. Subsequently, 1 ml of inactivated rabies virus was mixed with several concentrations of AgNPs (200 µg, 400 μg, 600 μg, and 800 μg). Six Naval Medical Research Institute mice per group were given intraperitoneal injections of the loaded vaccinations (0.5 ml) on days 1 and 7. The mice were given an intracerebral challenge of 0.03 ml of the challenge rabies virus (strain 11, 20 lethal dosage [20 LD50]) on the fifteenth day. Following the five-day latency period of the mouse rabies disease, the mice were observed for a further 21 days. Using the quick fluorescence focus inhibition test method, neutralizing antibodies against the rabies virus were also studied. The National Institutes of Health test was used to establish the ideal concentration of AgNPs for use as an adjuvant and its potency. Using the MTT assay, the in vitro toxicity of AgNPs was evaluated in the L929 cell line. In accordance with European Pharmacopeia 8.0, the in-vivo toxicity of AgNPs and AgNPs-loaded vaccines was also examined. After injecting the mice with the vaccine at doses of 15 mg/kg and 20 mg/kg loaded with AgNPs, the maximum percentage of viability was noted. The vaccines loaded with AgNPs (dosage 15 mg/kg) and containing alum had computed potencies of 1.303 and 1.897, respectively. AgNPs were not harmful, but the MTT assay showed that alum was poisonous at a dosage of 10 mg/ml. The in vivo toxicity further clarified the safety of the vaccination containing AgNPs in mice and dogs, respectively. The adjuvanticity impact of green produced AgNPs on veterinary rabies vaccination potency with no *in-vivo* toxicity was clarified in the current work for the first time (Asgary et al., 2016).

Jazayeri et al. evaluated a novel technique for the formulation and delivery of an oral DNA vaccine, a plasmid carrying the hemagglutinin (HA) gene of the avian influenza virus A/Ck/Malaysia/5858/04 (H5N1) (pcDNA3.1/H5) was developed via green synthesis of AgNP combined with polyethylene glycol (PEG). The cytotoxicity of the synthesized AgNPs was examined *in-vitro* using MCF-7 cells and *in-vivo* through cytokine expression analysis. No cytotoxic effects were observed in MCF-7 cells at a dose of $-5 \log_{10}$ AgNPs, with only 9.5% cell death relative to the control. One-day-old specific pathogen-free (SPF) chicks, immunized once via oral gavage with 10 µl of pcDNA3.1/H5 (200 ng/ml) nano-encapsulated with 40 μl AgNPs, exhibited no clinical symptoms. PCR effectively identified the AgNPs/H5 plasmid in the duodenum of the inoculated chicken as early as 1-hour post-immunization. Immunization of chickens with AgNPs/H5 augmented both pro-inflammatory and Th1-like expressions, however no significant changes were seen among the chickens inoculated with AgNPs, AgNPs/pcDNA3.1, and the control group. Furthermore, serum samples obtained from inoculated hens with AgNPs/H5 exhibited a rapid increase in antibodies against H5 by day 14 post-immunization. The peak average antibody titers were observed on day 35 post-immunization, at 51.2 ± 7.5 . AgNPs/H5 stimulated both CD4⁺ and CD8⁺ T cells in the inoculated hens as early as day 14 post-immunization, at $7.5 \pm 2.0\%$ and $20 \pm 1.9\%$, respectively. Consequently, a single oral dosage of AgNPs/H5 elicited both antibody and cell-mediated immune responses, along with increased cytokine production (Jazayeri et al., 2012).

Rozalen et al. created AgNPs-MTX conjugates with a confined size distribution, a controlled synthesis of methotrexate (MTX) silver nanoparticles (AgNPs-MTX) was carried out. Boronhydride and citrate were used as reduction and reduction/capping agents, respectively, in order to achieve this goal. AgNPs that were synthesized with varying quantities of MTX were found to have drug loading capabilities of 28, 31, and 40%, according to the calculations. *In-vitro* drug release experiments demonstrated that all conjugated quantities released between 77 and 85 percent of the initial MTX injected into the AgNPs. These release profiles were consistent across all conjugated levels. When it came to free MTX, the incorporation of the nanocarrier not only slowed down its release but also altered the pharmacokinetics with which it was administered. In accordance with a first order kinetic model, free MTX is released after three hours, however in the presence of AgNPs, a rapid initial release is observed during the first five hours, followed by a plateau after twenty-four hours. In this particular instance, AgNPs-MTX was appropriate for a Higuchi model, in which the solubilization of the substance is governed by a diffusion mechanism. The results that were obtained from flow cytometry of several cell lines that were treated with AgNPs-MTX revealed the combined anticancer impact of both reagents. After 48 hours of exposure, the percentage of surviving cells in a colon cancer cell line (HTC-116) was reduced to forty percent. Even though it was less pronounced, this effect was nevertheless substantial for a lung cancer cell line known as A-549. Last but not least, a zebrafish experiment with AgNPs-MTX did not demonstrate any substantial cytotoxic impact, so verifying the reduction in systemic drug toxicity that was accomplished by coupling MTX to AgNPs. Additionally, the reduction in toxicity that was found in the zebrafish model suggests that there is a possibility of an improvement in the utilization of AgNPs-MTX in chemotherapy for the treatment of human tumors (Rozalen et al., 2020).

Gholamali et al. successfully combined the pH-sensitive polymers, Ag nanoparticles, CMCh, and PVA in order to successfully construct the NCs hydrogels for the drug delivery system. Through the utilization of ECH as a crosslinker, CMCh-PVA hydrogels were successfully produced in an alkaline medium. Both NCs hydrogels containing silver NPs and CMCh-PVA hydrogels at a temperature of 25 °C were successful in reducing the amount of silver nitrate. As a result, the swelling ratio demonstrated its influence on pH under the pH 2.1 and 7.4 conditions. When compared to the pristine CMCh-PVA hydrogels, the swelling ratio of nanocomposite hydrogels made of CMCh-PVA/Ag was shown to be higher with a higher concentration of AgNPs. The agar diffusion method was utilized in order to investigate the antibacterial characteristics of the nanocomposite hydrogels that were synthesized. The antibacterial capabilities were tested against Gram-positive S. aureus and Gram-negative E. coli. In contrast to microorganisms such as S. aureus and E. coli, the NCs hydrogels made of CMCh-PVA/Ag have demonstrated excellent antibacterial characteristics. When it comes to antibacterial action, hydrogels that include a significant proportion of silver nanoparticles are also indicative of greater levels. It is possible to reduce the amount of medication that is released from hydrogels by increasing the concentration of silver NPs. This is because of the strong interactions that occur between the amine groups of naproxen and the carboxylic groups of caffeine. The presence of silver nanoparticles is one of the primary factors that contribute to the behavior of drug release. As a result of the longer route for the migration of naproxen from biocompatibility NCs hydrogels containing Ag nanoparticles to the buffer, the time it took for naproxen to be released from CMCh-PVA/Ag hydrogel was longer than it was for pure CMCh-PVA hydrogels (Gholamali et al., 2020).

In another study, doxorubicin (Dox), AgNPs, and chitosan are combined to create a hybrid nanoparticle system, which offers a novel approach to cancer treatment. The goal of this hybrid system is to reduce the systemic toxicity of doxorubicin while optimizing its distribution and efficacy. The study's primary discovery is the doxorubicin's pH-responsive release behavior from the Ch-AgNPs-Dox hybrid system. When the pH of the tumor microenvironment is acidic (5.5), as opposed to neutral (7.4), the nanoparticles release doxorubicin more efficiently. Because it assures a higher drug concentration at the tumor site while limiting the amount of the drug that is exposed to healthy tissues, this targeted release mechanism is essential for enhancing the therapeutic index of doxorubicin and decreasing its adverse effects, which include nephrotoxicity and cardiotoxicity. The MCF-7 breast cancer cell line was used for the in vitro cytotoxicity tests, which show that the Ch-AgNPs-Dox formulation had far stronger cytotoxic effects than free doxorubicin. The chitosan coating is responsible for this increased cytotoxicity because it makes it easier for the nanoparticles to internalize into cancer cells, which results in a more potent suppression of DNA synthesis and cell proliferation. The study also emphasizes how ROS produced by silver nanoparticles aid in the death of cancer cells, adding to the hybrid system's total anti-cancer effectiveness. The ability of Ch-AgNPs-Dox to slow tumor growth is demonstrated in vivo utilizing an Ehrlich tumor-bearing mice model. When mice are administered hybrid nanoparticles instead of Ch-AgNPs or free doxorubicin alone, the tumor volume is significantly reduced in the treated mice. These results are corroborated by histopathological examination of tumor tissues, which demonstrates widespread cell death along with necrosis and apoptosis in tumors treated with the Ch-AgNPs-Dox formulation. This study finds that a promising approach to targeted cancer therapy is provided by the hybrid nanoparticles of Ch-AgNPs-Dox. The anti-cancer effects of AgNPs, the controlled release of doxorubicin, and the biocompatibility of chitosan combine to create a multifunctional platform that may enhance the effectiveness and safety of cancer treatment. According to the results, this hybrid nanoparticle technology may be developed further for use in clinical settings, especially for the treatment of solid malignancies like breast cancer (Mohamed, 2020).

Given their remarkable optical properties, which are significantly impacted by localized and specific surface plasmon resonance, AgNPs are ideally suited for applications involving the delivery of drugs. Furthermore, recent advancements in enhancing the biocompatibility and stability of AgNPs through surface modification make nanostructured systems based on silver excellent candidates that are specific, selective, and versatile for such applications (Amooaghaie et al., 2015; Kumari et al., 2020; Panda et al., 2022; Pauksch et al., 2014).

1.2 Aim of the dissertation

Combining nanotechnology and green chemistry has become an interdisciplinary way that has increased the number of MNPs that are compatible with cells and their genes (Mulvihill et al., 2011). NPs that span a range of dimensions from 1 to 100 nm are widely acknowledged as intermediaries that link bulkier substances with atomic-scale substances (Altammar, 2023). Nanoscale materials exhibit exceptional and distinctive characteristics in comparison to their bulk counterparts. The observed idiosyncrasies can be credited to the inherent physio-chemical characteristics, accompanied by the surface-to-volume ratio of nano molecules (Tekade et al., 2017).

Broadly speaking, there are two fundamental methodologies employed in the production of NPs. The chemical synthesis of NPs involves a multitude of techniques, one of which is the utilization of photons of light in photochemical processes (dos Santos et al., 2019), physiochemical approaches involving γ-radiation (Sharma et al., 2020), chemical reduction techniques (Guzman et al., 2008), microemulsion methods (Sun et al., 2019), electrochemical procedures (Elemike et al., 2019), microwave irradiation processes (Pauzi et al., 2019), and techniques of laser ablation (Rafique et al., 2019). Each of these processes produces a significant quantity of NPs, but they are limited by the presence of harmful components as well as the expensive and labor-intensive equipment required. Several chemical compounds, including polyethylene glycol, tollens, sodium citrate, elemental hydrogen and sodium borohydride, when dissolved in aqueous mixture, they operate as reducing managers. The reducing chemicals facilitate the reduction of metal (M⁺) ions to their metallic (M⁰) state, causing the formation of NPs (Chouke et al., 2022) (see Figure 1.2).

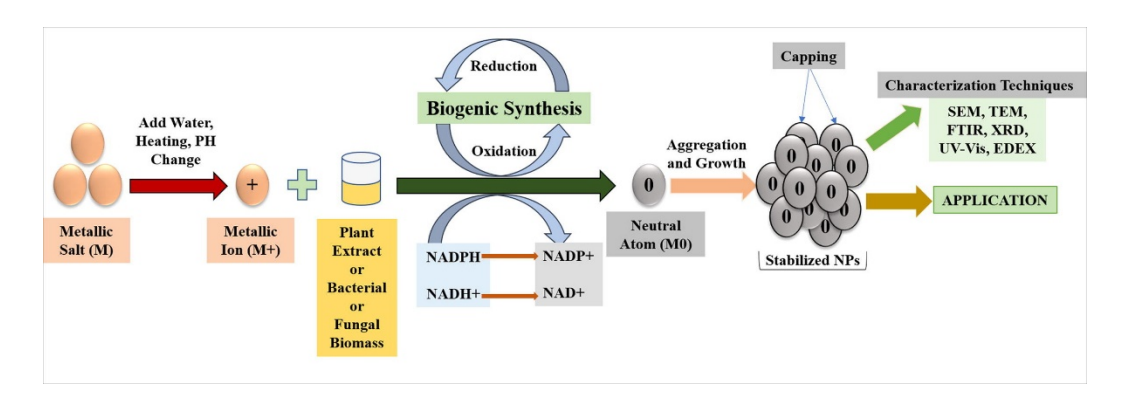


Figure 1.2. Illustration of NPs synthesis process (Adapted with permission from (Qamar & Ahmad, 2021))

Additionally, the utilization of green or biogenesis implies the employment of natural molecules as stabilizing, capping, and reducing agents, thereby replacing costly and hazardous chemicals. Because of this observation, researchers employ biosynthetic techniques (Qamar & Ahmad, 2021). There exist multiple factors contributing to this particular inclination. To begin with, it is important to note that biologically synthesized NPs exhibit distinct physicochemical features in comparison to NPs that are chemically synthesized (Joudeh & Linke, 2022). Furthermore, this approach demonstrates a relatively lower cost and a higher level of user-friendliness in comparison to the chemical approach, which involves the utilization of costly chemicals (Mukherjee & Patra, 2017). In addition, the chemical substances possess toxicity towards humans, animals, and notably the environment (Younas et al., 2022). Hence, the majority of professionals refer to green synthesis as a bottom-up methodology that involves substituting chemicals with plant extracts derived from several parts such as fruits, leaves, roots, and fruit peels (Madkour, 2018).

The production and application of AgNPs have caught significant attention in research papers, surpassing the study of other metallic NPs, despite variations in the number of publications utilizing the top-down strategy (Fahimirad et al., 2019). NPs possess distinct characteristics, namely their size and form, which contribute to their extensive selection of applications. NPs find extensive applications in diverse domains, involving biomedical science for drug delivery, rapid diagnosis, imaging, tissue regeneration and medical equipment) (Gosselin et al., 2022; Marassi et al., 2018; Prasher et al., 2020; Y. Su et al., 2019), anti-cancer agents (Y. Khan et al., 2017), antimicrobial agents (Alotaibi et al., 2022), Atherosclerosis (Junpeng Shi et al., 2014) and bioremediation (Heisnam et al., 2022).

Cardiovascular diseases (CVDs) are widely acknowledged as the primary reason of death on a global scale (Vaduganathan et al., 2022). Atherosclerosis is the primary underlying factor responsible for CVD, which encompasses disorders such as myocardial infarction (MI), heart failure, claudication and stroke. Atherosclerosis mostly affects the intima of several medium-large sized arteries, particularly at sites of arterial bifurcation (Nakhlband et al., 2018). The rising incidence of such disease necessitates innovative treatment and diagnostic strategies to address the related clinical and societal challenges. Advancements in nanotechnology and biomedical sciences have revealed the potential to use focused nano-machines for specific purposes such as diagnosis, and therapy. Nanomedicines, which are innovative methods for improving medication administration, imaging, and detection techniques, have demonstrated

significant potential in addressing cardiovascular illnesses i.e., Atherosclerosis (Omidian et al., 2023) (see Figure 1.3).

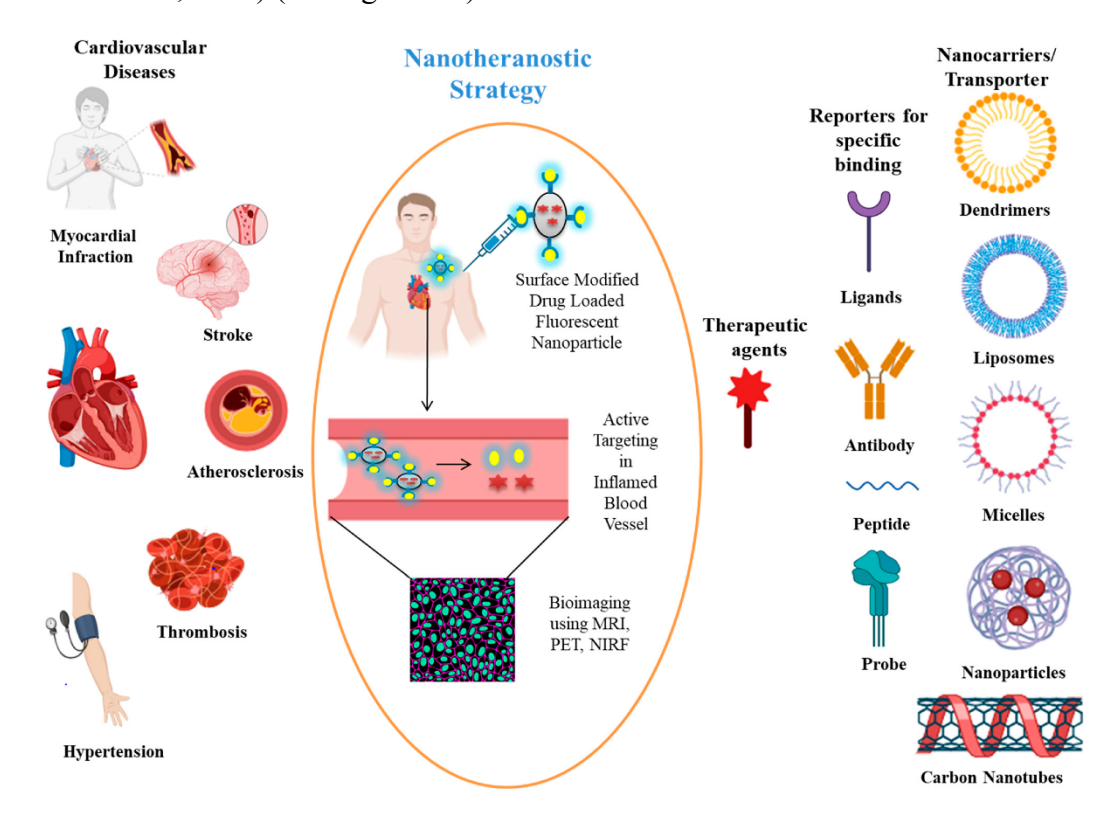


Figure 1.3. Application of NMs for the treatment of CVDs (Adapted with permission from (Ramchandani et al., 2023))

When comparing the impacts of rosuvastatin and AgNPs on hyperlipidemic rats, AL-Dujaili et al. discovered that the former significantly decreased serum levels of Endothelin and Obestatin, while the latter had no effect at all (Al-Dujaili & Al-Shemeri, 2016). Shi et al assessed the cytotoxicity of AgNPs and their influence on endothelial cell (EC) injury (Junpeng Shi et al., 2014). According to their findings, exposure to AgNPs results in the suppression of cell growth, harm to the cell membrane, and the initiation of programmed cell death. In addition, they asserted that AgNPs elevate the concentrations of adhesion molecules, inflammatory cytokines, and chemokines, and notably, they enhance the generation of ROS in HUVECs. Collectively, they proposed that AgNPs trigger the onset of early atherosclerosis by causing damage and impairment to the endothelial cells via the triggering of IκB kinase (IKK)/NF-κB. Conversely, certain studies have demonstrated a negative impact of AgNPs on angiogenesis (Gurunathan et al., 2009), which consequently affects CVDs.

Therefore, this dissertation aims to propose a sustainable approach to kill cancer cells and provide a new coating material for drug coated balloons (DCBs) for the remedy of atherosclerosis and peripheral artery disease (PAD). This scientific goal will be realized through the following partial goals:

- Selection of plants having reported anticancer molecules that act as capping agent for silver nanoparticles (AgNPs).
- Biosynthesis of AgNPs using plant extracts i.e., roots, leaves, and stems.

- Selection of Food and Drug Administration (FDA) approved polymers i.e., Polycaprolactone (PCL) and Polyethylene Glycol (PEG) for nanofibers (NFs).
- Incorporation of synthesized AgNPs into nanofiber via electrospinning techniques.
- Toxicological studies for assessing the potential of AgNPs as anti-cancer agents.
- Exploring the toxicological aspects of AgNPs incorporated NFs for their potential use as coating material for drug coated balloons to treat atherosclerosis and peripheral artery disease.

1.3 Objective of the dissertation

- a. By exposing the cancer cells to biosynthesized AgNPs, the cell viability of cancer cells will decrease in a dose dependent manner.
- b. AgNPs incorporated NFs will release Ag ion in a controlled manner for being used as coating material for drug coated balloons to treat atherosclerosis and peripheral artery disease.
- c. The toxicological studies for AgNPs incorporated NFs will provide information about suitable dosage of AgNPs that can be incorporated into NFs for drug coated balloons treat atherosclerosis and peripheral artery disease.

Chapter 2

Review of literature

2.1 Prevalence of cancer

Cancer stands as a obvious contributor to mortality rates and sets a substantial barrier to the advancement of life expectancy across the globe (Bray et al., 2021). Agreeing to the World Health Organization's (WHO) 2019 estimates, 112 out of 183 countries have cancer as the principal or secondary basis of death for those under the age of 70. In 23 countries, it is also the third or fourth leading cause of mortality (see Figure 2.1) (WHO, 2020). The rising incidence of cancer as the principal cause of death can be partially explained by the notable declines in the mortality rates from coronary heart disease (CAD) and stroke comparative to cancer in numerous countries. According to gender and kind of cancer, predictions for the number of new cases of invasive cancer in the US in 2022 have been released by a recent study. The study projects that 1,918,030 new instances of cancer will be diagnosed overall, or around 5250 new cases every day. In addition, it is projected that 98,000 new cases of melanoma in situ of the skin and 51,500 new cases of ductal carcinoma in situ of the female breast will be found in women (Siegel et al., 2022).

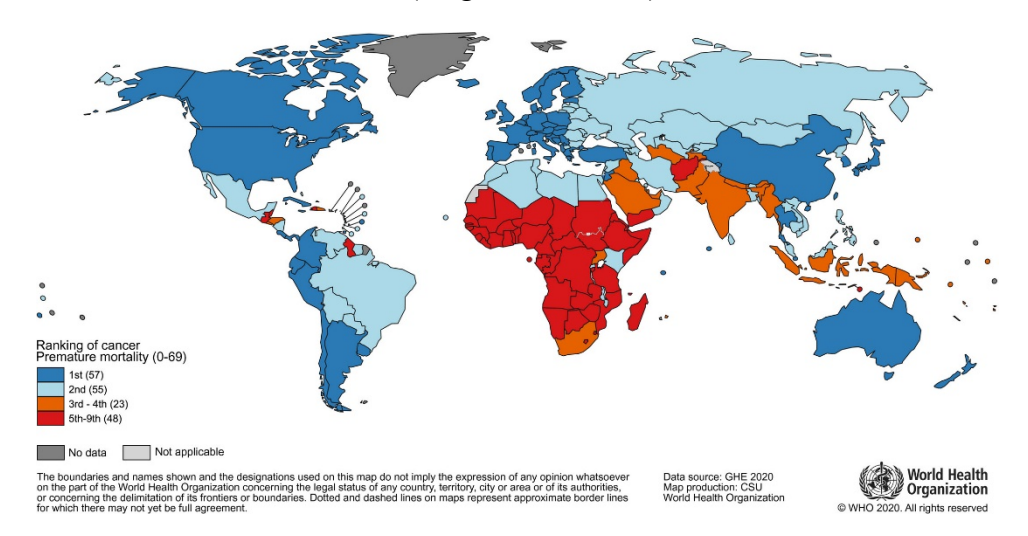


Figure 2.1. Cancer's ranking as a cause of death for individuals under the age of 70 in 2019 (Source: WHO)

Figure 2.2 illustrates the prevailing types of malignancies detected in males and females in the year 2020. In 2022, over 609,360 individuals in the United States are projected to succumb to cancer, resulting in an average of nearly 1700 fatalities each day. Colorectal, prostate, and bronchus (henceforth lung) malignancies comprise more than half (48%) of newly diagnosed cases in males; prostate cancer accounts for 27% of all diagnoses. 51% of all newly identified cases of cancer in women are breast, lung, and colorectal; breast cancer accounts for approximately one-third of these cases. Males experience the highest mortality rates due to lung, prostate, and colorectal cancers, while females are most susceptible to lung, breast, and colorectal cancers (see Figure 2.3) (Siegel et al., 2022). About 350 people every day lose their lives to lung cancer, which is more than the combined mortality toll from pancreatic, breast, and prostate cancers put together. Plus, it kills 2.5 times as many people as colorectal cancer, the

second prominent reason of cancer-related fatalities. Approximately 105,840 (or 81% of the total) of the 130,180 lung cancer deaths in 2022 will be directly caused by cigarette smoking, while an additional 3,650 deaths will be attributed to exposure to second-hand smoke. The tally comes to 26. When taking into account both sexes collectively, lung cancer ranks as the seventh preceding root of cancer death, with an additional 20,700 deaths attributable to factors other than smoking (Siegel et al., 2022).

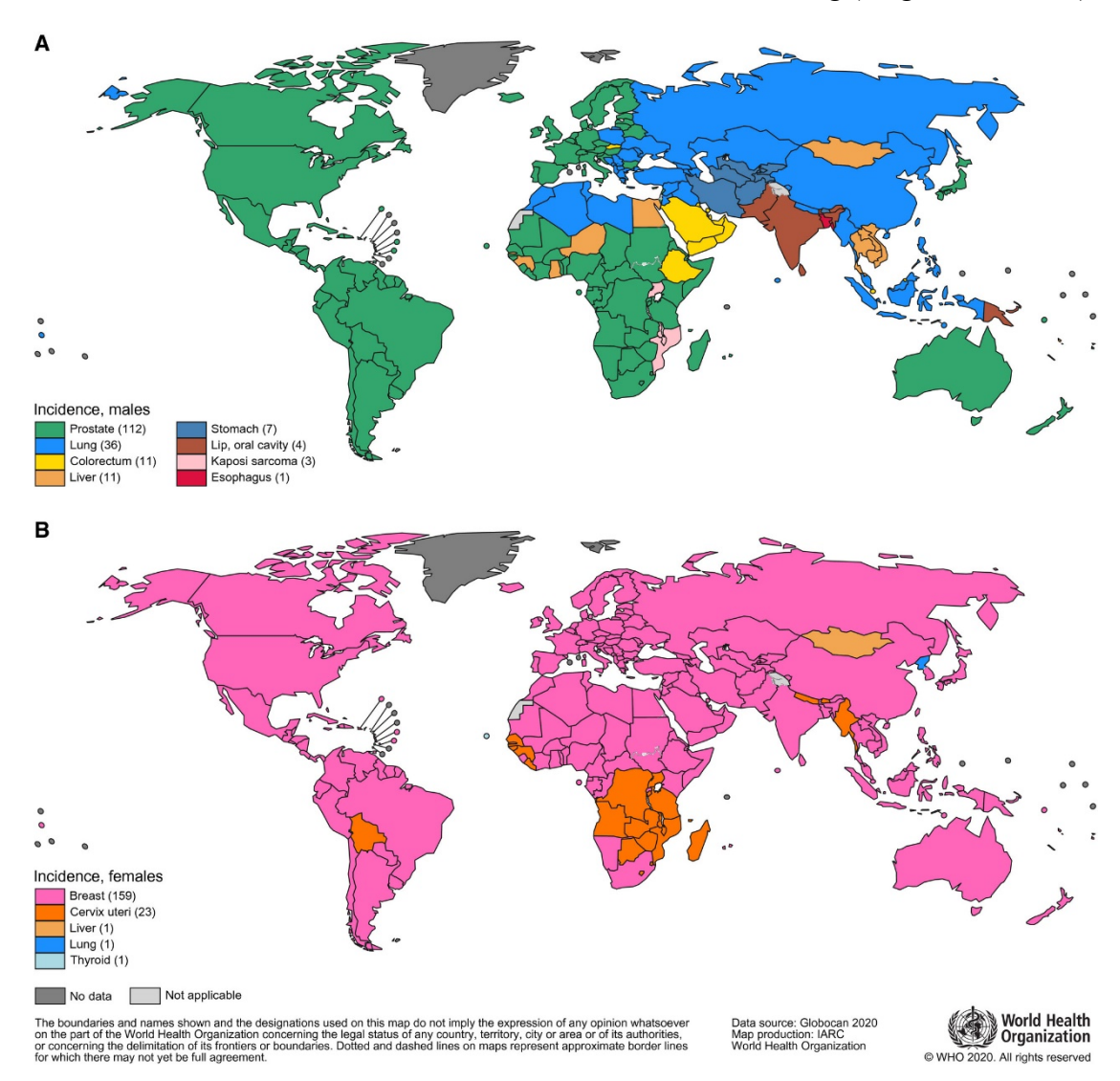


Figure 2.2. Most prevalent types of cancer categorized by gender (Source: WHO)



Figure 2.3. Top ten cancer types for the predictable total of new cancer cases and deaths in USA (Adapted with permission from (Siegel et al., 2022)).

2.2 Current cancer treatment

Currently, despite the availability of early detection techniques and sophisticated treatments, cancer stays a significant worldwide health issue characterized by a high occurrence and death rate. Due to their genetic abnormalities, cancer cells evade cell cycle regulatory systems and evade apoptosis (Greaves & Maley, 2012). While death rates for many forms of cancer have decreased due to the success of treatment approaches, the leading focus of cancer research remains on the development of improved therapeutics to further reduce mortality (see Figure 2.4). The advancement and transformation of cancer treatment has been driven by an enhanced comprehension of the molecular pathways that underlie cancer. The global prevalence of cancer patients is growing, leading to notable problems. Nevertheless, the quest for a therapy that yields the largest rate of positive responses while minimizing negative effects persists rapidly. The clinic employs many cancer treatment modalities, including radiotherapy, surgery, chemotherapy, stem cell transplant, photodynamic therapy, hormone therapy, targeted therapy, immunotherapy and hyperthermia (Miller et al., 2022). Combination therapies are frequently employed due to the resistance mechanisms exhibited by cancer.

Male			Female		
Prostate	3,523,230		Breast	4,055,770	
Melanoma of the skin	760,640		Uterine corpus	891,560	
Colon & rectum	726,450		Thyroid	823,800	
Urinary bladder	597,880		Melanoma of the skin	713,790	
Non-Hodgkin lymphoma	451,370		Colon & rectum	710,670	
Kidney & renal pelvis	376,280		Non-Hodgkin lymphoma	394,180	
Oral cavity & pharynx	311,200		Lung & bronchus	367,570	
Testis	303,040		Uterine cervix	300,240	
Leukemia	300,250	\	Ovary	246,940	
Lung & bronchus	287,050		Kidney & renal pelvis	230,960	
All sites	8,321,200		All sites	9,738,900	

Figure 2.4. Forecasted cancer survivorship rate in the United States in 2021 (Adapted with permission from (Miller et al., 2022))

While improvements in treatment have increased both progression free and survivorship rate, more work remains to be done to make cancer ultimately curable. Although there may be a suitable phase of cancer with long-lasting traits, contrary to popular belief, cancers are not transforming from fatal to chronic illnesses (Pizzoli et al., 2019). Except for a small percentage of individuals whose tumors respond well to traditional therapies, most cases include a chronic, cyclical pattern of remission and recurrence. When it comes to advanced and metastatic cancers, however, palliative care is often administered not for the aim of curing cancer but rather to alleviate symptom load and spiritual and psychological suffering (Henson et al., 2020).

2.3 Challenges in cancer treatment

Cancer is challenging to treat because of the properties of cancer cells. Cancer's cell and tissue biology, genetics, response to therapy and pathology are only a few examples of the staggering range and depth of its viability. Cancer cells avoid getting detected by immune system via variety of approaches as presented in Figure 2.5.

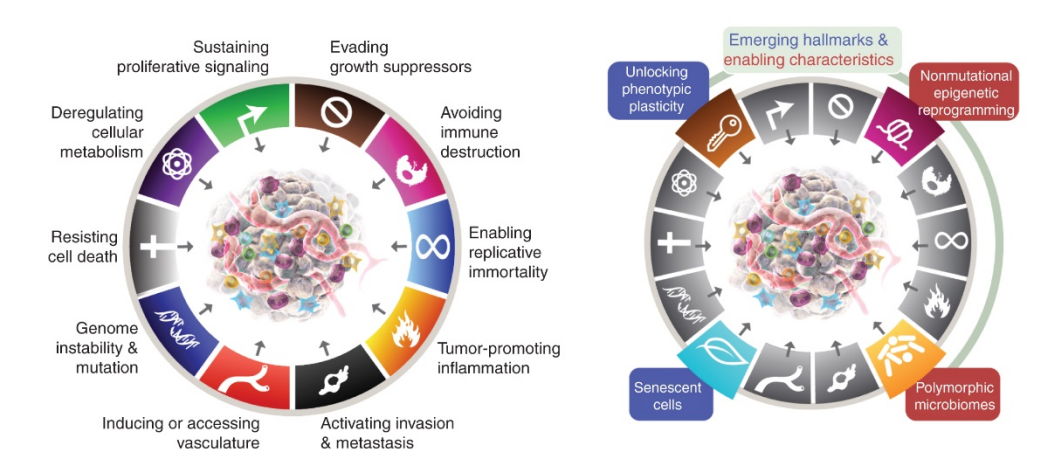


Figure 2.5. Illustration of how cancer cells survive therapy (Adapted with permission from (Hanahan, 2022))

2.3.1 Difficulty in targeting cancer stem cells (CSC)

More and more research points to the idea that malignant cells may often be traced back to a single cell that has stem cell features. These results should have a dramatic influence on the treatment of cancer. The underlying premise of conventional cancer therapy is that all somatic cells have an equal propensity to develop into malignant cells. The aforementioned strategies have proven ineffective in offering

sustained and durable cancer protection by reason of their absence of specificity. On the other hand, target-specific drugs, can shrink tumors by a significant amount, but they almost never eradicate cancer stem cells, with devastating consequences such as tumor recurrence once treatment is stopped.

2.3.2 Drug resistivity towards anti-cancer drugs

Normal stem cells possess distinctive mechanisms that enable them to safeguard themselves against detrimental xenobiotic substances, owing to their need for continual self-renewal and differentiation throughout an individual's lifetime. Stem cells often exhibit high levels of expression of ATP-binding cassette transporter proteins (ABC) (Begicevic & Falasca, 2017). These transporter proteins may harness the energy generated by ATP hydrolysis to enable the active movement of substances, allowing stem cells to expel harmful compounds from their internal cytoplasm to the extracellular environment, even when the concentration gradient is unfavorable (Fletcher et al., 2010). Several types of drug-resistant cancer cells have been observed to possess this protein, which leads researchers to believe that cancer stem cells are responsible for maintaining this trait. An example of this would be the drug resistance protein that is found in breast cancer cells. This protein is referred to as breast cancer resistance protein (BCRP) ABCG2, and it is a unique ABC transporter (Nakanishi & Ross, 2012). A number of other types of stem cells have been shown to contain this protein in the past, and it is responsible for the elimination of medications in breast cancer instances (Natarajan et al., 2012). The BCRP-ABCG2 protein was discovered to have a high level of expression in CD34+/CD38 cells, which are recognized as a subset of stem cells in Acute Myelogenous Leukemia (AML) (Raaijmakers et al., 2005). This protein plays an active role in the removal of drugs from these cells. CSCs can also employ alternate tactics to bestow drug resistance. The cells that are thought to be the origin of the tumor (CD34+ cells) in AML have been found to have a high expression of aldehyde dehydrogenase (ALDH), which is a protein that is frequently seen in hematopoietic stem cells. ALDH is an enzyme that performs the job of detoxification and gives resistance against alkylating medicines like cyclophosphamide because of its activity. According to the current perception of cancer stem cell biology, cancer stem cells (CSCs) are said to be a rare cell type that only makes-up a minute portion of tumor cells. Additionally, they are believed to be dormant. This presents an additional challenge in specifically targeting the CSCs using traditional chemotherapeutic medications, as these treatments primarily harm cells that are undergoing fast division. Due to their limited involvement in active cell division, CSCs are less susceptible to the effects of chemotherapeutic drugs (Yu et al., 2012).

2.3.3 Constraints of traditional chemotherapeutic drugs

Current chemotherapy medicines exhibit cytotoxicity towards both tumorous and healthy cells (Tilsed et al., 2022). The injection of these toxic drugs eradicates both the quickly dividing cancer cells and the healthy cells, resulting in significant adverse effects and potential patient mortality(Crawford, 2013). Unfocused radiation has a comparable deficiency of specificity (Baskar et al., 2014).

2.4 AgNPs as possible anti-cancer agents

The utilization of biologically manufactured silver theragnostic NPs for cancer therapy has the potential to serve as a viable and substitutional approach to the standard

approaches employed for the remedy of cancer (Londhe et al., 2023). The unique biological, physical, and chemical characteristics of AgNPs make them highly favorable candidates for targeted cancer therapy. Imaging facilitation is one of several potential uses for their many advantageous pharmacological qualities, including biocompatibility and cancer-killing capacity, plus their tiny size and huge surface area (Kah et al., 2023). The usage of biosynthesized AgNPs has garnered interest for its involvement in cancer detection and directed drug delivery systems (Gomes et al., 2021). AgNPs may either harm oncogenes in tumor cells or shield healthy cells from malignant cells (D. Kovács et al., 2022). They achieve this through methods that utilize the antioxidative and anticancer capabilities present in plants (Felimban et al., 2022). The choice of plant species, concentration of phytochemicals in plant parts and type of extract are crucial factors in the creation of AgNPs (Siakavella et al., 2020). The process of action varies among different AgNPs depending on the plant precursors they are derived from (Shaikh et al., 2021). The general synthesis mechanism is already described in figure 1.2 of chapter 1.

The potential of phyto-AgNPs, which are produced from natural products, to influence many biological pathways, prevent the growth of cancer cells, trigger apoptosis, and lessen metastasis has made them highly promising for the treatment of cancer. These organic substances have the potential to improve the overall therapeutic outcome when used with traditional chemotherapy medications (Gao et al., 2022). The synergistic effects stem from phytochemicals capacity to target various pathways, which might increase the effectiveness of chemotherapeutic treatments and possibly reduce the dosage needed of these medications, hence reducing toxicity. Drug resistance is one of the biggest obstacles to cancer treatment, as it frequently makes traditional chemotherapy ineffective. Inhibiting drug-metabolizing enzymes, decreasing drug efflux, downregulating drugs-related proteins, and inhibiting drug-metabolizing enzymes are just a few of the ways that phytochemicals might assist overcome multidrug resistance (MDR) (Ward et al., 2020). Because of these qualities, phytochemicals are useful allies in combination treatments intended to avoid MDR and enhance patient outcomes. The severe adverse effects of chemotherapy drugs are wellknown, and they frequently prevent them from being used in clinical settings. The study demonstrates how phytochemicals and chemotherapy together can lessen these harmful side effects. Phytochemicals have the potential to improve the quality of life for cancer patients by shielding normal cells from the cytotoxic effects of chemotherapy, enhancing the selectivity of therapeutic action against cancer cells, and lowering the total side effect burden. The advancement of nanomedicine platforms has created new opportunities for the efficient co-administration of chemotherapeutic medications and phytochemicals. Both kinds of medicine can be encapsulated by nanocarriers such liposomes, polymeric nanoparticles, micelles, and inorganic nanoparticles, which guarantee their steady delivery to tumor locations. Reducing adverse effects and enhancing therapeutic outcomes are dependent on decreasing systemic exposure while optimizing drug accumulation in malignant tissues by targeted delivery. The nanocarrier systems that have been effectively created for this use, showing notable advancements in therapy efficacy, tumor targeting, and pharmacokinetics (Jinfeng Shi et al., 2021). Co-delivery nanomedicines face various obstacles in their clinical translation, even with encouraging preclinical study outcomes. These include the possibility for erratic interactions between phytochemicals and chemotherapeutics, the challenge of creating nanocarriers that can stably encapsulate several medicines with varying physicochemical qualities, and the challenges of scaling up manufacturing for

clinical usage. Regulatory obstacles and the requirement for comprehensive clinical trials to guarantee safety and effectiveness are further major roadblocks to commercializing these innovative treatments.

Due to their potential towards killing cancer cells reserachers from korea utilized 58 plant extracts from Indonesia and Vietnam to synthesize AgNPs using an environmentally friendly approach. They chose six AgNP compounds from a total of fifty-eight, which were produced using extracts from *Hypotrachyna laevigata*, *Areca catechu*, *Maesa calophylla*, *Ardisia incarnata*, *Adinandra poilanei* and *Maesa laxiflora* (Ahn & Park, 2020). The evaluation of cell toxicity and generation of reactive oxygen species (ROS) in HeLa and A549 cells revealed that the AgNP samples synthesized from *Maesa calophylla*, *Ardisia incarnata*, and *Maesa laxiflora* revealed significant cytotoxicity and excessive ROS generation compared to the other six samples of AgNPs. The AgNPs, when exposed to HeLa and A549 cells, caused cell death particularly by necrosis, with a minor contribution from late apoptosis. Cell cycle research revealed a significant surge in the cell number during the S phase.

The AgNPs manufactured using green methods caused cell death, indicating potential for anti-cancer properties. Pannerselvam et al. synthesized AgNPs using *Peltophorum pterocarpum* as a nanotherapeutics against cancer cells (Pannerselvam et al., 2021). The in vitro cytotoxic effects of the produced AgNPs against malignant cells, including HepG2, MCF-7, and A549 cells, were evaluated. The results demonstrated that AgNPs possess the anti-cancer abilities. The IC₅₀ values against HepG2, A549, and MCF-7 cell lines were noted to be 69, 53, and 62 μg/ml, respectively. Pei et al. investigated the anti-cancer potential of biogenic AgNPs, produced from *Coptis chinensis* extract. Before subjecting the A549 lung cancer cells to AgNPs treatment with dosages of 10 μg/ml and 25 μg/ml, they examined the fundamental mechanism throughout the cell population. The antiproliferative action of AgNPs was complemented by a discernible reduction in the level of cell viability. In addition to that, anti-bacterial tests conducted with Gram(+) bacteria (*Staphylococcus aureus*) and Gram(-) bacteria (*Escherichia coli*) revealed a greater zone of inhibition against Grampositive bacteria (Pei et al., 2019).

The researchers from India explored the production of AgNPs by utilization the extract from leaf of *Uvaria narum*, a medicinal plant widely known as narumpana and its properties such as antibacterial, anticancer, antiangiogenic, and catalytic effects (Ajaykumar et al., 2023). The anti-angiogenic action of the AgNPs was demonstrated using the chick chorioallantoic membrane assay (CAM). AgNPs exhibited cytotoxicity against three fish cell lines: Cyprinus carpio koi fin, Oreochromis niloticus liver (onlL), and Cyprinus carpio gill (CyCKG) cells. AgNPs exhibited anti-cancer activity towards Dalton's lymphoma ascites (DLA) cells. In addition, the inhibitory effects of AgNPs against pathogenic microorganisms, including S. aureus and E. coli, were demonstrated. The findings of the study reveal that green produced AgNPs possess antibacterial, antiangiogenic, cytotoxic, and catalytic activities. These are all essential characteristics for a molecule that has exceptional clinical applications, as the study demonstrates. In their study, Wang et al. published an examination of the structure and biological features of AgNPs that were synthesized by employing the pericarp extract of muskmelon (Cucumis melo L.). After doing an XRD analysis, it was discovered that the biosynthesized AgNPs possessed a face-centered cubic crystalline structure. In addition, the energy-dispersive X-ray spectroscopy (EDAX) and scanning electron microscopy (SEM) demonstrated the presence of AgNPs that had a spherical shape and

had an average size of 25 nm. It was shown that the AgNPs were able to effectively inhibit the growth of both *Bacillus subtilis* and *E. coli*. Furthermore, the cytotoxicity test of AgNPs shown a substantial effectiveness in killing a number of cancer cells, including PC-3, HCT-116, HeLa, and Jurkat, in a manner that was dependent on the dose. IC50 values varied from 150 to 224 μ g/ml, and the observed cell viability ranged from 50% to 60% depending on the concentration of the compound. Biosynthesized AgNPs have been proven to have an anti-cancer effect on malignant cells, as evidenced by the lower cell viability (Y. Wang et al., 2020).

Likewise, Abu-Dief et al. prepared AgNPs from Delonix Regia Extract and tested the cytotoxicity of these NPs against three human cell lines: breast carcinoma cells (MCF-7), hepatic cellular carcinoma cells (HepG-2), and colon cancer cells (HCT-116) (Abu-Dief et al., 2020). The cytotoxic effect (IC₅₀) against the HepG-2, HCT-116 cell line, and MCF-7 cell line by AgNPs were observed to be 4.35, 6.2, and 5.12 μg/μl, respectively. These values were compared to the cytotoxic impact (IC₅₀) of Doxorubicin, which were 5.25, 4.25, and 4.45 µg/µl, respectively. The cytotoxicity of AgNPs is comparable to that of Doxorubicin, with MCF-7 and HepG-2 cell lines exhibiting greater sensitivity to AgNPs treatment compared to HCT 116 colon cancer cell lines. HepG-2 cells exhibited greater sensitivity to the inhibitory effects of AgNPs on cell growth, with an IC₅₀ value of 35 μg/ml. In contrast, the IC₅₀ value for the HCT-116 cell line was noted to be 6.2 µg/ml. The presence of AgNPs leads to a reduction in both the ability of cells to survive and their ability to move, as the DNA molecules become more tightly packed. Consequently, the capacity for replication is compromised when Ag⁺ ions interact with proteins and produce ROS, resulting in cell death due to oxidative stress.

Nadhe et al. synthesized AgNPs from two biologial sources bacteria (Acinetobacter sp.) (bAgNPs) and plant extract (Curcuma aromatica) (pAgNPs) and performed a comparative study of their anti-cancer capability against cervical cancer (HeLa) cell line (Nadhe et al., 2020). Both AgNPs exhibited a viability rate of 50% for peripheral blood mononuclear (PBMCs) cells when utilized at a high dose of 200 µg/ml. The IC₅₀ values for pAgNPs and bAgNPs against HeLa cells were 14 and 17.4 μg/ml, respectively. The use of ethidium bromide and acridine orange staining revealed that bAgNPs exhibited cytostatic effects, while pAgNPs induced apoptosis. The staining technique JC-1 indicated that the treatment with pAgNPs had an impact on the mitochondrial membrane potential, whereas the treatment with bAgNPs did not cause any changes. Flow cytometry analysis indicated that exposure of HeLa cells to both AgNPs resulted in cell cycle arrest. Moreover, it was observed that the use of pAgNPs induced apoptosis in these cells. Approximately 58% and 77% of HeLa cells were observed in the subG1 phase after being treated with pAgNPs and bAgNPs, respectively. Bacterial AgNPs had a cytostatic impact on HeLa cells by halting cell development in the subG1 phase. Conversely, plant based AgNPs induced the death of HeLa cells by impairing the mitochondrial membrane potential and triggering apoptosis.

According to a study by Tian et al., *A. marina*, a marine mangrove plant, is a great reducing agent for the synthesis of AgNPs and has strong anti-cancer effects on A549 cells. The plant extract used to create the synthetic Ag NPs contains a variety of functional groups that contribute to the reduction of Ag metal ions. It's interesting to note that Ag NPs influence significant mitochondrial membrane damage and exhibit outstanding anti-cancer action against A549 cells. Furthermore, fluorescent

microscopic investigation using DCF dye showed the extremely high amount of ROS generation. Every in vitro investigation verified that AgNPs was highly effective, concentration-dependently, against A549 cells. Additionally, *A. franciscana* treated with Ag NP showed a notable mortality rate at increasing concentrations due to the compound's enhanced toxicity. As a result, our findings indicated that Ag NPs were efficient against A549 lung cancer cells and had promise anti-cancer characteristics (Tian et al., 2020).

Gul et al. carried out green synthesis of AgNPs using annual meadow grass (*Poa annua*) for possible drug delivery system. Gas chromatography mass spectroscopy and phytochemical studies of *P. annua* extract revealed abundant amounts of flavonoids, phenols, and alkaloids, which act as reducing and stabilizing agents for AgNPs. For more than a month at 4 °C, the produced AgNPs (with a diameter of 36.66 ± 7.85 nm) remained stable in various solvents, including deionized water, phosphate-buffered saline, and dimethyl sulfoxide. The AgNPs-EDL@Starch composite is a new drug delivery system for cancer treatments that combines biogenic AgNPs with an anticancer medicine (*E. dracunculoides Lam.* plant extract) and a starch coating. Through the use of antioxidant assay ($61.42 \pm 0.04\%$ and $81.00 \pm 0.12\%$, respectively) and MTT assay against SCC7 cell lines ($\approx 60\%$ and $\approx 40\%$), the biocompatibility and anti-cancer impact of AgNPs and AgNPs-EDL@Starch were demonstrated. The largest dose of AgNPs (300 mg/kg) administered orally to Sprague Dawley rats (n = 3) for 7 days did not cause any noticeable cytotoxicity, according to their *in-vivo* results (Gul et al., 2021).

According to another study's findings, there is a lot of promise for employing extracts from *Curcuma longac* also known as turmeric, and *Zingiber officinale* also known as to create AgNPs that can be used as anti-cancer agents. AgNPs were tested *in-vitro* against HT-29 human colon carcinoma cells, the anti-cancer activity demonstrated encouraging findings with a dose-dependent cytotoxic effect, especially at an IC₅₀ value of 150.8 μ g/ml. According to these results, organically produced AgNPs may have superior anti-cancer capabilities than chemically produced nanoparticles, making them a potentially safer and greener option. The potential application of plant-based AgNPs in the creation of fresh anti-cancer treatments is highlighted by this work (Venkatadri et al., 2020).

In another study, Murugesan et al. proposed an environmentally gentle method for producing AgNPs by utilizing Gloriosa superba Linn aqueous extract with an aim to use these NPs as anti-cancer angents (Murugesan et al., 2021). GST-AgNPs were experimented against A549 cell lines in order to determine their effectiveness as an anticancer agent in vitro. We evaluated the sensitivity of vero cells and A549 cells to the GST-AgNPs at concentrations ranging from 10 to 100 µg/ml following a treatment period of 24, 48, and 72 hours. The findings indicated that there was a significant dosedependent but also time-dependent action. In contrast to the cells that were not exposed to any treatment, the number of viable cells was reduced. At a concentration of 50 µg/ml, the Vero cells did not exhibit any impact; nevertheless, when the concentration was increased to 125 µg/ml, they were influenced. These findings provide conclusive evidence that GST-AgNPs have a deadly effect on lung cancer cells, but normal cells are not affected by this effect. The conclusion of the study proves that GST-AgNPs displayed cytotoxic effects on A549 cells. This was demonstrated by the fact that there was an increase in cell mortality after the treatment with GST-AgNPs was administered. It is clear that the cytotoxicity that was brought about by GST-AgNPs followed a pattern that was dose-dependent. At 24, 48, and 72 hours after treatment with biosynthesized GST-AgNPs, which demonstrated an IC₅₀ value of 46.54 µg/ml, adjustments in the morphology of A549 cancer cells were seen. These variations were observed in the cells. Furthermore, it was seen that the cell inhibition rate of GST-AgNPs was 11.95% and 65.08% when the doses were 10 and 60 µg/ml, respectively. The minimum inhibitory concentration (IC50) of GST-AgNPs that were produced through biological means was found to be 46.54 µg/ml over a period of twenty-four hours. Subsequently, there was a decline in the number of cells accompanied by inadequate cell cohesion. After 24 hours of treatment with biologically generated GST-AgNPs at a concentration of 46.54 µg/ml, the fluorescent stain revealed the presence of living, apoptotic, and necrotic cancer cells. The viable cells demonstrated a typical green nucleus, but the nonviable cells showcased an intact orange nucleus. Nevertheless, the early apoptotic cells exhibited a vividly green nucleus. Conversely, the cells undergoing late apoptosis exhibited chromatin condensation and nuclear disintegration, which appeared in an orange hue. The application of GST-AgNPs resulted in the generation of ROS within cancer cells, which subsequently caused harm to the cellular constituents, ultimately resulting in cell demise. They provided information that cell death can be triggered by biosynthesized GST-AgNPs by the production of superoxide radicals and reactive hydroxyl species. Their data presented offered definitive proof of the cytotoxic impact of GST-AgNPs on the A549 lung cancer cell line.

A very recent work created bio-genic AgNPs using the bacterium Paraclostridium benzoelyticum strain 5610. AgNPs were investigated for their anti-inflammatory efficacy of AgNPs exhibits the lowest inhibition activity for COX-2 (13.16 \pm 0.46%) and the maximum inhibitory action (42.68 \pm 0.62%) for 15-LOX. AgNPs have demonstrated notable inhibitory effects on the AGEs of elastases (66.25 \pm 0.49%), with visperlysine AGEs (63.27 \pm 0.69%) coming in second. Additionally, following 24-h of treatment, the AgNPs exhibit considerable toxicity against the HepG2 cell line, demonstrating a 53.543% drop in cell viability. The anti-inflammatory activity showed that the bio-inspired AgNPs had a strong inhibitory effect. All things considered, biogenic AgNPs can be used to treat anti-aging conditions. In addition, because of their antioxidant and anti-cancer properties, NPs can be a helpful therapeutic option for a range of conditions, such as bacterial infections, cancer, and other inflammatory diseases (Faisal et al., 2023).

To improve chemotherapy and reverse drug resistance, chemotherapeutic medications must have both accurate tumor-targeting and great anti-cancer efficiency. Combining multifunctional agents ought to be a fruitful tactic for achieving synergy. Muhammad et al. have effectively created new multi-functionalized medicine nanocrystals in our research to enable the co-administration of an organic medication called Paclitaxel (PTX), inorganic silver nanoparticles (AgNPs), and a tumor-targeting agent. More specifically, polydopamine (PDA) was coated on PTX nanocrystals that had been created as a template earlier. In order to create and deposit AgNPs in situ and provide locations for the grafting of the tumor-targeting peptide NR1 (RGDARF), the PDA layer was employed as the connecting link. The result was that these NR1/AgNP-decorated drug nanocrystals showed significantly improved cellular uptake efficiency, in vitro anti-cancer activity, and an anti-migratory effect against a range of cancer cells. These effects were caused by the AgNPs and PTX working in concert, improving cellular uptake efficiency through NR1-receptor interaction, pH-responsive drug release, and the nano-scaled nature of the material. Specifically, these NR1/AgNP-

decorated PTX nanocrystals demonstrated strong anti-cancer effectiveness and few side effects, all while maintaining good selectivity and biocompatibility. Furthermore, the potency of these unique pharmacological nanocrystals to induce apoptosis was significant, leading to nuclear damage, mitochondrial malfunction, rupture of cell membranes, excessive production of reactive oxygen species, and breakage of double-stranded DNA. With a higher Bax-to-Bcl-2 ratio and the activation of pro-apoptotic P53 and caspase 3, the possible functional mechanism and molecular foundation of these novel pharmacological nanocrystals are significant to the regulation of mitochondriamediated apoptosis (Muhammad et al., 2020).

Another study investigated the potential medical uses for AgNPs made from a leaf extract from Juniperus chinensis. The study compares the effectiveness of these bio-functionalized nanoparticles against the commercial chemotherapeutic medication cisplatin in order to assess the anti-cancer and anti-metastatic capabilities of these particles on human lung cancer cells (A549). The MTT test was utilized to assess the cytotoxic effects of AgNPs on both normal HEK293 cells and malignant A549 cells. The outcomes showed that AgNPs were selectively harmful to cancer cells, as seen by their dose-dependent cytotoxicity against A549 cells and negligible effects on HEK293 cells at lower concentrations. For A549 cells, the concentration of AgNPs at which 50% of cells are inhibited was found to be 9.87 µg/ml; this value was less than that of cisplatin, indicating that AgNPs have a greater ability to suppress the growth of cancer cells. Subsequent analyses of AgNPs' molecular processes showed that they cause A549 cells to undergo apoptosis. Compared to cells treated with cisplatin, cells treated with AgNPs showed a considerable upregulation in the expression levels of important apoptotic genes, including p53, caspase-3, and caspase-9. Flow cytometric analysis, which revealed a larger percentage of apoptotic cells in the AgNPs-treated group, further supported this. Furthermore, it was shown that AgNPs suppressed the expression of the genes MMP2 and MMP9, which are linked to metastasis, preventing cancer cells from migrating and invading. These results were corroborated by the scratch wound healing and Matrigel invasion experiments, which showed that AgNPs considerably and more potently inhibited the A549 cells' capacity to spread than cisplatin. AgNPs treatment significantly increased the amount of ROS produced in A549 cells, which is a proven way to cause apoptosis. AgNPs-treated cells showed a more marked increase in ROS levels than cisplatin-treated cells, indicating that ROS formation plays a major role in AgNPs lethal effects. Additionally, it has been demonstrated that AgNPs can stop the cell cycle in the G0/G1 phase, halting the growth of cancer cells by keeping them from entering the DNA synthesis (S) phase. This was linked to the overexpression of the tumor suppressor gene p53, which encourages cell cycle arrest and apoptosis, and the downregulation of cyclin D1, a protein essential for cell cycle progression. These NPs showed less toxicity to normal cells and were superior to cisplatin in causing apoptosis, suppressing cell growth, and preventing metastasis. According to this, bioorganic-capped AgNPs may prove to be a useful therapeutic agent for the treatment of lung cancer, providing a less harmful substitute for traditional chemotherapy (Noorbazargan et al., 2021).

Likewise, another study used the natural phytochemicals found in the *Ardisia gigantifolia* extract to reduce silver nitrate (AgNO₃) into AgNPs, which are subsequently examined for their ability to prevent the growth and spread of stomach cancer cells. Two gastric cancer cell lines, AGS and MKN45, were used in a variety of in vitro experiments to evaluate the anti-cancer effect of Arg-AgNPs. After 24 and 48

hours of treatment, respectively, the MTT assay findings showed that Arg-AgNPs effectively and dose-dependently suppressed cell proliferation, with IC₅₀ values of 1.37 and 0.65 mg/ml for AGS cells and 1.03 and 0.96 mg/ml for MKN45 cells. These results show that the nanoparticles have a strong anti-cancer effect and are superior to many conventional treatments. Subsequent analysis of the mechanism of action showed that in both gastric cancer cell lines, Arg-AgNPs cause cell cycle arrest at the G0/G1 phase. It is important to note that this cell cycle arrest stops the cells from entering the DNA synthesis (S) phase, which inhibits the cells' ability to proliferate. Particularly, the administration of Arg-AgNPs led to a considerable decrease in the number of cells in the S phase, an indication of slowed cell division and growth, and a rise in the fraction of cells in the G0/G1 phase. The wound-healing assay revealed that Arg-AgNPs not only prevented cell proliferation but also inhibited the migration of cancer cells. Furthermore, the study showed that Arg-AgNPs significantly inhibited the ability of the stomach cancer cells to migrate, even at low concentrations, indicating their potential to impede the progression of cancer. The discovery that Arg-AgNPs induce cellular senescence is another important one. A permanent growth pause that stops damaged or malignant cells from proliferating is called cellular senescence. The anti-cancer potential of Arg-AgNPs was further supported by the study, which demonstrated a significant rise in senescent cells after treatment with the substance. Senescent cells were detected using SA-β-gal staining. Finally, the investigation brought attention to the part that reactive oxygen species (ROS) play in Arg-AgNPs' ability to fight cancer. Chemically reactive substances known as ROS have the ability to cause oxidative stress in cells, which can result in cell damage and death. The study revealed that the treated gastric cancer cells had much higher ROS levels due to the presence of Arg-AgNPs, which probably played a role in both the observed cell cycle arrest and the induction of apoptosis (Le et al., 2023).

A different study investigated the production of AgNPs from Phyllospongia lamellosa extracts. The study looks into the biological activities of these NPs, namely their ability to fight inflammation and cancer. Detailed metabolomics analysis and molecular docking studies are used to bolster the findings. Significant anti-cancer activity against estrogen-positive (MCF-7) and multidrug-resistant (MDA-MB-231) human breast cancer cell lines is demonstrated by the study's biological evaluation of the produced AgNPs. When applied to MCF-7 cells, the IC₅₀ values of the AgNPs made using the chloroform extract (CE-SNPs) show notably strong anti-cancer properties, surpassing those of the reference medication, taxol. On the other hand, these nanoparticles show a selective toxicity towards cancer cells, with IC₅₀ values similar to those of taxol and modest toxicity against normal breast cells (MCF-10a). The sponge extract contains a range of terpenoids, especially triterpenes and sesterterpenes, according to the metabolomics study. These substances are well-known for having anticancer qualities, and it's possible that their presence adds to the AgNPs' biological action. Moreover, molecular docking studies imply that these substances might target the protein secreted phospholipase A2 (sPLA2), which is linked to the development of cancer, in order to achieve their anti-cancer actions. The study evaluates the antiinflammatory potential of AgNPs by assessing their capacity to inhibit cyclooxygenase (COX) enzymes, which are important mediators of inflammation, in addition to their anti-cancer effect. AgNPs are found to have moderate to poor inhibitory effect against COX-1 and COX-2, with the free AgNPs and those loaded with the sponge extract demonstrating the lowest levels of activity against COX-2, according to the results. In spite of this, the nanoparticles' selectivity indices (SI) surpass those of the reference medications, suggesting that they may find use in anti-inflammatory applications. According to the study's findings, *P. lamellosa* extracts' green-synthesized AgNPs show great potential as anti-cancer agents, especially when it comes to estrogen-sensitive breast cancer. A better understanding of the underlying mechanisms is provided by the metabolomics and docking investigations, which indicate that certain metabolites targeting sPLA2 are responsible for the anti-cancer effect (Al-Khalaf et al., 2021).

A study from Turkey examined the anticancer properties of chemically synthesized AgNPs, Bio-AgNPs derived from Cumin seeds, and extract from Cuminum cyminum L. (Cumin) seeds on MCF-7 and human breast adenocarcinoma metastatic cell line (AU565). Using the MTT assay, the cytotoxic and anticancer properties of AgNPs and Bio-AgNPs were ascertained. Based on the cytotoxicity investigation, Bio-AgNPs seem to be less harmful than AgNPs against J774 macrophage cells, as indicated by their respective IC50 values of 0.75 and 1.25 µg/ml. Conversely, at non-toxic doses like 0.25 and 0.5 µg/ml, Bio-AgNPs showed notable inhibitory effects on human breast cancer cells. On the other hand, AgNPs were more harmful than Bio-AgNPs on breast cancer cells at higher doses. Upon examining the cytotoxic and anticancer properties of cumin extract, it was determined that at the examined doses, it killed 50% of the MCF-7 cells while having no inhibitory effect on J774 cells. It's interesting to note that the cumin extract had no inhibitory effects on AU565 cells. However, on both cell lines, AgNPs and Bio-AgNPs shown strong anticancer properties. At the highest concentrations administered (12.5 µg/ml), the percentage of AgNPs that inhibited MCF-7 and AU565 cell lines was determined to be 95% and 97%, respectively. In a similar vein, we found that the highest concentrations of Bio-AgNPs inhibited 87.5% and 96% of MCF-7 and AU565 cells respectively. Given the comparatively toxic-free characteristics of Bio-AgNPs made from C. cyminum L. seed extracts, it is possible to predict that this formulation will lead the way in the near future in the creation of novel anticancer drugs based on nanotechnology for the treatment of breast cancer (Dinparvar et al., 2020).

Another extensive investigation on the possible uses of AgNPs in cancer treatment and their biogenic manufacture utilizing the leaf extract of the seagrass species Cymodocea serrulata. The study's main objectives were to characterize the resultant nanoparticles, synthesize them in an environmentally responsible manner, and assess their antibacterial, anticancer, and anti-inflammatory properties. The disc diffusion method is used to assess the antibacterial efficacy of the biogenically produced AgNPs against Gram-positive (B. subtilis, P. aeruginosa) and Gram-negative (S. aureus, E. coli) microorganisms. The outcomes reveal noteworthy antibacterial activity, wherein the nanoparticles exhibit greater effectiveness in comparison to the conventional antibiotic gentamycin, particularly at reduced concentrations (50 and 100 μg/ml). By measuring the cytotoxicity of the AgNPs against a variety of human cancer cell lines, such as lung cancer (A549), breast cancer (MDA-MB-231 and MCF-7), and hepatic cancer (HepG2) cells, the study also explores the anticancer potential of the AgNPs. The results of the cytotoxicity tests show that the AgNPs have cytotoxic effects that are dose-dependent, and the IC₅₀ values show strong anticancer activity. With an IC₅₀ value of 57.3 \pm 2.5 µg/ml, the AgNPs are particularly effective against the MCF-7 breast cancer cell line, indicating their potential as a chemotherapeutic treatment. Furthermore, the human red blood cell (HRBC) membrane stabilization method is used to evaluate the anti-inflammatory characteristics of the AgNPs. The findings indicate that the AgNPs have noteworthy anti-inflammatory properties, surpassing both the standard anti-inflammatory medicine diclofenae and the leaf extract of *C. serrulata*, with an IC₅₀ value of $30.08 \pm 1.4 \,\mu\text{g/ml}$ (Venmani et al., 2023).

All these studies provided information on possible cancer killing mechanism which encompasses a variety of effects, including halting the cell cycle, inhibiting the development of new blood vessels, damaging cell membranes and causing leakage, inducing DNA damage, destroying mitochondria, causing misfolding of proteins, and leading to programmed cell death known as apoptosis (Ramzan et al., 2022) (see Figure 2.6).

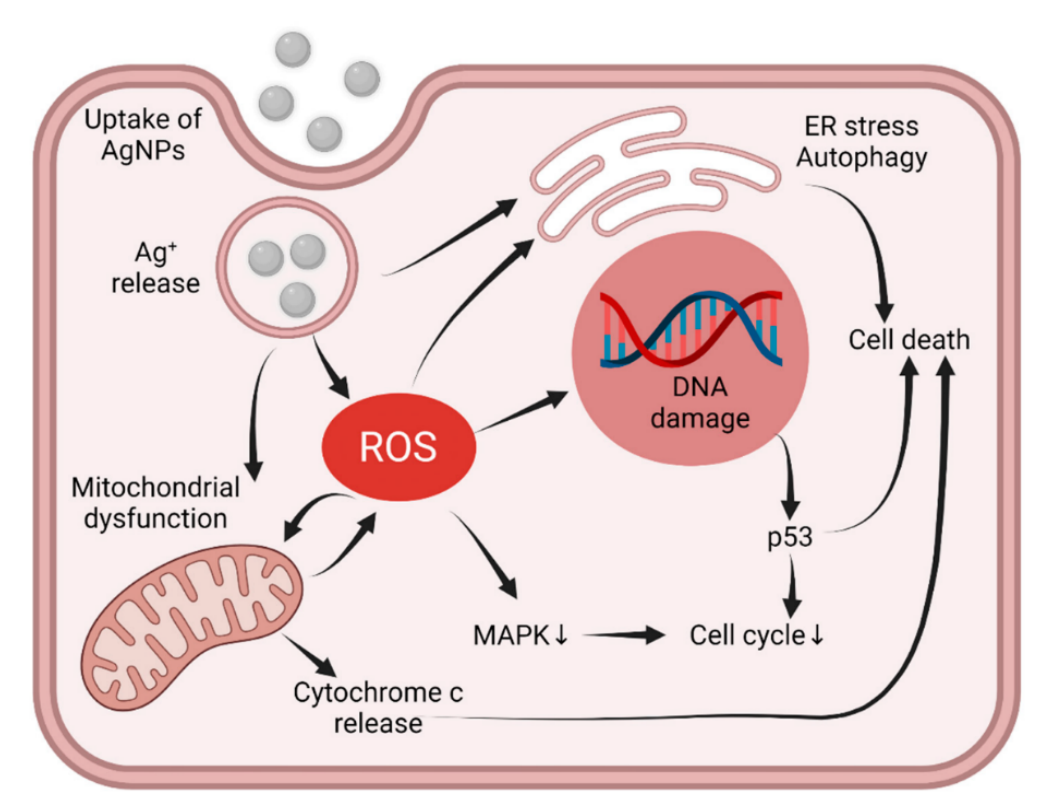


Figure 2.6. Diagram of cancer cell killing mechanism of AgNPs (Adapted with permission from (Dávid Kovács et al., 2022))

2.5 Global prevalence of peripheral artery disease (PAD)

Lower extremities peripheral arterial disease (PAD) is a disorder triggered by the buildup of fatty deposits in the blood vessels of the legs, resulting in narrowing or blockage of the arteries (see Figure 2.7). This can cause symptoms such as intermittent leg pain, reduced blood flow, and difficulty performing daily activities (Creager, 2020). PAD is an escalating global public health issue characterized by its increasing incidence. It is widespread, impacting over 200 million individuals globally (F. G. Fowkes et al., 2013). Unfortunately, it frequently goes unnoticed and receives inadequate treatment.

While there has been substantial research on PAD in high-income nations, the impact of this disease in nations with lower socioeconomic development has been neglected (F. G. R. Fowkes et al., 2017). Nevertheless, low and middle income nations are experiencing an epidemiological transition characterized by a significant rise in the occurrence and impact of cardiovascular illnesses (S. Yusuf et al., 2001). This trend is likely attributed to the processes of industrialization, urbanization, and an upsurge in

metabolic risk factors. In spite of the fact that the prevalence of PAD is higher in high-income countries, the majority of people who have PAD around the world live in countries with low and intermediate incomes. This is the case even when population size is taken into consideration (Song et al., 2019).

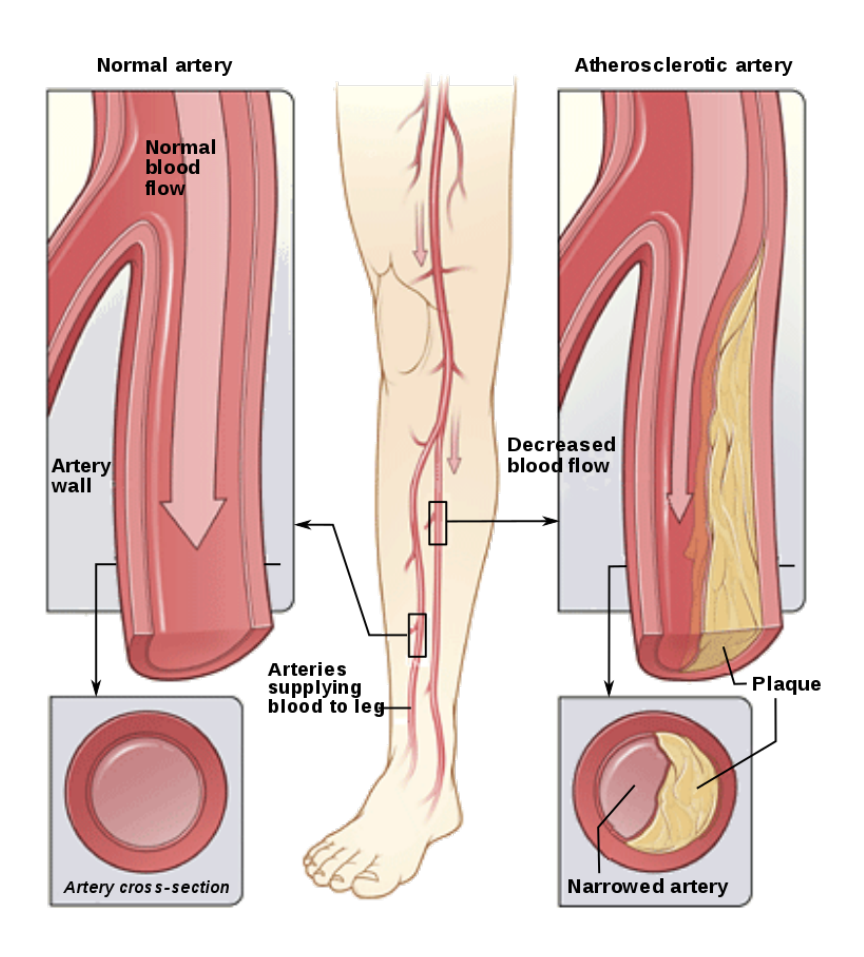


Figure 2.7. Demonstration of PAD presence in leg

Recently a risk factors study (GBD 1990-2019) on PAD calculated three summary measures including years of life lost (YLLs), years lived with disability (YLDs), and disability-adjusted life years (DALYs) in order to compare the burden of disease across different locations. They used direct technique to calculate agestandardized rates per 100,000 people according to the GBD population standard (see Figure 2.8). The outcome of the study demonstrated that the global prevalence of PAD among individuals aged 40+ years was estimated to be 1.52%, affecting a total of 113 million people. Among these cases, 42.6% were reported in countries with a low to moderate socio demographic index (SDI). The occurrence of PAD worldwide was more pronounced among the elderly population, namely 14.91% in those aged 80-84 years. Additionally, the occurrence tended to be higher in females compared to males. The percentage of total peripheral artery disease DALYs in 2019 that can be attributed to modifiable risk factors was 69.4%. Nations with high SDI had the highest prevalence of PAD, whereas nations with low SDI had the lowest prevalence. However, the rates of disability-adjusted life years (DALYs) and death followed U-shaped curves, with the highest burden observed in both the low and high SDI quintiles (Kim et al., 2023).

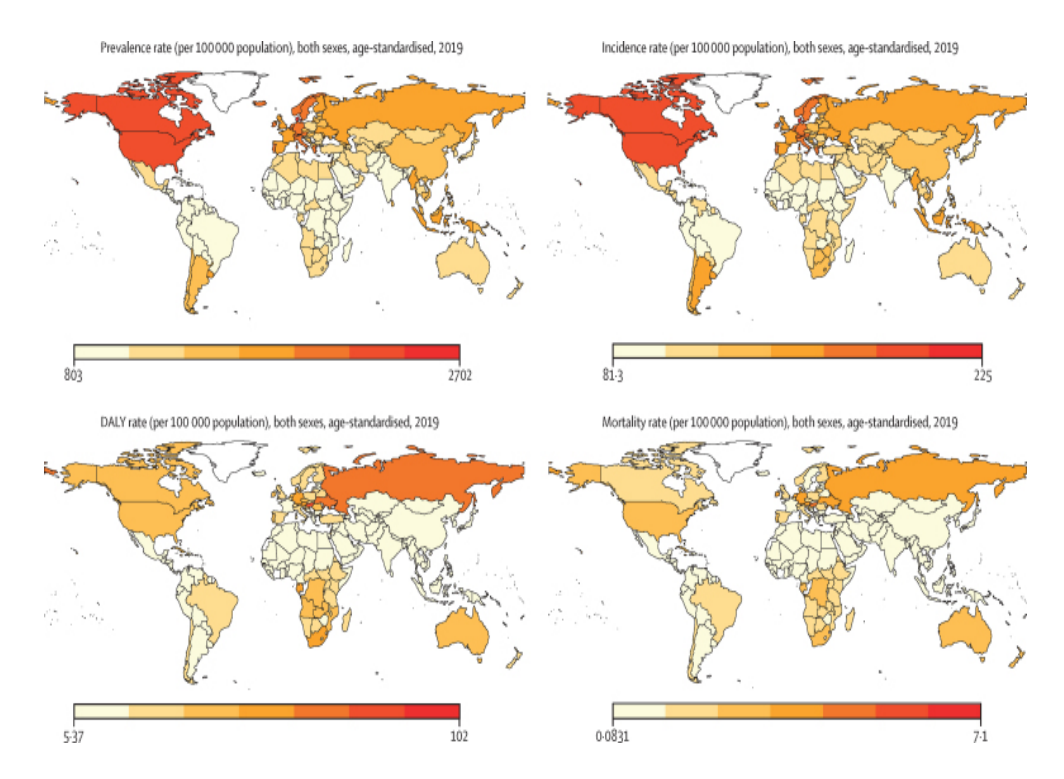


Figure 2.8. Geographic dispersion of age-adjusted rates of PAD in the year 2019 (Adapted with permission from (Kim et al., 2023))

2.6 Prevalence of peripheral artery disease (PAD) in Serbia

Approximately 15% of the entire adult population is believed to exhibit certain characteristics of chronic venous insufficiency (CVI) (Beebe-Dimmer et al., 2005). In general, the prevalence of PAD in the adult population ranges from 3% to 4% (Cornejo Del Río et al., 2017). In Serbia, not many studies have been carried out on the prevalence of PAD in Serbian population. Some studies have been published which provided an insight on its prevalence in association with patient condition i.e., hemodialysis patients, patients with carotid artery disease, and lower extremity amputations cases due to PAD or related illness.

A cross-sectional descriptive study was published in 2016 by the researchers from the Clinical Center of Vojvodina, and Faculty of Medicine, University of Novi Sad, Serbia. They examined a total of 162 patients. The findings of their study indicated that the risk variables associated with chronic venous insufficiency (CVI) included elevated body mass index (BMI), hypertension, prolonged periods of standing while employment, and a positive family history of CVI. Within the same sample, it was discovered that 28 individuals, accounting for 17.28% of the patients, exhibited PAD. The pertinent risk factors for PAD in the current investigation included elevated diabetes, hypertension, BMI, and a positive familial history of PAD. The analysis of the incidence of PAD in patients with severe forms of CVI compared to a control group revealed a statistically significant difference (p = 0.0275) with odds ratio of 3.375. Following multivariate analyses, the adjusted odds ratio remained statistically significant (Matic et al., 2016).

Another cross-sectional study a total of 156 hemodialysis patients were included. This study was conducted by medical professionals from Clinical Hospital Center Zvezdara, Belgrade, Serbia along with medical professionals from Primary

Health Center, Palilula, Serbia and researcher from Medical Faculty, University of Belgrade, Serbia (Ašćerić et al., 2019). PAD was detected in 55 out of 156 individuals, with a prevalence of 35.3%. The patients diagnosed with PAD were notably older $(67\pm10~\text{years}~\text{vs}.~62\pm11~\text{years},~p=0.014)$ and had a higher prevalence of diabetes mellitus (p=0.022) and anemia (p=0.042). Additionally, they exhibited significantly lower levels of serum albumin (p=0.005), total cholesterol (p=0.024), and iron (p=0.004), as well as higher levels of glucose (p=0.002) and C-reactive protein (p<0.001). Furthermore, the patients with PAD had lower dialysis adequacies (p=0.040) compared to those without PAD. Through multivariate analysis, it was found that there is a higher level of C-reactive protein (odds ratio = 1.03, p=0.030), a higher likelihood of vascular access by Hickman catheter (odds ratio = 4.66, p=0.045), and a higher chance of experiencing symptoms of PAD (odds ratio = 5.20, p<0.001) as independent factors associated with PAD in hemodialysis patients.

Similarly, researcher from Medical Faculty, University of Belgrade, Serbia conducted a study with an objective to evaluate the frequency of polyvascular disease in individuals with carotid artery disease (CAD) and PAD, as well as to ascertain the risk characteristics of patients with polyvascular disease (Vlajinac et al., 2019). The study comprised a total of 1045 consecutive patients who visited their department with either CAD or PAD. They recorded that CAD was recorded in 366 people, accounting for 35% of the total. PAD was documented in 199 participants, representing 19% of the total. Polyvascular disease, which involves many blood vessels, was reported in 480 participants, making up 46% of the total. When comparing CAD with PAD, it was shown that PAD was more frequently associated with polyvascular disease (p = 0.002) and was accompanied by a greater number of other atherosclerotic illnesses (p = 0.02). Patients with polyvascular disease, as opposed to those with atherosclerotic disease in only one territory, exhibited a higher prevalence of hypertension (p ranging from 0.03 to < 0.001), dyslipidemia (p < 0.001), elevated levels of high-sensitivity C-reactive protein (p = 0.005) at 3 mg/l or higher, and a greater likelihood of being current smokers (p < 0.001) or former smokers (p ranging from 0.03 to 0.001). Based on their results they observed a significant occurrence of symptomatic polyvascular disease in patients diagnosed with either CAD or PAD. The risk profile exhibited a higher degree of severity in patients with polyvascular disease compared to those with disease confined to a single vascular area.

2.7 Application of NPs for the treatment of PAD

The therapy of PAD can be categorized as invasive and non-invasive therapies. Non-invasive therapy for the treatment of PAD encompasses various approaches, including preventive management of associated risk factors such as hypertension, smoking, and hypercholesterolemia (Lu & Creager, 2004). This can be achieved through physical rehabilitation and the use of medications such as statins, beta blockers, lipid inhibitors, Ramipril, diuretics, and cell-based therapy (Hamburg & Balady, 2011). Nevertheless, many treatment techniques exhibit limitations. Preventive treatments are solely efficacious for individuals who possess the motivation and dedication to successfully finish the program, and the majority of these programs are not encompassed by health insurance. Although widely employed, the medicinal technique may have adverse effects. When given as either individual medications or in combination to individuals with PAD, there is a risk of experiencing severe bleeding, cardiac consequences, and liver issues (Harris et al., 2016). Alternatively, invasive therapies for PAD such as endovascular intervention, surgical bypass, bare metal stents,

and angioplasty balloon catheters have been documented as therapy options (King III & Meier, 2000; Payne, 2001; Shammas et al., 2012). Although these therapeutic approaches enhance blood circulation to tissues and organs, their effectiveness is constrained by the scarcity of venous vessels, inability to treat diseased vessels, compromised blood flow at the donor site, restricted applicability in severely diseased arteries, significant blood loss, post-operative bleeding complications, and the compression of lipid plaques against the endothelial wall, thereby impeding their removal from the diseased arterial vessels (Adlakha et al., 2010; Chang et al., 2016). Stent implantation has been associated with stent fractures and increasing complications, necessitating repeated insertion and revascularization procedures (Adlakha et al., 2010). Additional constraints encompass vascular injury and removal of endothelial lining due to stents or balloon angioplasty. Moreover, the positioning of arteries like the femoral and popliteal makes them susceptible to difficulties after stent implantation, such as dislocation or stent fractures, due to the stresses of straining, bending, and crushing applied on the muscles (Dys et al., 2013).

Hence, it is vital to prioritize the development of dependable diagnostic instruments and efficacious therapeutic alternatives for PAD in order to enhance patient's quality of life and mitigate the incidence of illness and death. Currently in its nascent phase, nanotechnology has great potential as a viable alternative for developing therapeutic, diagnostic, and theranostic methods to identify and cure PAD (see Figure 2.9). Nanotechnology holds great potential in enhancing global health for individuals with PAD, encompassing its applications in disease prevention, diagnosis, and therapy. This technology shows promising results in reducing both morbidity and death rates. Given the significant prevalence of cardiovascular illnesses and their associated high rates of illness and death in Western countries, the recent introduction of nanomedicine/nanotechnology offers a promising alternative implementing therapeutic interventions to report this health crisis. Researchers and medical professionals are continuously working to utilize diverse types of nanostructures, such as polymer nanoparticles, in order to develop targeted drug delivery methods and minimize the toxicity and side effects of medications.

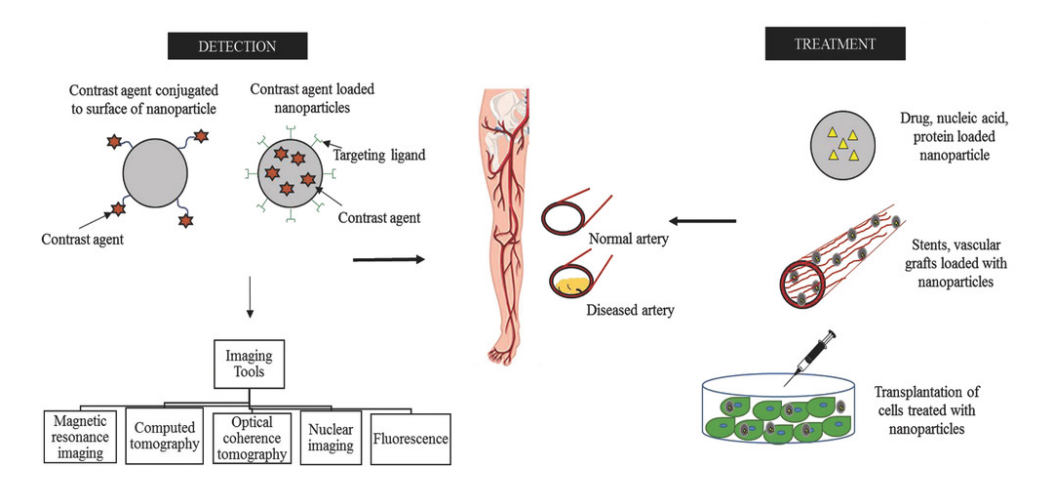


Figure 2.9. Schematic illustration of NPs application towards PAD (Adapted with permission from (Noukeu et al., 2018))

The limitations of bare metal stents (BMSs) and drug-eluting stents (DESs), such as restenosis and stent thrombosis, prompted the creation of new systems designed to be placed in arteries to address these issues. The FDA has approved several

commonly used DES, such as those that release sirolimus, paclitaxel, zotarolimus, and everolimus (Jeremias & Kirtane, 2008). Nevertheless, these metallic components, frequently covered with polymers containing medicinal substances, frequently lead to restricted medication release and availability. These NPs shield the medication from quick elimination, so maximizing its therapeutic effectiveness. The use of Paclitaxel (PTX) loaded magnetic NPs coated stents resulted in a significant increase in the retention of magnetic NPs inside arterial tissue, with a tenfold improvement compared to the use of PTX alone. This led to the inhibition of smooth muscle cell (SMC) proliferation at the site of damage, and consequently, a reduction in restenosis when compared to the use of PTX without magnetic NPs (Chorny et al., 2010). Furthermore, the incorporation of NPs into biomedical substances (BMS) could enable targeted drug delivery by positioning the NPs exactly at the site of harm. Coating stents with PTX loaded PLGA NPs led to an 80% reduction in smooth muscle cell migration into the artery lumen (Johnson et al., 2010). Additionally, it enhanced endothelial cell migration and proliferation compared to stents that released PTX. In addition, the efficacy of therapies is boosted through the combination of NPs with BMS. The utilization of stents containing liposomal alendronate (161 nm) in the arteries of lipid-fed rabbits resulted in a notable rise in the diameter of the inner space, a reduction of almost 90% in the number of monocytes, and a decrease in the infiltration of macrophages and excessive growth of new tissue in these rabbits that received the treatment (Danenberg et al., 2003). In addition, stents coated with PTX-loaded albumin NPs that were placed in rabbit arteries showed a decrease in neointimal thickness, unlike the control group of rabbits who received 0.9% saline. The utilization of pitavastatin-loaded NP-eluting stents resulted in an enhancement of the rate at which endothelial cells healed and a reduction in stenotic occurrences in porcine arteries (Kolodgie et al., 2002; Tsukie et al., 2013). In atherosclerotic rabbits, the presence of neointimal hyperplasia was reduced after the implantation of stents carrying prednisolone NPs (TRM-484) compared to nonstented arteries (controls). Introducing NPs to biomedical substances results in the prevention of blood clot formation and narrowing of blood vessels, while also encouraging the growth of endothelial cells (Joner et al., 2008). In canine femoral arteries, for instance, vascular stents coated with polydopamine immobilized heparine/poly-l-lysisne NPs prevented thrombus formation, inhibited neointimal hyperplasia, and promoted endothelial regeneration when compared to control arteries treated with a dopamine coated titanium stent (T. Liu et al., 2014). Furthermore, there has been investigation into the utilization of stents that are coated with magnetic mesoporous silica NPs (MMSNPs) and carbon nanotubes (CNTs) (Lemos et al., 2013). The stents showed great mechanical flexibility and compatibility with blood, and investigations conducted inside living organisms showed that the blood arteries treated with these stents were quickly covered with a layer of endothelial cells, faster than those treated with DES.

Incorporating NPs with BMS has several benefits, such as minimizing the risk of drug elimination by cells, ensuring drug closeness to the damaged artery, and prolonging drug release to prevent the advancement of thrombosis and restenosis. Nevertheless, there exist certain constraints that hinder the technique from surpassing the aforementioned procedures. Initially, this technique is intrusive and induces significant discomfort in patients. Additionally, the stents are composed of metal materials that have a greater likelihood of anastomosis, perhaps exacerbating the complexity of the condition (Zilla et al., 2007). Moreover, the absence of an endothelium allows blood to come into direct touch with the damaged inner surface of

the artery, and the composition of these stents may encourage the accumulation of proteins and the formation of blood clots, which can further block the sick artery. The application of this technology is restricted to micro blood arteries, so it is not accessible to all patients with PAD. Finally, it is important to note that the NPs may not be uniformly dispersed across the stent, thus leading to incomplete treatment within the artery.

A recent study from Poland examined the antibacterial capabilities and biosafety of lipoic acid (LA) coated LA-AgNPs vs uncoated AgNPs (Hajtuch, Santos-Martinez, et al., 2022). The project will determine whether coating silver nanoparticles with lipoic acid can maintain their antibacterial activity while enhancing their biosafety profile, particularly in the vascular microenvironment. Both AgNPs and LA-AgNPs showed strong antibacterial activity against a wide range of microorganisms, including those usually linked with catheter-related bloodstream infections. The pathogens investigated were E. faecium, S. aureus, K. pneumoniae, A. baumannii, P. aeruginosa, and K. aerogenes. While uncoated AgNPs had slightly higher antimicrobial efficiency against the majority of pathogens, lipoic acid-coated nanoparticles also shown significant antibacterial activity, showing that the coating did not significantly impair their bactericidal characteristics. The study focused primarily on the cytotoxic effects of both types of nanoparticles on HUVECs. The study found that uncoated AgNPs caused considerable cytotoxicity in HUVECs, resulting in lower cell viability, increased formation of reactive oxygen species (ROS), and greater rates of apoptosis. In contrast, the LA-AgNPs lacked these cytotoxic effects. The lipoic acid coating appeared to inhibit ROS production, apoptosis, and mitochondrial membrane depolarization in HUVECs, indicating a dramatically enhanced safety profile for the coated nanoparticles. The study also looked into the effects of AgNPs and LA-AgNPs on human platelets and red blood cells. Uncoated AgNPs induced mitochondrial depolarization in platelets, indicating mitochondrial malfunction, which is critical because platelets rely largely on their mitochondria for energy production and activity. Furthermore, uncoated AgNPs were discovered to cause hemolysis, or the breakdown of red blood cells, resulting in the release of hemoglobin and lactate dehydrogenase (LDH). When nanoparticles enter the bloodstream, they have hemolytic activity, which poses severe hazards. In contrast, LA-AgNPs did not cause mitochondrial dysfunction in platelets or hemolysis in RBCs, indicating that the coated NPs are more biocompatible. The lipoic acid coating's protective effect is due to its antioxidant characteristics, which reduce the oxidative stress caused by uncoated silver nanoparticles. This coating slows the dissolution of silver ions, which is principally responsible for the cytotoxic effects observed with bare AgNPs. The study indicates that, while both uncoated and lipoic acid-coated silver nanoparticles have excellent antibacterial characteristics, the latter is far safer for prospective biological uses, particularly in the vascular environment. The lipoic acid coating dramatically lowers the cytotoxicity, hemolytic activity, and mitochondrial damage associated with silver nanoparticles, while maintaining antibacterial efficiency. These findings indicate that LA-AgNPs may be a safer alternative for use in medical devices such as vascular catheters, where reducing the risk of cytotoxicity and hemolysis is crucial. More in vivo investigations are needed to corroborate these findings and fully explore the potential of LA-AgNPs in therapeutic situations.

AgNPs functionalized with the antiplatelet medication eptifibatide (EPI) are being investigated in another study for possible uses as a covering for medical devices and in the treatment of cardiovascular disease (Hajtuch, Iwicka, et al., 2022). The study aims to assess the safety and effectiveness of these NPs in thrombosis and vascular health by blocking platelet aggregation and regulating endothelial cell function. EPI-AgNPs efficiently suppresses platelet aggregation, a crucial step in the production of blood clots, which is one of the main findings. According to the study, functionalized NPs have a greater ability than free eptifibatide medication to suppress platelet aggregation. The distinct characteristics of the nanoparticles, which enable improved platelet engagement and more efficient eptifibatide transport to the intended target, are responsible for this increased efficacy. According to the study, EPI-AgNPs prevent platelet mitochondria from malfunctioning in addition to inhibiting platelet aggregation. When compared to platelets treated with the free medication, those treated with EPI-AgNPs exhibited less damage to the mitochondria and better mitochondrial respiration. This defense against mitochondrial damage is important because impaired mitochondrial function in platelets can worsen thrombotic situations by producing more ROS. By controlling blood clotting and vascular tone, endothelial cells—which line the inside of blood vessels—play a critical role in preserving vascular health. The study discovered that endothelial cell activity was efficiently regulated by EPI-AgNPs. In particular, the NPs increased the synthesis of anti-thrombotic factors like tissue plasminogen activator (tPA) and cyclic guanosine monophosphate (cGMP) and blocked the release of pro-thrombotic factors like von Willebrand factor (vWF). EPI-AgNPs may be able to assist in balancing the production and breakdown of clots, lowering the risk of thrombosis while maintaining regular vascular function, according to this dual action. The possible toxicity of nanoparticles is a major worry when using them in medicinal applications. The cytotoxicity of EPI-AgNPs on human platelets, endothelial cells, and red blood cells (RBCs) was evaluated in the study to address this. The hopeful results demonstrated that at concentrations effective for antiplatelet activity, EPI-AgNPs did not significantly diminish cell viability or promote hemolysis, or the destruction of red blood cells. This implies that the use of these nanoparticles in the human circulatory system is safe and biocompatible. The impact of EPI-AgNPs on the larger coagulation system, which includes several coagulation factors and pathways, was also investigated in this study. Crucially, prothrombin time (PT), activated partial thromboplastin time (APTT), and fibrinogen levels were not substantially affected by the nanoparticles. This suggests that EPI-AgNPs selectively prevents platelet aggregation without altering the coagulation balance in any way, which is important to prevent unanticipated bleeding consequences. According to the study's findings, EPI-AgNPs offers a novel and promising strategy for controlling cardiovascular illnesses and thrombosis prevention. These NPs provide a possible dual-action therapeutic platform by maintaining platelet mitochondrial function, efficiently suppressing platelet aggregation, and modifying endothelial cell activity without considerable damage. Their clinical utility may also be increased by their capacity to be coated on medical equipment, such as vascular catheters.

A recent publication examined the possible antioxidant and antihypertensive properties of AgNPs loaded with caffeic acid (CA) using a rat model of hypertension brought on by nitric oxide (NO) deprivation (Kalaiarasi et al., 2022). The need to develop more potent treatments for hypertension, which continues to be a major risk factor for cardiovascular illnesses worldwide, drove this investigation. The effectiveness and safety profile of AgNPs-CA in the treatment of oxidative stress and hypertension are presented in the paper, with special attention to their capacity to bring about equilibrium in settings where NO is insufficient. The results of the study showed

that AgNPs-CA successfully lowered the blood pressure in hypertensive rats that were induced by the nitric oxide synthase inhibitor L-NAME (N-Nitro-L-arginine methyl ester). When compared to hypertensive rats who were not treated, there was a notable drop in blood pressure, suggesting that AgNPs-CA have potent antihypertensive effects. When L-NAME was given, oxidative stress indicators such lipid hydroperoxides (LOOH) and thiobarbituric acid reactive substances (TBARS) increased in the heart, liver, kidney, and aorta, among other organs. Treatment with AgNPs-CA dramatically decreased these indicators, indicating their strong antioxidant action. This shows that AgNPs-CA can mitigate the oxidative stress brought on by a lack of NO, which is a vital component in the development of hypertension. In L-NAME-treated hypertensive rats, the study found a significant reduction in the activity of enzyme antioxidants such as glutathione peroxidase (GPx), catalase (CAT), and superoxide dismutase (SOD). Restoring these antioxidants' activity to nearly normal levels with CA-AgNPs therapy is essential for lowering oxidative damage in hypertensive circumstances. Likewise, the administration of AgNPs-CA restored the levels of non-enzymatic antioxidants, including vitamins C and E, which had been decreased in hypertensive rats. The synergistic effects of caffeic acid and silver nanoparticles are responsible for AgNPs-CA antihypertensive properties. One naturally occurring phenolic acid that has been shown to have both vasodilatory and antioxidant effects is caffeine. It lowers blood pressure by scavenging free radicals and increasing the generation of NO. Conversely, caffeic acid may be more easily delivered and stabilized by silver nanoparticles, increasing its bioavailability and potency. The fact that the study shows that AgNPs-CA had no appreciable negative effects on the animals supports the possibility that they could be a safe therapeutic alternative. This is especially crucial because traditional antihypertensive medications frequently have drawbacks such low absorption, need for frequent dosage adjustments, and adverse effects.

2.8 Drug Coated Balloons (DCBs) for the treatment of PAD

In 1977, Andreas Grüntzig pioneered the use of balloon angioplasty (BA) as a therapy for coronary artery disease. This breakthrough marked a major advancement in the field of cardiology and laid the foundation for modern interventional cardiology (Axel et al., 1997). DCBs have developed as a potential replacement to DESs in situations where long-term insertion of stents is not optimal. The idea of delivering anti-proliferative drugs by balloon angioplasty has been in existence for a considerable period. The first documented evidence dates back to 1986, when Goldman et al. showed the successful administration of horseradish peroxidase (PRXC1A) to human and canine arteries using a polyurethane catheter with numerous lumens (Goldman et al., 1987).

To achieve long-term prevention of restenosis, it is crucial to administer and retain the necessary drugs. The limus family of pharmaceuticals, liberated by last-generation DESs in a controlled approach from an implanted stent, has been found to be the most efficient class of anti-proliferative drugs (Dangas et al., 2013). In contrast, DCB releases drugs in a different way. The DCBs directly apply the drug onto the surface of the balloon (Figure 2.10A). Upon insertion and inflation of the balloon within the designated artery, the drug coating comes into contact with the arterial wall. Subsequently, the medication is released from its enclosure and diffuses into the surrounding tissue. DCBs eliminate drugs from the body by inducing "transient matrix

disruption." When the balloon is inflated and subsequently deflated, it disrupts the integrity of the coating. This facilitates the penetration of the medication into the vascular tissue. Conversely, drug-eluting stents are inserted into an artery to offer synthetic support and gradually dispense the medication (Figure 2.10B). The majority of stents consist of a metallic framework encased in a polymer coating that contains the medication. Drug release from DES primarily occurs through two mechanisms: diffusion-controlled release and erosion-controlled release.

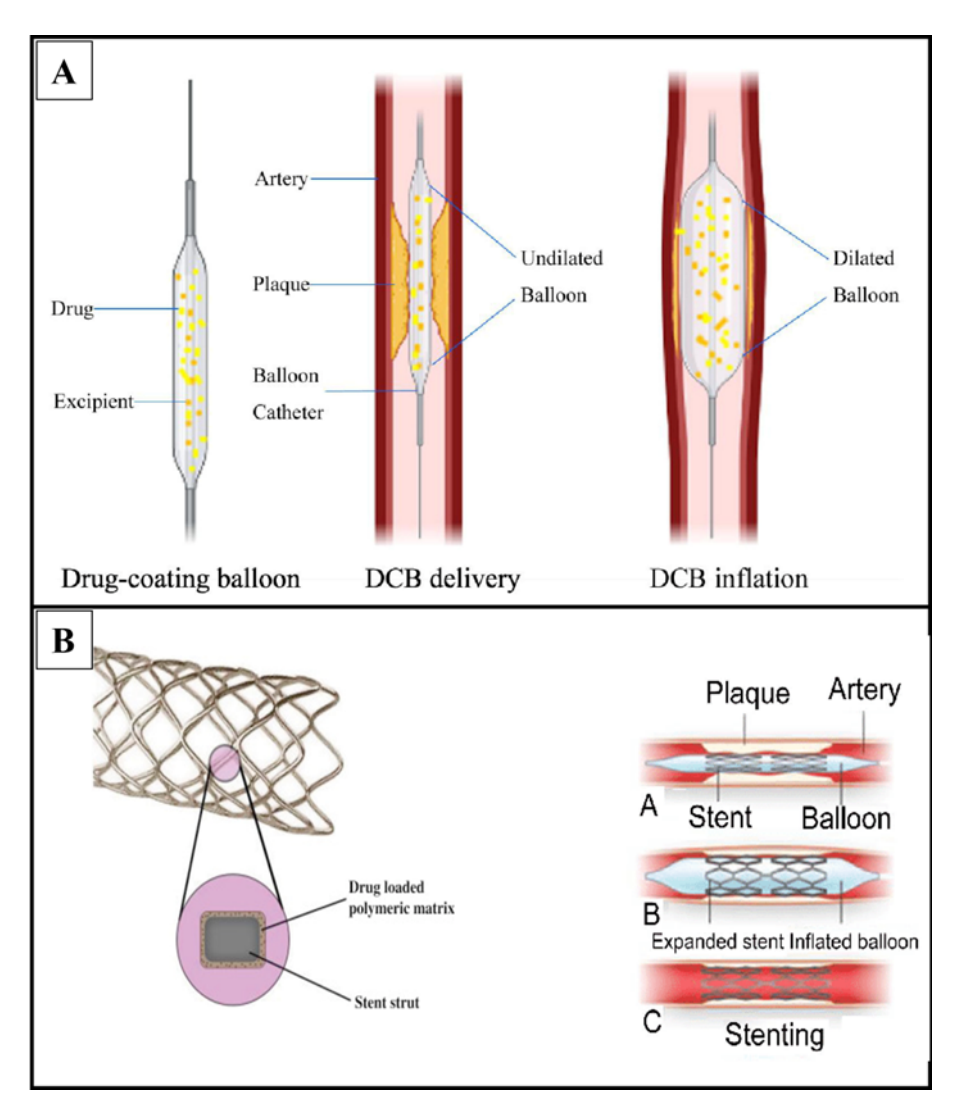


Figure 2.10. Illustration of drug release from (A) DCBs and (B) DESs (Adapted and modified with permission from (Cao et al., 2022; Deb et al., 2019; Qamar et al., 2023; Thangavel et al., 2014))

The efficiency of the treatment relies on the prompt administration of a specific dosage of an anti-proliferative medication, which is expected to gradually integrate into the vessel wall. In 1990, Edelman et al. investigated heparin as one of the initial drugs for local administration. The researchers showed that the drug does not accumulate within the vessel wall over time due to its solubility characteristics (Edelman et al., 1990). Professor Bruno Scheller published the first agent with positive outcomes in 2001. In a pig model of restenosis, he showed that the solubility of paclitaxel significantly increased when combined with contrast agents. This enabled the delivery of a concentrated dose directly into the coronary artery, resulting in a significant

reduction in neointimal proliferation (Scheller et al., 2002). A preliminary version of the DCB was developed by combining paclitaxel with contrast medium and administering it onto the surface of a balloon (Scheller et al., 2004). The initial clinical results sparked enthusiasm in this field, leading to the development of more drug-coated balloons (DCBs). Programs were created with the aim of reproducing this technological method by utilizing hydrophilic carriers to transport paclitaxel over the vessel wall following balloon dilatation. Paclitaxel is included in all commercially available drugcoated balloons (DCBs) because of its ability to dissolve fats and its resistance to chemical changes. Paclitaxel has been demonstrated to impede cell migration and proliferation by permanently disrupting intracellular microtubules, leading to the inhibition of cell duplication during metaphase and anaphase of mitosis (Rowinsky & Donehower, 1995). While all DCB technologies utilize the same fundamental drug, they exhibit variations due to differences in excipients, production process, dosage, and balloon surface technology. However, as of current scientific advancements, the scientists are moving towards nanotech approach. In this approach researchers are now focusing on coating DCBs with NPs to open a new horizon of technological advancement. Hence, there is a need to explore more opportunities to coat DCBs with NPs and NFs to enhance drug retention and stable release.

2.9 Electrospinning technique for coating material

In 1600, William Gilbert observed the formation of a conical water droplet when an electric field was applied, leading to the concept of electrospinning (Gilbert, 1956). Over a century later, Stephen Gray observed the electrohydrodynamic atomization of a water droplet, resulting in the generation of an exceedingly thin stream (Gray, 1731). Abbé Nollet conducted the first known electrospraying experiment in 1747, demonstrating that water could be sprayed as an aerosol when it flowed through a vessel that was electrostatically charged and placed near to the ground (Nollet, 1748). After that, Lord Rayleigh looked into the behaviors of charged droplets in great detail. In 1882, he made a theoretical calculation of the maximum number of charges that a liquid droplet could have before it released liquid jets from the surface (Rayleigh, 1882). The electro spraying method and electrospinning technique are similar in that they both depend on the employment of a high voltage to release liquid jets (Bailey, 1984). The primary differences between electrospinning and electrospraying are related to the viscoelasticity and viscosity of the liquid, which influence the behavior of the jet. Unlike electro spraying, which produces particles by breaking the jet into droplets, electrospinning maintains the jet's continuous flow while creating threads.

Electrospinning is an electrohydrodynamic process in which a jet is generated by electrifying a liquid particle; the jet subsequently undergoes stretching and elongation to fashion fibers (Xue et al., 2019). The fundamental electrospinning arrangement is rather straightforward, as shown in Figure 2.11, making it available to practically any laboratory (Long et al., 2019). The principal components consist of a conductive collector, a syringe pump, a high-voltage power source, and a spinneret, which is a blunt-tipped hypodermic needle. Both alternating current (AC) and direct current (DC) are viable options for power sources. During electrospinning, the liquid protrudes from the spinneret due to surface tension, forming a pendant particle (Duft et al., 2003). A charged projectile is discharged from the electrified droplet as a result of the electrostatic repulsion between the same-sign surface charges. Prior to undergoing violent lashing motions, the jet initially expands in a straight line due to bending instabilities (Reneker & Yarin, 2008). A solid fiber or fibers are deposited on the

grounded collector as a result of the jet's rapid solidification as it is stretched into finer dimensions. The electrospinning process can be broadly broken down into four steps: (1) charging the liquid droplet and creating a cone-shaped or Taylor cone-shaped jet; (2) extending the charged jet in a straight line; (3) thinning the jet in the presence of an electric field and creating electrical bending instability, also called whipping instability; and (4) solidifying and collecting the jet as solid fibers on a grounded collector (Liao et al., 2018).

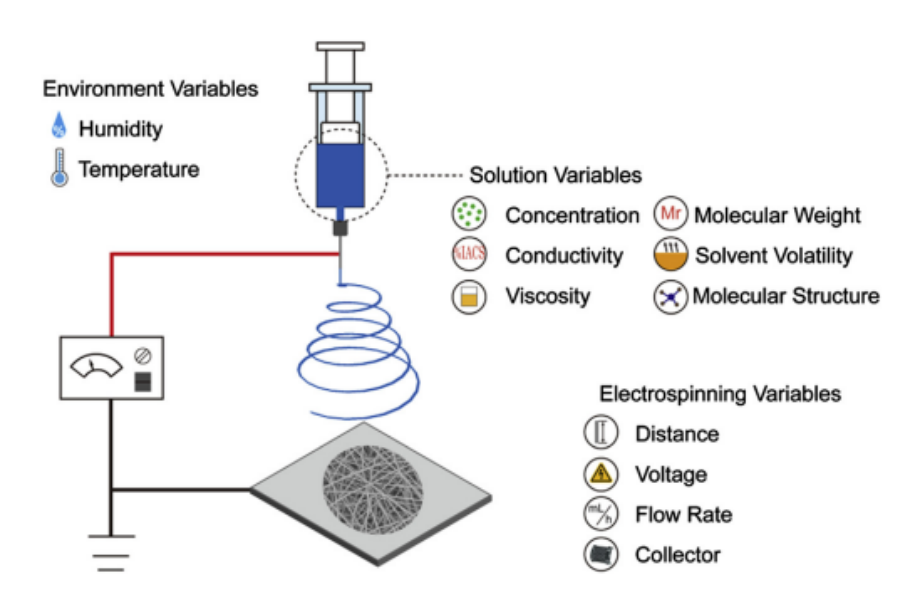


Figure 2.11. Illustration of electrospinning equipment (Adapted with permission from (Long et al., 2019))

Electrospun nanofibers (NFs) are an efficient material that may be applied directly to an implant to enhance its biocompatibility and provide extra topographic characteristics or biological signals. For instance, Biotronik produced the commercial coronary balloon-expandable stent system known as PK Papyrus. It was created by covering a single stent's surface with elastic polyurethane NFs, which offered a high degree of bending flexibility. Active proteins may potentially be included into the nanofibers. In one example, vascular endothelial growth factor and heparin-loaded PLCL NFs were placed on an inflatable stent to treat aneurysms (J. Wang et al., 2015). After being implanted into a rabbit model, the encapsulated biological effectors were able to suppress thrombus and promote fast endothelialization, despite the high elasticity of PLCL NFs improving the stent's expansion range. In order to maintain the parent artery's long-term patency, the aneurysm was completely destroyed by the NFs-covered stent, which isolated the aneurysm dome from the blood supply.

Electrospinning is a straightforward and adaptable technology that may generate NFs suitable for a range of biological applications. Through the optimization of electrospinning settings and potential integration with other techniques, it is possible to systematically produce controlled and replicable physical, biological, and chemical stimuli on electrospun NFs. Therefore, before creating an NFs-based scaffold, it is imperative to thoroughly evaluate the essential cues, characteristics of the scaffold, and particular demands of various applications. The primary obstacle in the present phase of advancement is in the intricacy of producing diverse structured 3D scaffolds using electrospinning techniques, specifically those composed of NFs. Nevertheless, there has

been few research undertaken on the design and production of NFs-based, 3D scaffolds, and even fewer on incorporating topographic, physicochemical, and biological cues within the same scaffold. As such, there is an urgent need to establish a simple and adaptable technique for modifying the 3D architecture of a scaffold for the treatment of PAD and atherosclerosis.

Chapter 3

Material and Method

3.1 Selection of plant

The plants were selected based on their use in Serbian culture and reported medicinal properties. It was observed that herbal tea is commonly used among people. Therefore, two of the locally most used herbal tea Bosiljak (*Ocimum basilicum L.*) and Borovnica (*Vaccinium myrtillus*) were selected for the preparation and synthesis of AgNPs.

3.2 Extraction and preparation of O. basilicum and V. myrtillus tea extract

The assortment of dried shredded parts (leaves and stem) of *O. basilicum* (Boslijak) and *V. myrtillus* (Borovnica) was acquired at a health store in the central business district of Kragujevac. Following their acquisition, samples of tea were taken to the Bioengineering Laboratory at the Faculty of Engineering in Kragujevac, Serbia. It took around 45 minutes to bring 10 g of *O. basilicum* and 15 g of *V. myrtillus* tea in 150 ml and 100 ml of distilled water to a boil while constantly stirring the liquid at a temperature between 90 and 100 °C, respectively. The temperature of the liquids was allowed to gradually decrease until it reached room temperature. To achieve a higher level of purity, the extract was filtered through what-man paper. After that, we kept the extract at a temperature of 4 °C until we were ready to utilize it.

3.3 Synthesis of AgNPs using O. basilicum and V. myrtillus tea extract

To make AgNO₃ (silver nitrate) solution, AgNO₃ was bought from Fisher Scientific, UK. About 16.99 g/mol of AgNO₃ was mixed with 100 ml of purified water to make a 1 M solution of AgNO₃. In order to make AgNPs, 30 ml of *O. basilicum* tea extract was mixed with 70 ml of a 1 M solution of AgNO₃. While on the contrary, for *V. myrtillus*, 50:50 ratio was used. After the solution was mixed, it was stirred all the time until it turned dark brown to black (see Figure 3.1). The AgNPs that were made from *O. basilicum* and *V. myrtillus* were termed as OBTe-AgNPs and VMTe-AgNPs.

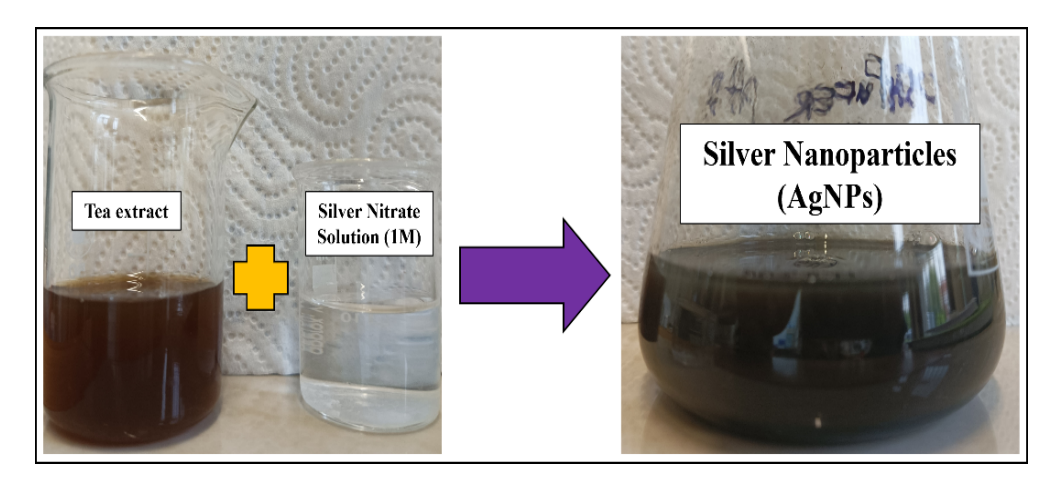


Figure 3.1. Illustration of AgNPs synthesis process

3.4 Preparation of polymer solution for electrospinning

Poly(ϵ -caprolacton) (PCL) with an average Mn \sim 80,000, 440744-500G) and poly(ethyleneglycol) (PEG) with an average Mn \sim 4,000, 81240-1 kg, were procured from Sigma-Aldrich, United States of America. The compounds Chloroform (CHCl₃) and N,N-Dimethylformamide (DMF, 99.5%) were obtained from Macron Fine Chemicals (4444-25) and Fisher Scientific (D/3841/17), respectively. All compounds in this study were utilized without undergoing additional purification.

The technique was executed in accordance with the previously outlined procedures (Virijević et al., 2023). The solutions under investigation were made by dissolving the PCL and PEG in solvents CHCl₃ and DMF, with a volume ratio of 50:50. After that according to weight of polymer, the various concentrations (1%, 2% and 3%) of OBTe-AgNPs were added into prepared mixture separately. The solutions were stirred at a speed of 800 rpm for a duration of 24 h at ambient temperature. After a duration of 24 h, the mix solutions were fully dissolved and prepared for the process of electrospinning. The procedure was executed with a vertical position configuration. After preparing the solutions, they were transferred into 10 ml syringes using a 21G needle and an applied voltage of 15 kV. The flow rate that was applied was 1 ml/h. The duration of each run of the process was 30 s. A collector made of aluminum plate was utilized.

3.5 Electrospinning of OBTe AgNPs incorporated polymer

Our own electrospinning apparatus at BioIRC Doo was utilized in this investigation. The components of this setup are a syringe pump, a collector plate, and a high voltage source. The needle is an NIPRO brand from Japan and is size 21G. We built the program in-house, and it controls the complete process. After the relative humidity and temperature of the room were measured, the polymer solution along with the various concentrations (1%, 2% and 3%) of OBTe-AgNPs was transferred to a syringe and a needle was connected. A suitable voltage was used to start the electric field. The solution falls to the top of the extended needle, forming the Taylor cone, as the electric field intensity increases. It is already well-known that electrostatic forces caused the solvents from the polymer solution to evaporate, and that these forces also caused the production of nanofibers. Following their collection on the aluminum plate collector (see Figure 3.2B), the fibrous scaffolds were transferred to the Petri dishes. The inverted microscope (Delta Optical Genetic PRO, Poland) was used at 40x magnification to examine nanofiber samples (see Figure 3.2A).

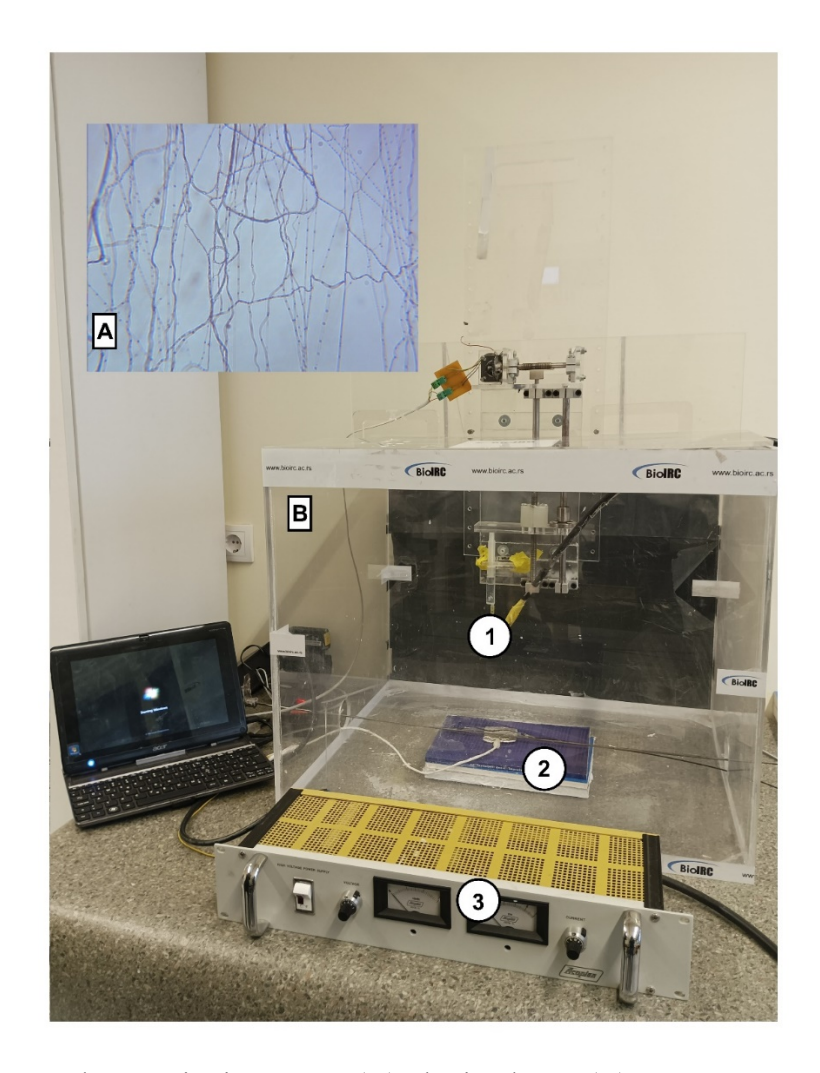


Figure 3.2. Electrospinning set up (A) obtained NFs (B) components of electrospinning (1) syringe pump (2) collector plate (3) high voltage source.

3.6 Characterization of AgNPs, and tea extracts

The characterization of AgNPs was carried out using various instruments. Lambda 365 Ultraviolet Visible (UV-Vis) spectroscopy (PerkinElmer Inc., USA) was utilized to initially characterize OBTe-AgNPs and VMTe-AgNPs at ambient temperature (25 °C) between 200 and 900 nm. In order to examine the dimensions and morphology of OBTe-AgNPs, and VMTe-AgNPs, we employed the following instruments: a TESCAN MIRA3 field emission scanning electron microscopy (FESEM) manufactured by The Tescan Group in the Czech Republic; a Malvern Instruments Zetasizer Nano ZS ZEN 3600 (Malvern, UK) for dynamic light scattering (DLS); and an FEI Talos F200X microscope (Thermo Fisher Scientific, USA) equipped with an X-FEG source and energy dispersive X-ray spectroscopy (EDS) signal detection at maximum acceleration. The functional groups accountable for encapsulating Ag to generate AgNPs from the tea extract of *O. basilicum* and *V. myrtillus* were examined by means of Nicolet 6700 Fourier transform infrared (FTIR) spectroscopy (Thermo Fisher Scientific, USA) at 4 cm⁻¹ transmittances. The spectral range was 500 to 4000 cm⁻¹.

3.7 Characterization of OBTe-AgNPs incorporated NFs

It is critical to investigate the structural changes in polymers before and after integration of biogenic OBTe-AgNPs. The FTIR spectra of PCL-PEG NFs, OBTe-AgNPs, and three variants of OBTe-AgNPs-NFs were acquired using Spectrum TWO FTIR (L1600401) spectroscopy (PerkinElmer, UK) across a range of 400-4000 cm-1 at a resolution of 4 cm-1. The SEM analysis of all OBTe-AgNPs-NFs was performed utilizing a TESCAN MIRA3 field emission scanning electron microscopy (FESEM) manufactured by The Tescan Group in the Czech Republic. The dried NFs roughness was analyzed using the NT-MDT atomic force microscope's NTEGRA receiver. Intermittent contact was the mode of operation that was applied. On the other hand, the freeware Gwyddion v2.66 (Nečas & Klapetek, 2012) and WSxM 4.0 software platform's beta 9.3 version was used to analyze the results (Horcas et al., 2007).

3.8 Anticancer and antiatherosclerosis properties of green synthesized AgNPs

3.8.1 Cell culture

In this investigation, human cervical immortalized (HeLa) cancer cells were utilized. From CLS Cell Lines Service GmbH in Germany, cell lines were acquired. While on the other hand, the MDA-MB-231 breast cancer epithelial cells were obtained from Collection of Authenticated Cell Cultures (ECACC). While on the contrary, the human umbilical vein endothelial cells (HUVEC) were purchased from Lonza, Switzerland. Supplements added to the DMEM cell growth medium (Thermo Fisher Scientific, United States of America) contained the following: 1% Pen-Step, 1% L-glutamine, 10% fetal bovine serum (FBS), 1% sodium pyruvate, 0.5% mercaptoethanol, and 0.5% glucose; these were utilized to cultivate the HeLa cell lines. Sub-cultivation of cells occurred when they had attained 85% confluence.

3.8.2 Cell viability analysis in cell lines

The first step was the seeding of cells in a 96-well plate, with 10,000 cells being placed in each well along with 100 µl of medium. To guarantee that the cells adhered to the substrate, the plate was then placed in a CO₂ incubator at 37 °C for a period of twenty-four hours. Subsequently, the medium was extracted from every well, and 100 ml of complete medium was introduced into the control cells. Meanwhile, the OBTe-AgNPs, which were dissolved in full medium and included concentrations of 0.5, 1, 5, 10, 20, and 40 µg/ml, were introduced into the remaining wells in six separate duplicates. While for VMTe-AgNPs the dose concentration range was 10, 20, 40, and 60 μg/ml. While on the other hand, small pieces of OBTe incorporated NFs having 1%, 2%, 3% concentration of AgNPs/wt were added to cells. Once more, the plate was placed in the CO₂ incubator and heated to 37 °C for a period of twenty-four hours. After the incubation period, the medium was removed from each well and replaced with a new 100 ml of complete medium. Additionally, 25 ml of MTT, with a concentration of 5 mg/ml, was added to the mixture. After that, the plate was placed in the CO₂ incubator and allowed to incubate for three hours at 37 °C. Following the incubation period, the medium containing MTT was extracted from every well, and then 150 ml of DMSO was introduced into every well. It took twenty minutes for the plate to be incubated in a dark environment. After everything was said and done, the absorbance at 492 nm was measured in order to evaluate the outcomes of the experiment.

3.9 Reactive oxygen species production in AgNPs exposed cells

3.9.1 Glutathione (GSH) concentration analysis in cell lines

In the beginning, 30,000 cells were sown in each well of a plate containing 100 ul of media. The cells were then allowed to stick to the substrate by incubating the plate for 24 hours at 37 °C in a CO₂ incubator. Subsequently, the media was drained from each well, and 100 µl of the whole medium was added to the control cells. Meanwhile, 100 μl of OBTe-AgNPs was added to the remaining wells, each in six replicates, at the appropriate concentration (1, 5, 10, 20, 40 µg/ml). While on the other hand, for VMTe-AgNPs the dose concentration range was 20, 40, and 60 μg/ml. The plate was then kept in the CO₂ incubator at 37 °C for a set 24 hours of incubation. Following incubation, the plates were centrifuged at 1000 g for 10 minutes (RCF). Then, 100 µl of cold 2.5% sulfosalicylic acid (SSA) was added to each well after the medium was removed from each well. After that, the plates were incubated for fifteen minutes in a refrigerator. The plates were then centrifuged once more for 15 minutes at 1000 g (RCF). Next, 50 µl of supernatant was poured onto fresh plates from each well. 100 µl of 5,5' -dithio-bis (2nitrobenzoic acid) (DTNB), which had been made right before, was put into each well. The plates were incubated at room temperature for five minutes. Ultimately, the experiment's results were analyzed by measuring the absorbance at 405 nm.

3.9.2 Nitrite (NO₂⁻) concentration analysis in cell lines

In the beginning, 30,000 cells were sown in each well of a plate containing 100 μ l of media. The cells were then allowed to stick to the substrate by incubating the plate for 24 hours at 37 °C in a CO₂ incubator. Subsequently, the media was drained from each well, and 100 μ l of the whole medium was added to the control cells. Meanwhile, 100 μ l of OBTe-AgNPs was added to the remaining wells, each in six replicates, at the appropriate concentration (1, 5, 10, 20, 40 μ g/ml). While on the other hand, for VMTe-AgNPs the dose concentration range was 20, 40, and 60 μ g/ml. The plate was then incubated for a further twenty-four hours at 37°C in the CO₂ incubator. Following the incubation period, each well's 50 μ l of supernatant was moved to a fresh plate. After that, each well received 50 μ l of sulfanilamide reagent, and the plate was incubated for ten minutes in a dark environment. Subsequently, 50 μ l of 0.1% N-(1-Naphthyl) ethylenediamine dihydrochloride (NEED) was introduced into every well, and the plate was once more incubated for ten minutes in a dark environment. Ultimately, the experiment's results were analyzed by measuring the absorbance at 492 nm.

3.9.3 Super oxide anion radical (O2°-) concentration analysis in cell lines

A plate was inoculated with 30,000 cells per well, with 100 μ l of medium. Following this, the plate was incubated at 37 °C in a CO₂ incubator for 24 hours, which permitted the cells to adhere to the substrate. Subsequently, the medium was withdrawn from each well and 100 μ l of complete medium was introduced into the control cells. For the remaining wells, 100 μ l of OBTe-AgNPs was added in six replicates, with concentrations of 1, 5, 10, 20, and 40 μ g/ml. While on the other hand, for VMTe-AgNPs the dose concentration range was 20, 40, and 60 μ g/ml. The plate underwent an additional incubation period of 24 hours at a predetermined temperature of 37 °C in the CO₂ incubator. After the incubation period concluded, the medium was meticulously extracted from each well and a new 100 μ l of complete medium was introduced into each well, accompanied by 10 μ l of Nitro Blue Tetrazolium Chloride (NBT) at a

concentration of 2.5 mg/ml. Once more, the plate was incubated in the CO_2 incubator for three hours at 37 °C. After that, the medium containing NBT was withdrawn by aspiration, and the cells underwent a comprehensive rinsing procedure utilizing heated PBS solution. After being rinsed with 100 μ l of methanol, the cells were dried for 30 minutes in a laminar chamber. In order to streamline the subsequent analysis, each well was treated with 100 μ l of potassium hydroxide (KOH) and incubated at room temperature for 15 minutes. Following this, 100 μ l of dimethyl sulfoxide (DMSO) was added to each well, followed by 15 minutes of incubation in a dark environment. At 630 nm, the absorbance of the samples was then measured in order to assess the results of the experiment.

3.10 Gene expression analysis of apoptotic genes in HeLa cells

In order to determine whether exposure to OBTe-AgNPs induces cell death via the apoptotic pathway, qRT-PCR was used to examine the genes encoding apoptosis, including $Cas\ 3$, Bax, $Cas\ 8$, Bcl-2, $Cas\ 9$, and a housekeeping gene β -actin.

3.10.1 RNA isolation from HeLa cells

A stringent sequence of procedures was rigorously adhered to in order to extract RNA from cells. To begin, a volume of 5 ml of the medium was meticulously transferred from a vial to a test tube. Following this, 1 ml of trypsin-EDTA solution was utilized to separate the cells from the plate. The elevated cells were subsequently transferred to an additional test tube containing the medium. Subsequently, a 10-minute centrifugation process was conducted at 1200 revolutions per minute (rpm) at ambient temperature. To preserve the integrity of the cells, they were immediately deposited on ice. Once the supernatant was removed, 1 ml of Trizol® was introduced into the cell precipitate, followed by a vigorous homogenization process that continued until the mixture achieved clarity. Following the transfer of the homogenized solution to an Eppendorf tube, it was centrifuged at 4 °C for 5 minutes at 12000 rpm. The supernatant that was obtained was transferred with caution to fresh containers. After adding 200 µl of chloroform, the mixture was vigorously agitated for a duration of 15 seconds. After allowing the mixture to rest undisturbed at ambient temperature for two to three minutes, it was centrifuged at 12,000 rpm for fifteen minutes at 4°C. While the water phase on top was transferred to fresh Eppendorf tubes so as not to come into contact with the tube walls. The genetic material was precipitated using 500 µl of isopropanol. Following this, the tube was gently inverted several times and left undisturbed at room temperature for a duration of 10 minutes. After the specified incubation period, the samples underwent centrifugation at 4 °C for 10 minutes at 12000 rpm. The genetic material precipitate was rinsed with 1 ml of ice-cold 70% ethanol after the supernatant was discarded. Following a subsequent 5 minutes of centrifugation at 4 °C at 7600 rpm, the ethanol was meticulously extracted, and the specimens were subsequently desiccated within a laminar flow chamber. Subsequently, 30 µl of PCR water was added to each sample, followed by incubation at 55 °C for a duration of 5 minutes. Before conducting concentration measurements, the samples underwent homogenization via pipette. UV-vis mRNA concentration measurement is performed using Drop Duo plates; plates are cleaned prior to use by opening them and rinsing them with ethanol and a towel. Subsequently, 2 µl of the mRNA sample diluted in PCR water to the circleshaped plates. Following the ascertainment of the mRNA concentration, the samples were stored at -80 °C.

3.10.2 Reverse transcription polymerase chain reaction (RT-PCR)

The RT-PCR analysis was conducted in accordance with the manufacturer's instructions using a commercially available High-Capacity cDNA Reverse Transcription Kit (Applied Biosystems, USA). The reaction was carried out in four stages with a total volume of 20 μl: (I) the initial step (25 °C for 10 minutes); (II) the reverse transcription step (37 °C for 120 minutes); (III) enzyme inactivation (85 °C for 5 minutes); and (IV) 4 °C for ∞. The cDNA obtained from reverse transcription, which was executed on a MultiGeneTM OptiMax thermal cycler (Labnet International Inc., USA) for subsequent relative gene expression analysis.

3.10.3 Quantitative reverse transcription polymerase chain reaction (qRT-PCR)

The relative expression of genes was evaluated in a 20 μ l total reaction volume using a commercially available SG/ROX qPCR Master Mix (2x) (EURx, Gdańsk, Poland). The PCR reaction was conducted utilizing the Drawell Gentier96 Real-Time PCR system (China). The conditions for thermocycling were as follows: (I) 15 minutes at 95 °C; (II) 40 cycles of 15 seconds at 95 °C, followed by 30 seconds of annealing at 55 °C and 30 seconds of extension at 72 °C; (III) One minute of cooling at 4 °C. Utilizing Gentier96 Real-Time PCR software, the data was analyzed. The outcomes were derived utilizing the $2^{-\Delta\Delta Ct}$ method. The differences between the Δ Ct1 values of the genes under investigation and the Δ Ct1 values of the housekeeping gene (β -actin) are denoted by the $\Delta\Delta$ Ct values ($2^{-\Delta\Delta Ct}$ = Δ Ct1- Δ Ct2). The candidate gene primers are detailed in Table 3.1.

TO 11 24 D 1	1	•	11	•	/F3 .	2 1
Table 3.1. Forward	and reverse	nrimer us	sed in the 6	experiment (\	റ്റ്
I MAIC CITY I OI WAI G	wild it it is	PIIIII OI	,	orth or illine ile		\sim ,

Analyzed genes	Forward primer sequence	Reverse primer sequence
Bcl-2	GATAACGGAGGCTGGGATGC	GACTTCACTTGTGGCCCAGAT
BAX	GCTTCAGGGTTTCATCCAGGA	CAATCATCCTCTGCAGCTCCA
Cas 3	GCACCTGGTTATTATTCTTGGC	GGACTCAAATTCTGTTGCCACC
Cas 8	TTCAGCAAAGGGGAGGAGTTG	GTGTGTTCCATTCCTGTCCCT
Cas 9	ACTTTCCCAGGTTTTGTTTCC	CAAGATAAGGCAGGGTGAGGG
β-actin	CTCACCCTGAAGTACCCCATC	AGGTCTCAAACATGATCTGGG

3.11 Apoptosis and necrosis analysis using Annexin FITC Assay in HeLa cells

In accordance with prior research, apoptosis, cell viability, and necrosis were evaluated utilizing the BD FACSVerseTM flow cytometer (BD Biosciences, USA). The initial version of BD FACSuite program examined at least 10,000 events. The Annexin V FITC/Propidium iodide (PI) reagent was used following the instructions provided by the manufacturer. Annexin V is categorized as an intracellular protein family constituent because it has a strong attraction to phosphatidylserine (PS). PS is normally found only on the intracellular side of the plasma membrane in living cells. However, in the specific situation of early apoptosis caused by the loss of membrane asymmetry,

PS moves to the outer side of the plasma membrane. In contrast, necrotic and late-stage apoptotic cells will display a favorable staining reaction to PI due to the dye's capacity to penetrate the nucleus and attach to DNA.

3.12 Silver ion release study

Atomic absorption spectroscopy 3300 from Perkin Elmer, United States was used to study the release behavior of Ag ions from OBTe-AgNPs loaded PEG-PCL composite NFs mats. For the release process, 25 ml of deionized water was added to a separate 100 ml container. This container already contained a small amount (47.1, 49.2, and 42.9 mg) of electrospun NFs with concentrations of 1%, 2%, and 3% AgNPs/wt, respectively. A mixture was stirred using a magnetic stirrer set at a speed of 450 RPM. Subsequently, a 3ml aliquot of medium was collected at a certain time point and subsequently replenished with fresh media to ensure consistent volume.

3.13 Statistical analysis

The results were shown as the mean (\pm standard error) of three separate experiments. All data were subjected to the student t-test and ANOVA at the standard distribution curve in regard to statistical values. A p-value below 0.05 was universally regarded as indicative of statistical significance.

Chapter 4

Results

4.1 Characterization and toxicological studies of OBTe-AgNPs

4.1.1 Characterization of OBTe-AgNPs and O. basilicum tea extract

Several methods, such as UV-Vis Spectroscopy, FTIR, and FESEM, were used to find out how OBTe-AgNPs were formed. We confirmed the formation of AgNPs by using UV-Vis spectroscopy to measure absorption in the 200-900 nm range. Figure 4.1A shows that AgNPs had a clear peak at 344 nm, which was in the range of 315–390 nm. FTIR was used to look for any possible proteins that might be involved in reducing, bio-capping, or effectively stabilizing Ag⁺ ions to Ag⁰ in the O. basilicum tea extract. FTIR showed several peaks between 500 and 4000 cm⁻¹, with 3310 cm⁻¹, 2105 cm⁻¹, and 1636 cm⁻¹ being the most noticeable (see Figure 4.1B). A 100-kx FESEM study of the size and shape of OBTe-AgNPs showed that they have an average diameter of 55 nm and an oval shape (see Figure 4.1C). When the DLS data was analyzed, it showed that the solution mostly had OBTe-AgNPs that were 173 nm in size because they had clumped together (zeta potential = -30.8, polydispersity index (PDI) = 0.474) (see Figure 4.1D). On the other hand, EDS analysis showed that there was Ag in the solution (see Figure 4.2A), and TEM analysis showed that the OBTe-AgNPs were spread out more clearly in terms of size. The TEM test showed that OBTe-AgNPs are about 35 nm in size on average (see Figure 4.2B). The picture made it very clear that the solution was made up of OBTe-AgNPs of different sizes, which matches what the FESEM test showed.

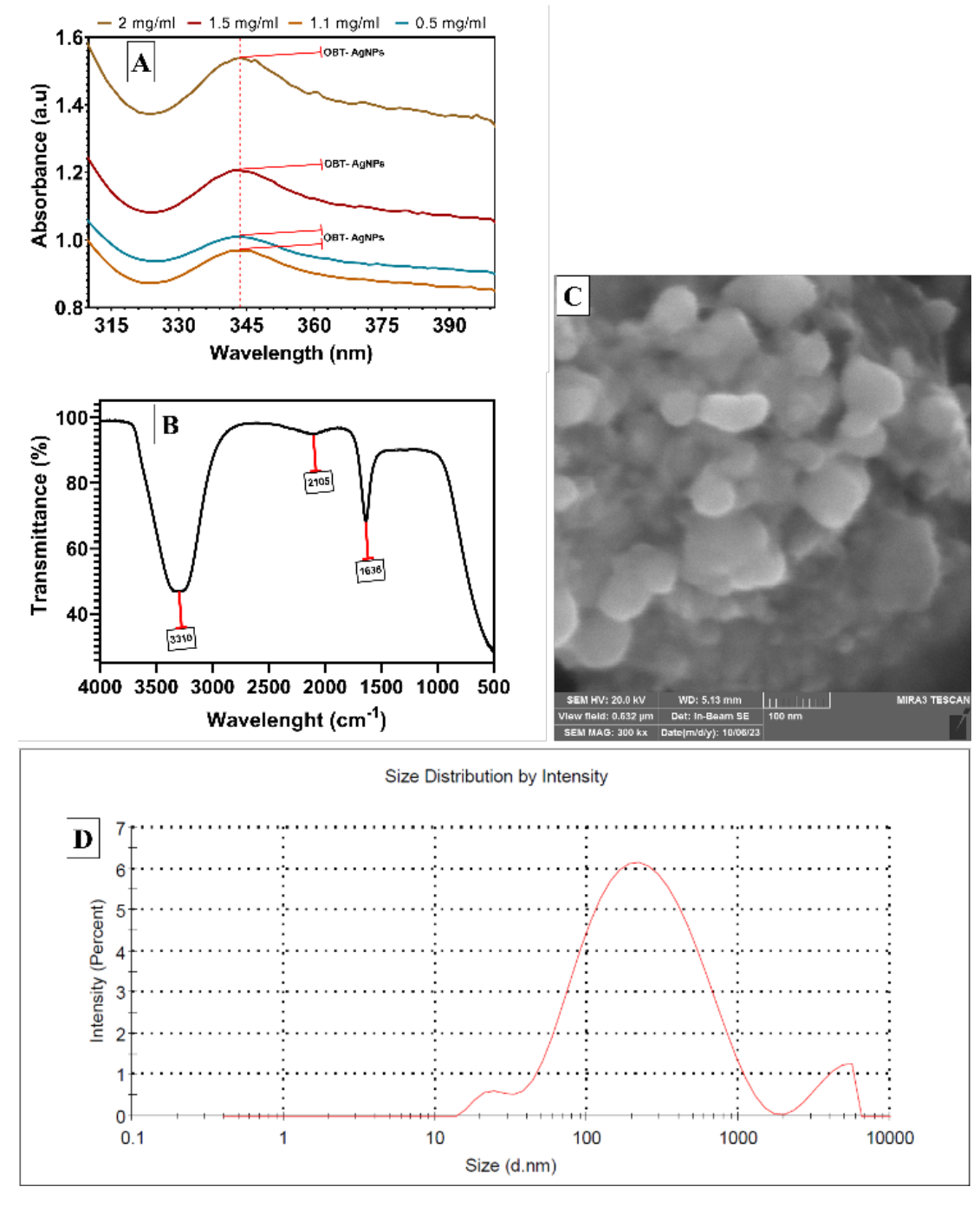


Figure 4.1. Characterization of OBTe-AgNPs (A) UV-Vis spectra (B) FTIR spectra of *O. basilicum* tea extract (C) FESEM micrograph (D) DLS size distribution

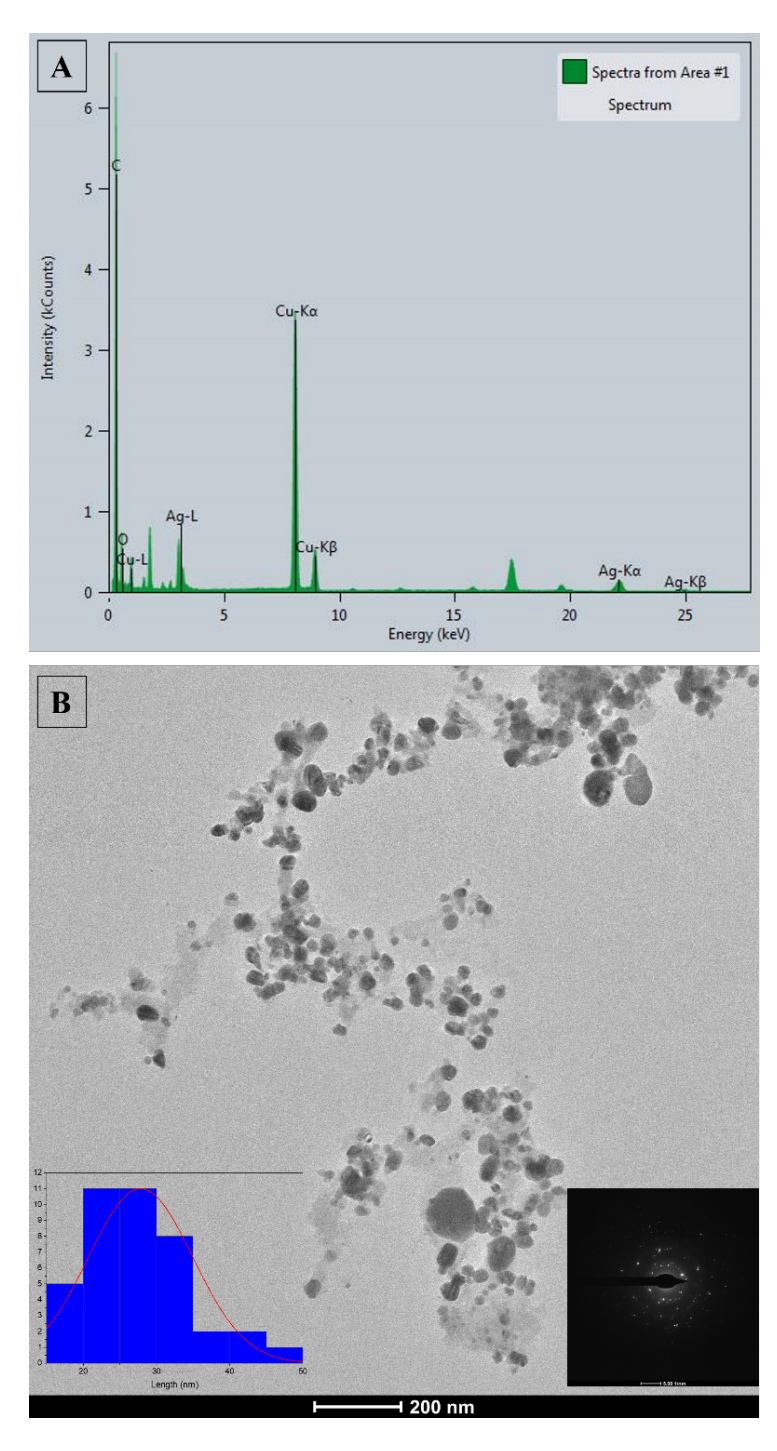


Figure 4.2. (A) EDS analysis revealing Ag-presence (B) TEM micrograph of OBTe-AgNPs with crystal shape and size distribution

4.1.2 OBTe-AgNPs stability against Temperature and pH

Altering the pH of the solution was employed to assess the pH stability of the synthesized OBTe-AgNPs. We used pH levels of 2, 4, 8, and 11 to investigate how pH impacts the stability of OBTe-AgNPs. The solution's pH was modified by adding 2 M hydrochloric acid and 1 M sodium hydroxide. The UV-Vis spectrophotometer was used to measure the absorbance of the reaction mixture. Figure 4.3A illustrates the pH effect of the created OBTe-AgNPs. At pH 11, the absorption peak at 435 nm suggests nonuniform particle size generation, but at pH 2, 4, and 8, the peak implies uniform

particle size formation. The thermal stability of the produced OBTe-AgNPs was evaluated by exposing the reaction mixture to different temperatures (25, 40, 60, 80, and 100 °C) for 30 minutes, as shown in Figure 4.3B. The highest intensity peak at 340 nm was seen at temperatures of 80 and 100 °C, as shown in Figure 4.3B. Absorption increased in direct proportion to the temperature increase. Raising the temperature of the combination accelerates the rate of OBTe-AgNPs synthesis under standard conditions. At high temperatures, the particles become polydisperse.

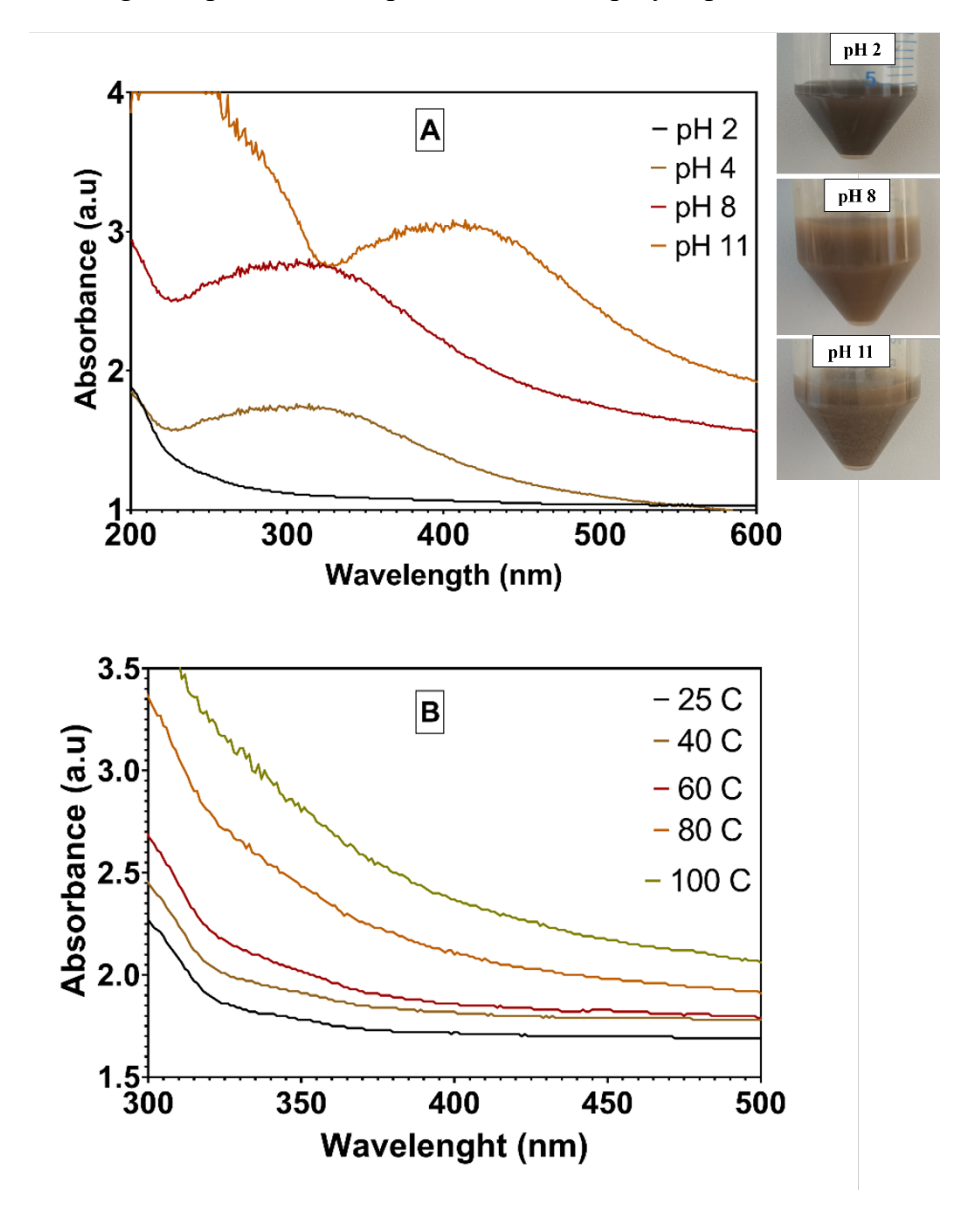


Figure 4.3. Effect of (A) pH and (B) temperature on the stability OBTe-AgNPs

4.1.3 Influence of OBTe-AgNPs on cell viability

The goal of this study was to determine the optimal concentration of OBTe-AgNPs for cancer cell targeting by studying their ability to trigger cell death. Hence, 0.5, 1, 5, 10, 20, and 40 μ g/ml of OBTe-AgNPs were added to HeLa cells. Figure 4.4 shows the results of the MTT experiment, which were used to measure cell viability. At increasing concentrations, the vitality of HeLa cells was observed to decline in a dose-dependent manner, with a significant drop (p < 0.001). At 5, 10, 20, and 40 μ g/ml, the

viability was 55.8%, 59.28%, 46.3%, and 36.73%, respectively, as shown in Figure 4.4. And the IC₅₀ was $21.78 \pm 0.68 \,\mu\text{g/ml}$.

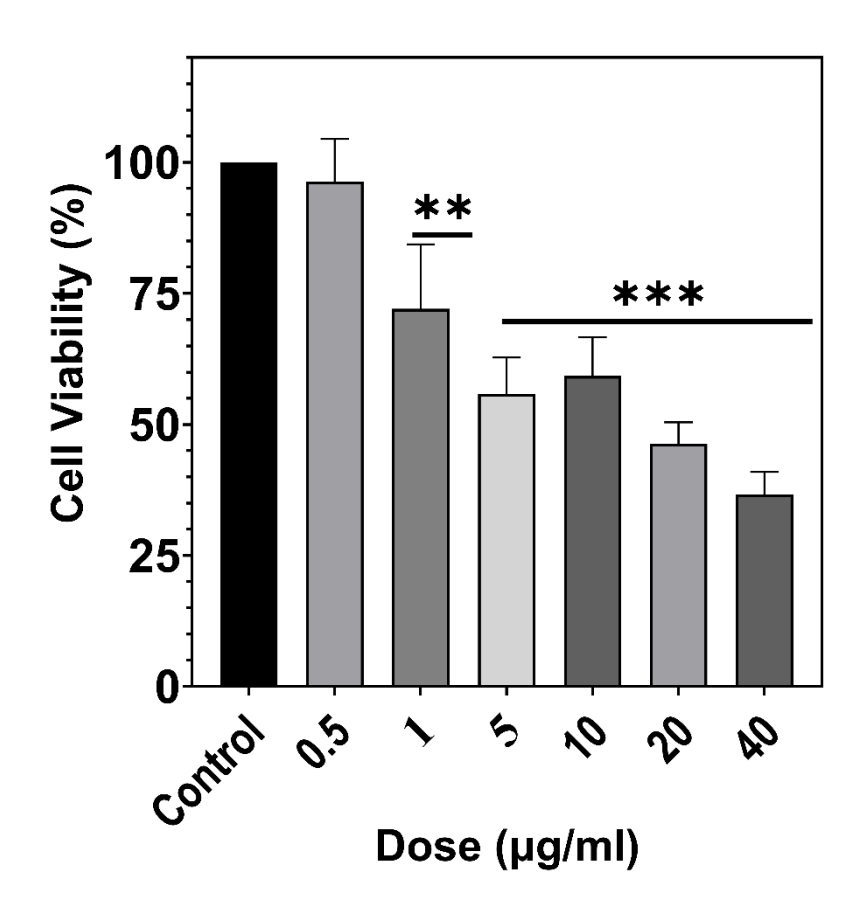


Figure 4.4. Cytotoxicity of OBTe-AgNPs against HeLa cells. Each data point represents the mean \pm SE of three independent replicates. ** and *** represents statistically significant from control at p < 0.01 and p < 0.001, respectively

4.1.4 ROS production in HeLa cells upon exposure to OBTe-AgNPs

A biomarker of the amount of oxidative stress in cells is the levels of glutathione (GSH), superoxide anion radical ($O_2^{\bullet-}$), and nitrite (NO_2^{-}). Figure 4.5A shows that there was a dose-dependent rise in GSH level in cells treated to OBTe-AgNPs. In 20 µg/ml (32.7 µM, p < 0.05) and 40 µg/ml (40.21 µM, p < 0.005) treated group GSH levels were significantly greater than those at lower concentrations. Similarly, as the dose of OBTe-AgNPs increased, nitrite and superoxide anion radical concentrations in cells likewise increased. Nonetheless, after 24 hours of treatment, the results demonstrated a notable shift in the level of super oxide anion radical (see Figure 4.5B) at 40 µg/ml (185.82 µM, p < 0.05). In contrast, nitrite levels (see Figure 4.5C) were found to be significantly higher at 20 µg/ml (30.58 µM, p < 0.05) and 40 µg/ml (38.6 µM, p < 0.001), respectively. Nitrite, superoxide anion radical, and glutathione levels followed a pattern comparable to that of cell death (see Figure 4.4).

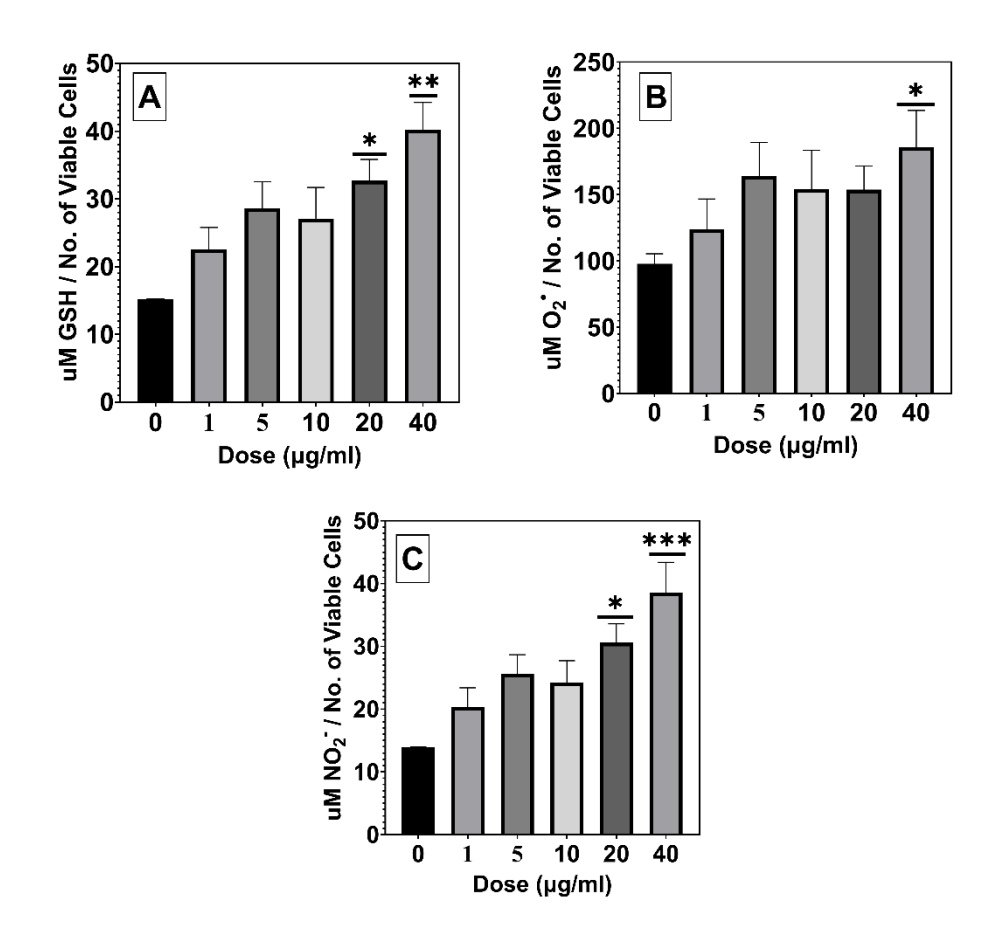


Figure 4.5. ROS production upon exposure to OBTe-AgNPs in HeLa cells. * , ** and *** represents statistically significant from control at p < 0.05, p < 0.005 and p < 0.001, respectively

4.1.5 Apoptotic gene expression in HeLa cells

When compared to the control, we found that the levels of Cas~3, 8, 9, and antiapoptotic Bcl-2 were significantly higher in the cells that were treated with OBTe-AgNPs at concentrations of 5 and $40~\mu g/ml$. In all genes that were studied, the treatment at a dose of $40~\mu g/ml$ had a more significant impact compared to the $5~\mu g/ml$ concentration, with the exception of Cas~8. In both treatments, the levels of Bax were shown to be low on Figure 4.6.

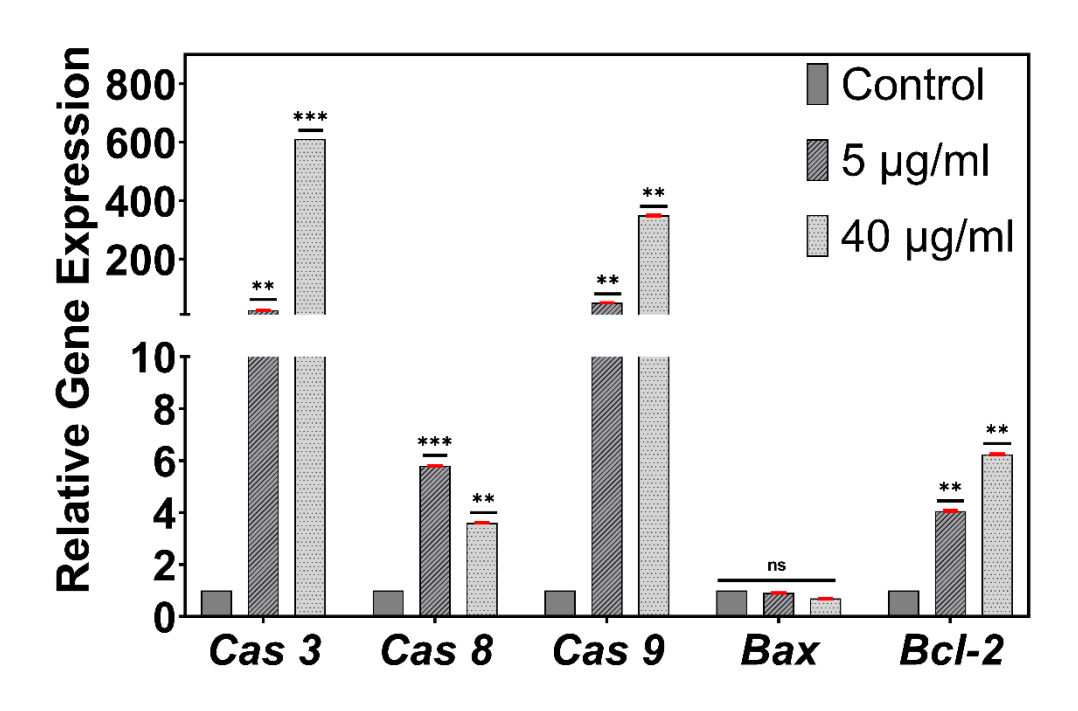


Figure 4.6. Relative gene expression of the *Cas 3, 8, 9*; pro-apoptotic *Bax*; and anti-apoptotic *Bcl-2*. ** and *** represents statistically significant from control at p < 0.005 and p < 0.001

4.1.6 Annexin FITC assay for apoptosis analysis in HeLa cells

The viability and type of cell death after treatment with OBTe-AgNPs at two concentrations (5 and 40 μ g/ml) for 24 hours were examined in the study using the flow cytometry method. Compared to the control, both doses significantly reduced viability, with the higher concentration showing a larger cytotoxic effect. At both concentrations, apoptosis was the most common form of cell death. Even so, at both dosages, necrosis was observed in a tiny percentage of cells. Figure 5.7 displays the findings of the flow cytometry analysis.

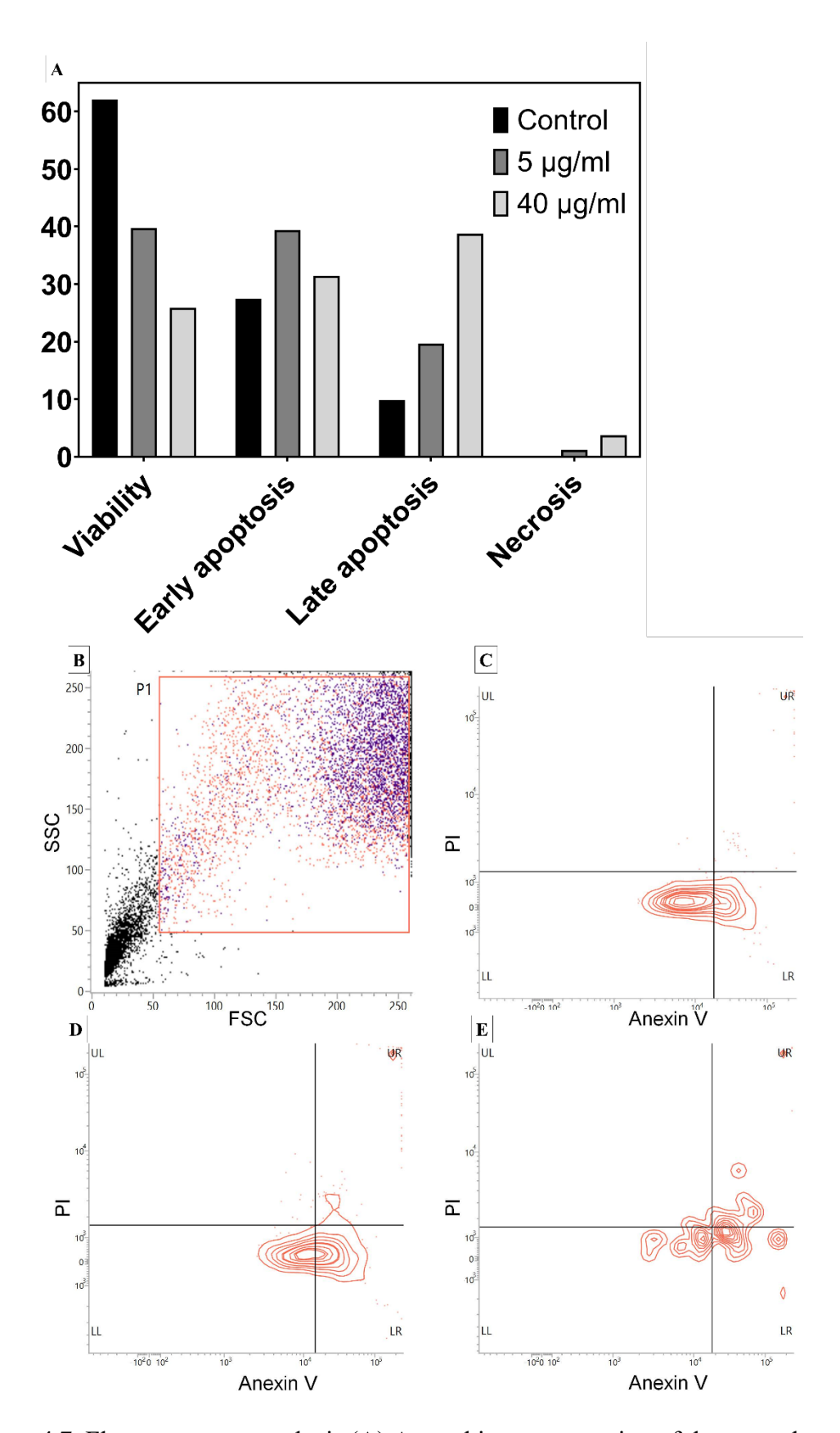


Figure 4.7. Flow cytometry analysis (A) A graphic representation of the several phases of cell demise in control, 5 μ g/ml and 40 μ g/ml group (B) Overlapping of cell

4.2 Characterization and toxicological studies of VMTe-AgNPs

4.2.1 Characterization of VMTe-AgNPs and V. myrtillus tea extract

A variety of methods, including UV-visible spectroscopy, FESEM, DLS, FTIR, and TEM, were utilized in order to verify the synthesis of VMTe-AgNPs. The manufacturing of VMTe-AgNPs was initially validated through the examination of UVvis spectra in the wavelength range of 200-800 nm. It is clear from looking at figure 4.8A that VMTe-AgNPs had a peak at 305 nm at several different concentrations. According to the findings of the FESEM analysis performed at a magnification of 100 kx, the average size and shape of the VMTe-AgNPs was seen to be 52 nm and round (see Figure 4.8B). At a magnification of 100 nm, TEM analysis offered more specific information regarding size and shape. When viewed using a TEM, the average size of the VMTe-AgNPs was 80 nm, and they had an oval form (see Figure 4.8C). Due to the claustration of VMTe-AgNPs, the solution contained a majority of VMTe-AgNPs with an average cluster size of 196 nm (see Figure 4.8D). The zeta potential of the solution was -27.9, and PDI was 0.269. The FTIR technique was utilized in order to search for biomolecules from the *V. myrtillus* tea extract that have the potential to assist in the reduction, bio-capture, or stabilization of Ag⁺ ions to Ag⁰. From 400 to 4000 cm⁻¹, the FTIR spectroscopy exhibited a multitude of peaks. The absorption peaks at 3281.13 cm^{-1} , 2916.51 cm^{-1} , 2849.27 cm^{-1} , 1613.56 cm^{-1} , 1318.58 cm^{-1} , 1030.48 cm^{-1} , 779.13 cm⁻¹, 516.10 cm⁻¹, and 466.23 cm⁻¹ were the most notable of these peaks (see Figure 4.8E).

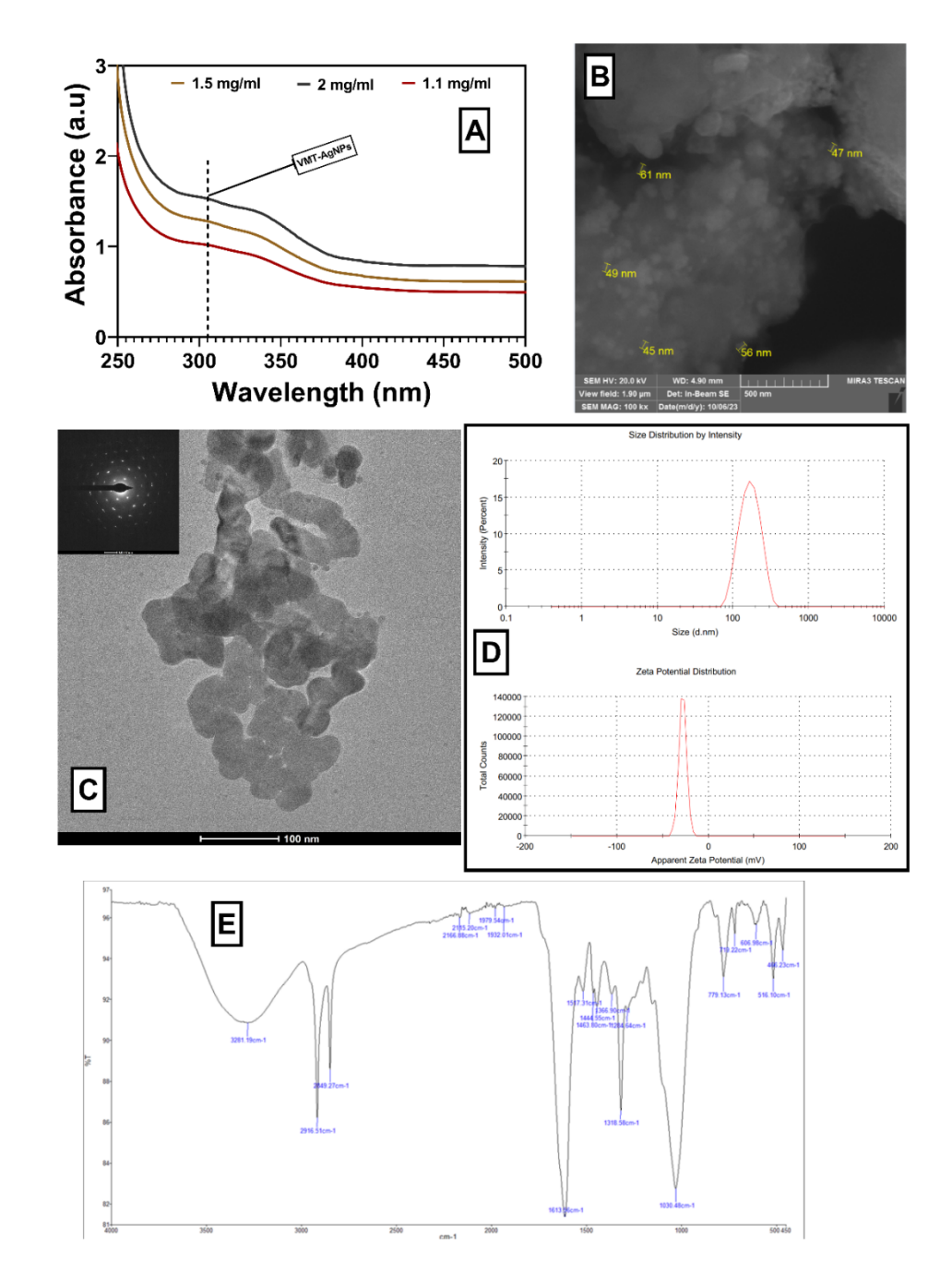


Figure 4.8. Characterization of VMTe-AgNPs (A) UV-Vis spectra of VMTe-AgNPs (B) FESEM micrograph of VMTe-AgNPs (C) TEM micrograph of VMTe-AgNPs (D) DLS size distribution of VMTe-AgNPs (E) FTIR spectra of *V. myrtillus* tea extract

4.2.2 VMTe-AgNPs stability against Temperature and pH

To determine whether or not VMTe-AgNPs are stable, temperature and pH were subjected to a range of variations. A UV-Vis spectroscopy was utilized in order to determine the absorbance of the reaction mixture over a wavelength range that extended from 200 to 800 nm. The reaction mixture was heated to varying temperatures for a period of 45 min at 25, 40, 60, 80, and 100 °C (see Figure 4.9A). This was done in order to test the thermal stability of the VMTe-AgNPs. According to the data presented in Figure 4.9A, an increase in temperature was accompanied by a comparable increase in

the amount of absorption. The fact that there was no discernible change in the stability of VMTe-AgNPs, on the other hand, provides evidence that VMTe-AgNPs are stable across a wide range of temperature settings. When the temperature of the combination is elevated, the rate of synthesis of VMTe-AgNPs also increases, even when the temperature is set at room temperature. Nevertheless, when the particles are pushed to higher temperatures, they go through a process called poly dispersion. In contrast, we explored the relationship between pH and the stability of VMTe-AgNPs by using pH values of 2, 5, 6, 10, and 11 in our investigation. In order to alter the pH of the solution, sodium hydroxide with a concentration of 1 M and hydrochloric acid with a concentration of 2 M were utilized. A representation of the pH effect of the VMTe-AgNPs that were created can be found in Figure 4.9B. The formation of particles with dimensions that are not uniform is shown by the absorption peak that occurs at 550 nm regardless of pH 2, 10, or 11. To the contrary, the peak is indicative of the formation of particles with diameters that are homogeneous when the pH is between 5 and 6.

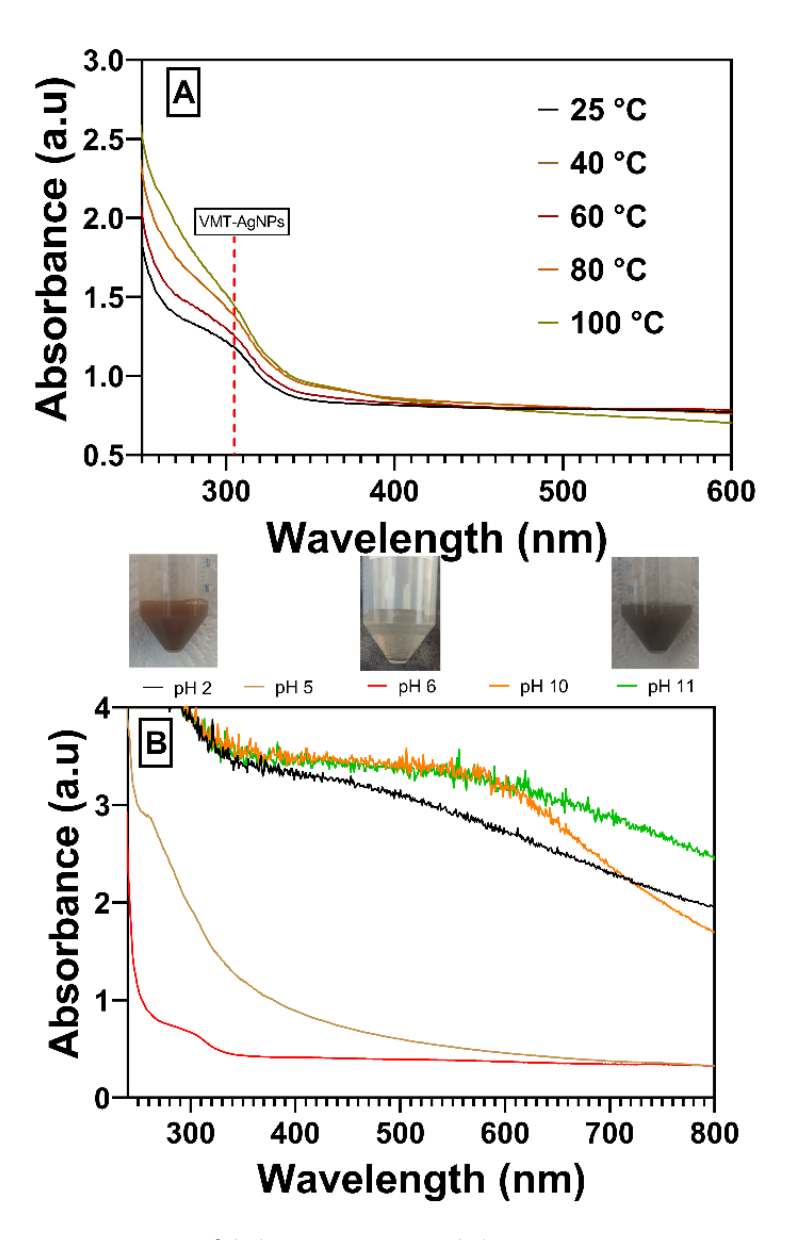


Figure 4.9. Impact of (A) Temperature (B) pH on VMTe-AgNPs stability

4.2.3 Influence of VMTe-AgNPs on cell viability

The cells were subjected to different concentrations (10, 20, 40, 60 µg/ml) for both 24 and 72 h in order to study and determine the optimal dosage of VMTe-AgNPs as an anti-cancer and anti-atherosclerotic agent. As shown in figure 4.10, the cell viability was assessed using the MTT assay. Increasing doses of VMTe-AgNPs were associated with a decline in MDA-MB-231 and HUVAC cell viability (see Figure 4.10). The viability of MDA-MB-231 cells was found to be 32.41% (p < 0.01) and 25.2% (p < 0.01) after 24 h in groups of 40 and 60 µg/ml relative to the control, respectively. The cell viability was found to be dramatically reduced to 21.35% and 11.2%, respectively, after 72 h in the same dosing group (p < 0.001), as shown in Figure 4.10A. In the 24 and 72 h group, the IC₅₀ value was determined to be 29.69 \pm 1.47 and 20 \pm 1.30 µg/ml, respectively.

The HUVEC cell lines exhibited a similar pattern of cell viability decline that was dosage dependent. The vitality of HUVEC cells was found to be 64.22% (p < 0.05), 32.89% (p < 0.001), 28.5% (p < 0.001) and 16.47% (p < 0.001) in 10, 20, 40 and 60 µg/ml, respectively, after 24 h. There was a substantial decrease in cell viability to 55.32% (p < 0.05), 28.54% (p < 0.01), 22.74% (p < 0.01), and 8.19% (p < 0.001), respectively, after 72 h in the same dosing group (see Figure 4.10B). In the 24 and 72 h group, the IC50 value was determined to be 17.72 \pm 1.25 and 20.38 \pm 1.31 µg/ml, respectively. A dose-dependent reduction in cell viability was noted in both cell lines, suggesting that VMTe-AgNPs may have anti-cancer and anti-atherosclerotic properties.

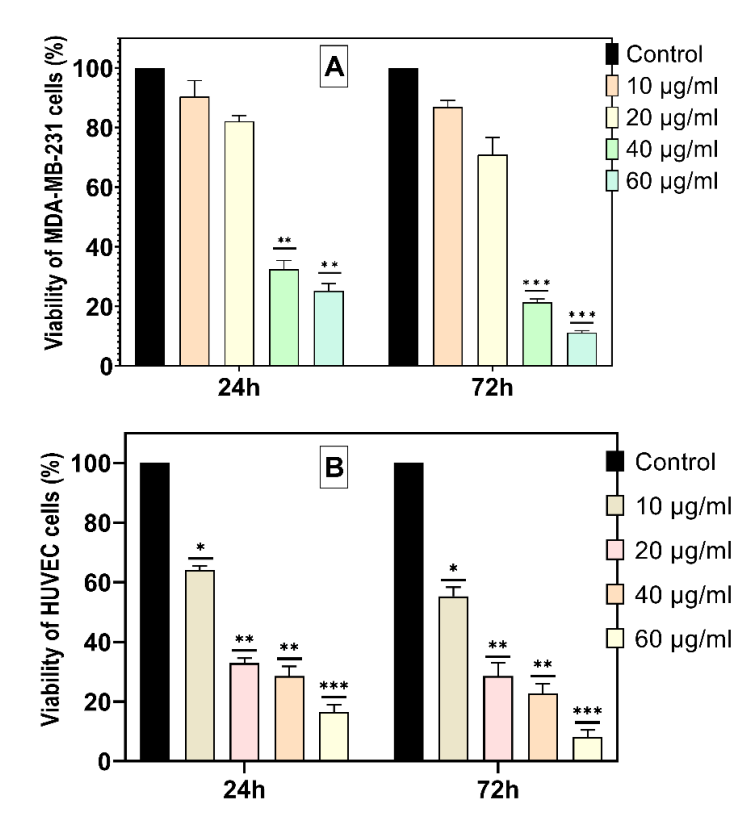


Figure 4.10. Cytotoxic efficacy of VMTe-AgNPs against (A) MDA-MB-231 and (B) HUVEC cell lines. * Represents statistically significant from control at p < 0.05, ** Represents statistically significant from control at p < 0.01, *** Represents statistically significant from control at p < 0.001

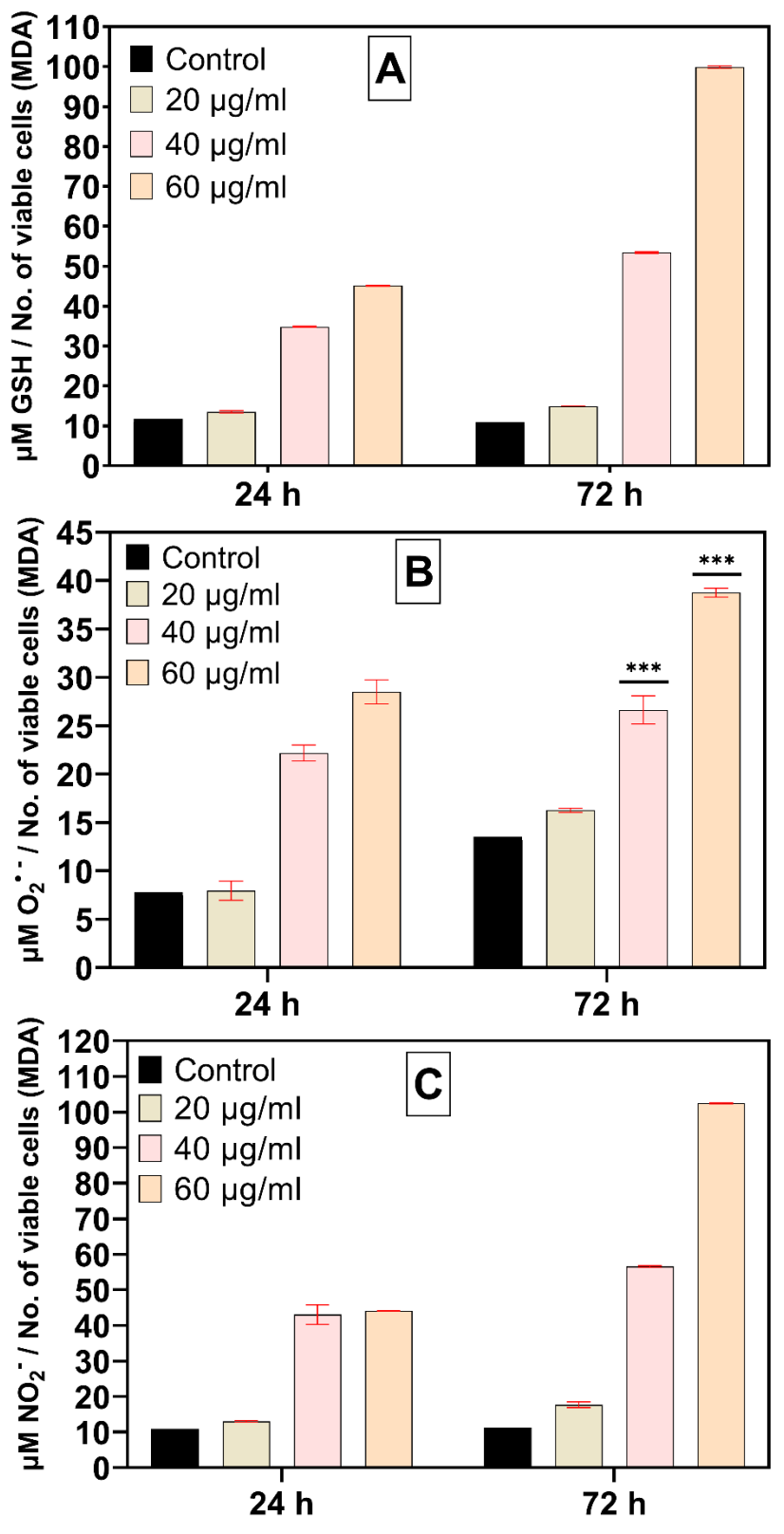
4.2.4 ROS production in cells after VMTe-AgNPs exposure

The levels of glutathione (GSH), nitrite (NO_2^-), and superoxide anion radical ($O_2^{\bullet -}$) are three markers that can be employed to ascertain the extent of oxidative stress within cells. Exposure of cells to VMTe-AgNPs revealed, in both cell lines, that ROS concentrations rise with increasing dosage values.

After 24 h of exposure to VMTe-AgNPs in MDA-MB-231, we observed a dose-dependent elevation in GSH concentration as a response to oxidative stress. The concentrations at 20, 40, and 60 μ g/ml were measured as 13.53, 34.82, and 45.1 μ M, respectively. However, these values were not statistically significant when compared to the control concentration of 11.71 μ M (see Figure 4.11A). However, it was noted that there was a dose-dependent rise in GSH concentration at concentrations of 20 μ g/ml (14.97 μ M), 40 μ g/ml (53.44 μ M), and 60 μ g/ml (99.91 μ M) after a treatment period of 72 h. Notwithstanding the observed increase in dosage, it was determined that the rise in all dose groups was not statistically significant in comparison to the control group (10.99 μ M) (see Figure 4.11A).

In a similar vein, we noted a comparable rise in the concentration of superoxide anion radical ($O_2^{\bullet-}$) following a 24-72 h exposure to VMTe-AgNPs, which was dependent on the dosage. Following a 24 h period, the concentrations in dose groups 20, 40, and 60 µg/ml exhibited an upward trend as the dosage increased. Specifically, the concentrations were measured to be 7.95 µM, 22.19 µM, and 28.49 µM, respectively (see Figure 4.11B). No significant increase in concentration was detected in any of the dosing groups when compared to the control group (7.79 µM). In contrast, it was discovered that after a duration of 72 h, there were statistically significant elevations in the concentration of $O_2^{\bullet-}$ at concentrations of 40 µg/ml (26.63 µM, p < 0.001) and 60 µg/ml (38.74 µM, p < 0.001) as compared to the control group (13.52 µM) (see Figure 4.11B).

Furthermore, both the 24 h and 72 h treatment groups exhibited a comparable rise in nitrite (NO_2^-) concentration, which was dependent on the dosage. Following a 24 h period, it was discovered that the concentration in dosage groups 20, 40, and 60 µg/ml exhibited a rising trend as the dose increased. Specifically, the concentrations were measured to be 13.04 µM, 43.05 µM, and 44.16 µM, respectively, as seen in Figure 4.11C. Nevertheless, we noted a lack of statistical significance in the observed rise in concentration across all dosage groups when compared to the control group (11.24 µM). In contrast, following a 72-h period of exposure, we found comparable dose-dependent elevations in NO_2^- concentration at dose of 20 µg/ml (17.68 µM), 40 µg/ml (56.59 µM), and 60 µg/ml (102.43 µM), which were not statistically significant when compared to the control group (11.23 µM) (see Figure 4.11C).



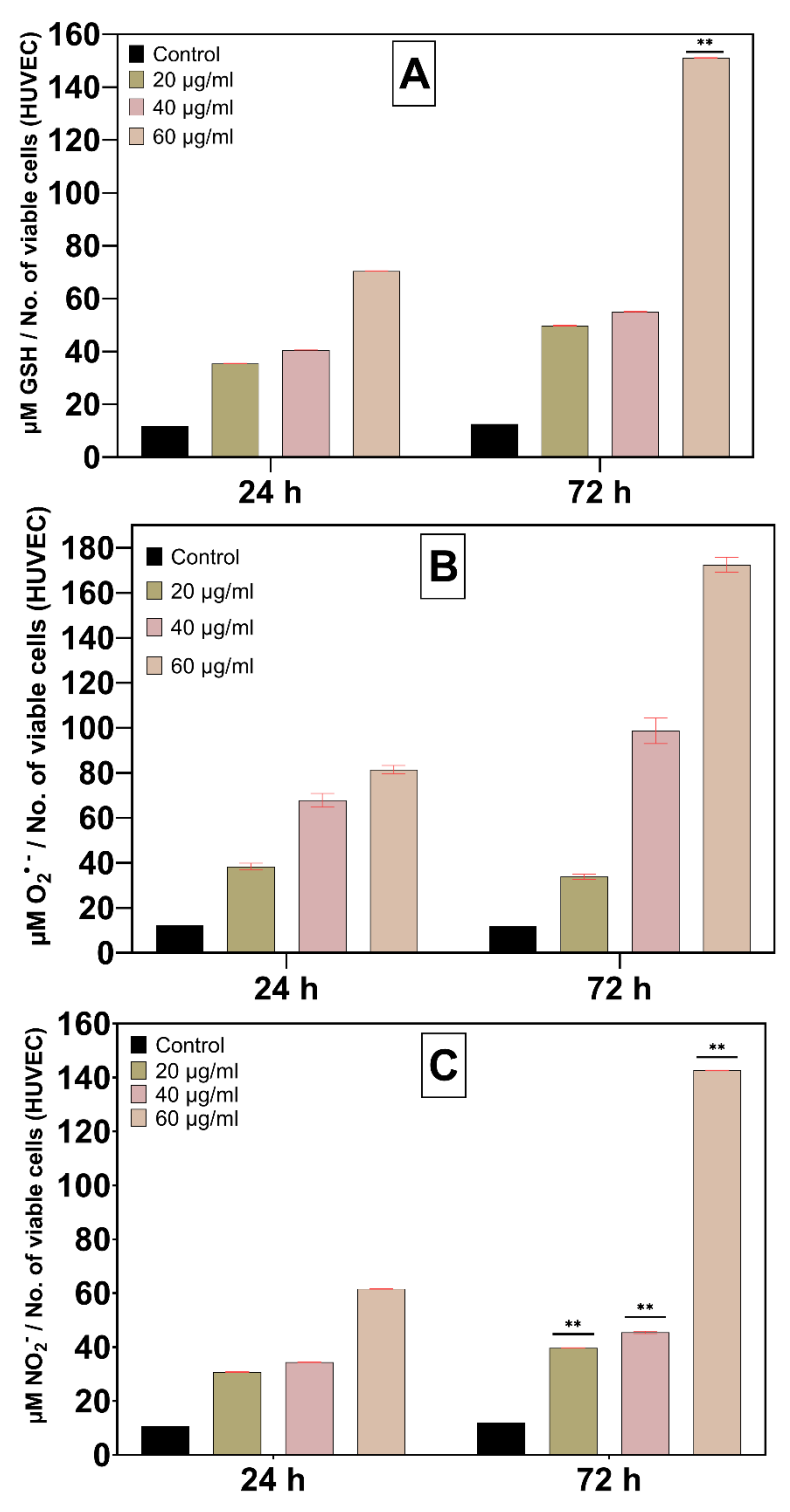
*** Represents statistically significant from control at p<0.001

Figure 4.11. ROS production upon exposure to VMTe-AgNPs in MDA-MB-231 cells

In the HUVEC cell line, a dose-dependent elevation in GSH levels was seen following a 24-h exposure to VMTe-AgNPs, as a response to oxidative stress. The concentrations at 20, 40, and 60 μ g/ml were measured to be 35.42, 40.55, and 70.46 μ M, respectively. However, these values were not statistically significant when compared to the control concentration of 11.84 μ M (see Figure 4.12A). However, it was noted that there was a dose-dependent rise in GSH concentration at concentrations of 20 μ g/ml (49.76 μ M), 40 μ g/ml (55.04 μ M), and 60 μ g/ml (151.05 μ M) after a treatment period of 72-h. Although there was an increase in dosage, only the group receiving a dose of 60 μ g/ml showed statistical significance (p < 0.01) compared to the control group (12.52 μ M) (see Figure 4.12A).

In a similar vein, we noted a comparable rise in the concentration of superoxide anion radical ($O_2^{\bullet-}$) following a 24-72 h exposure to VMTe-AgNPs, which was dependent on the dosage. Following a 24-h period, the concentrations in dose groups 20, 40, and 60 µg/ml exhibited an upward trend as the dosage increased. Specifically, the concentrations were measured to be 38.42 µM, 67.78 µM, and 81.39 µM, respectively (see Figure 4.12B). The concentration in all dosing groups was found to be statistically non-significant when compared to the control group (12.43 µM). In contrast, it was discovered that after a duration of 72 h, there were similar statistically non-significant elevations in the concentration of $O_2^{\bullet-}$ at concentrations of 20 µg/ml (33.90 µM), 40 µg/ml (98.64 µM), and 60 µg/ml (172.44 µM) as compared to the control group (11.77 µM) (see Figure 4.12B).

Furthermore, both the 24 h and 72 h treatment groups exhibited a comparable rise in nitrite (NO_2^-) concentration, which was dependent on the dosage. After a duration of 24-h, it was discovered that the concentration in dosage groups 20, 40, and 60 µg/ml exhibited a rising trend as the dose increased. Specifically, the concentrations were measured to be 30.71 µM, 34.37 µM, and 61.61 µM, respectively (see Figure 4.12C). A statistically non-significant difference was detected in the concentration of all dosage groups compared to the control group (10.60 µM). In contrast, our findings indicate that there were statistically significant elevations in NO_2^- levels at concentrations of 20 µg/ml (39.66 µM, p < 0.01), 40 µg/ml (45.47 µM, p < 0.01), and 60 µg/ml (142.62 µM, p < 0.01) as compared to the control group (12.01 µM) (see Figure 4.12C).



** Represents statistically significant from control at p<0.01

Figure 4.12. ROS production upon exposure to VMTe-AgNPs in HUVEC cells

4.3 OBTe-AgNPs incorporated nanofibers as a coating material for drug coated ballons

As seen in previous experiments that the biogenic AgNPs have the potential to be used as a multifunctional agent against multiple diseases i.e., cancer and atherosclerosis. Therefore, biogenic AgNPs were incorporated into PEG-PCL NFs to explore the potential of biogenic AgNPs as a drug excipient for drug coated balloons for removing atherosclerosis plaque.

4.3.1 Characterization of OBTe-AgNPs incorporated nanofibers

FTIR analysis of OBTe-AgNPs-NFs was conducted to observe the integration of biogenic OBTe-AgNPs into NFs. The spectra of OBTe-AgNPs-NFs exhibited distinct peaks at around 1700 cm⁻¹, indicating the stretching of C=O bonds, and in the region of 1100-1200 cm⁻¹, indicating the stretching vibrations of C=O=C bonds and -COO= bonds, which are specific to NFs. In contrast, the spectra of biogenic OBTe-AgNPs do not exhibit any distinct absorption bands in this region, suggesting the successful formation of AgNPs-NFs as shown in figure 4.13.

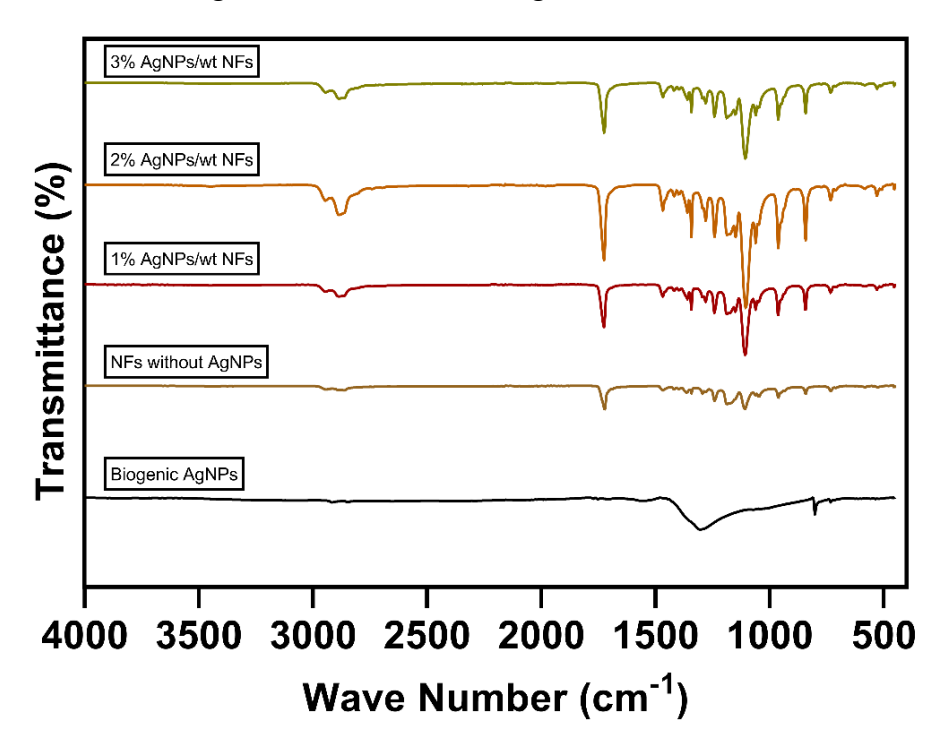


Figure 4.13. FTIR spectra of OBTe-AgNPs-NFs and biogenic OBTe-AgNPs

In addition, the FESEM was employed to observe the morphological distinctions among all the different forms of OBTe-AgNPs-NFs (as shown in figure 4.14). The mean diameter of OBTe-AgNPs-NFs with concentrations of 1%, 2%, and 3% was observed to be 179.29 ± 18.65 nm, 181.55 ± 12.67 nm, and 194.80 ± 17.80 nm, respectively. The diameter of the fibers in all versions of OBTe-AgNPs-NFs ranged from 168.21 to 216.26 nm. Conversely, NFs without AgNPs had an average diameter of 472.68 ± 51.33 nm, ranging from 406.84 to 572.95 nm.

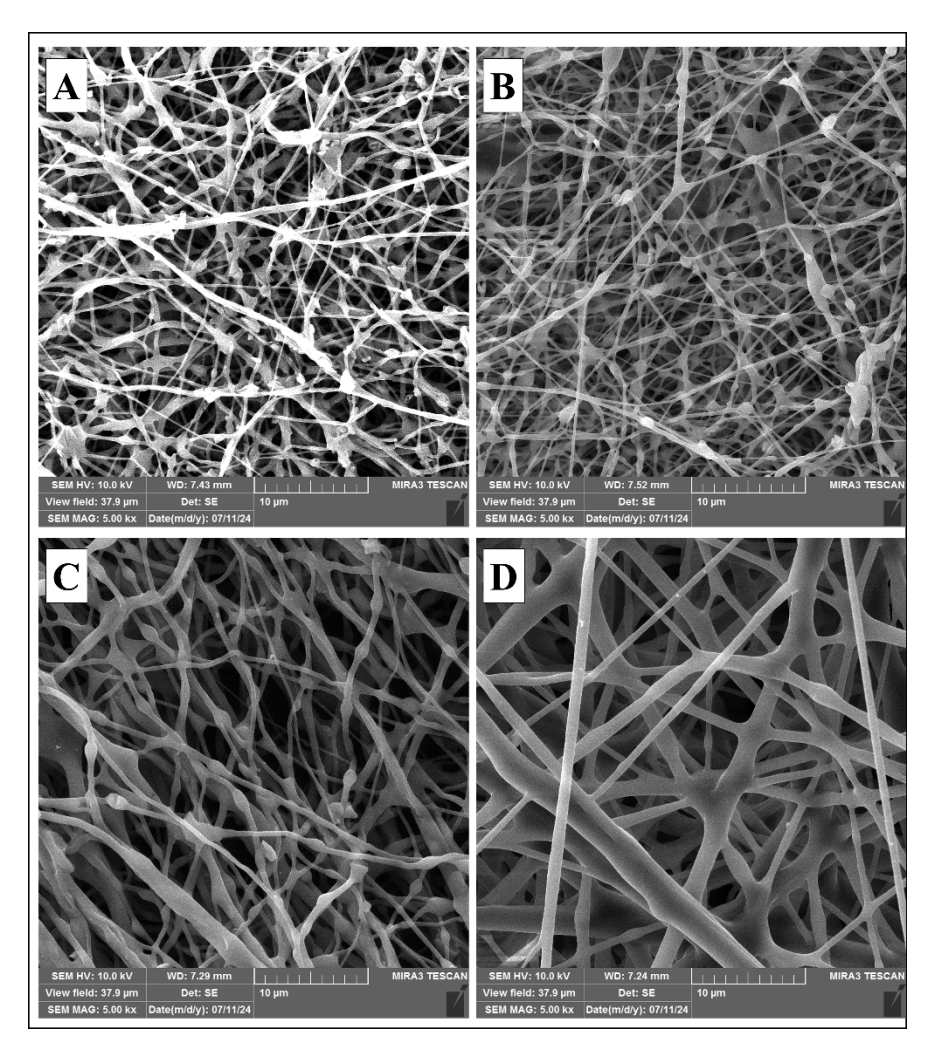


Figure 4.14. FESEM images of produced NFs (A) 1% OBTe-AgNPs-NFs (B) 2% OBTe-AgNPs-NFs (C) 3% OBTe-AgNPs-NFs (D) PCL-PEG NFs only

The surface roughness was examined and assessed using AFM. Two viable ways to describe a surface's roughness parameter are as an average along the surface's centerline or as the distance between the two extremes of the surface's irregularities. The 1%, 2%, and 3% OBTe-AgNPs-NFs had average surface roughness (Ra) values of 72.77, 98.34, and 149.01 nm, respectively, according to our research. Surface roughness increases as the percentage of OBTe-AgNPs incorporated into NFs increases. Figure 4.15 shows that when the fraction of incorporated OBTe-AgNPs increases, more OBTe-AgNPs collect on the surface of NFs. Findings from the AFM corroborate those from the FESEM pictures and the Ag ion release profile.

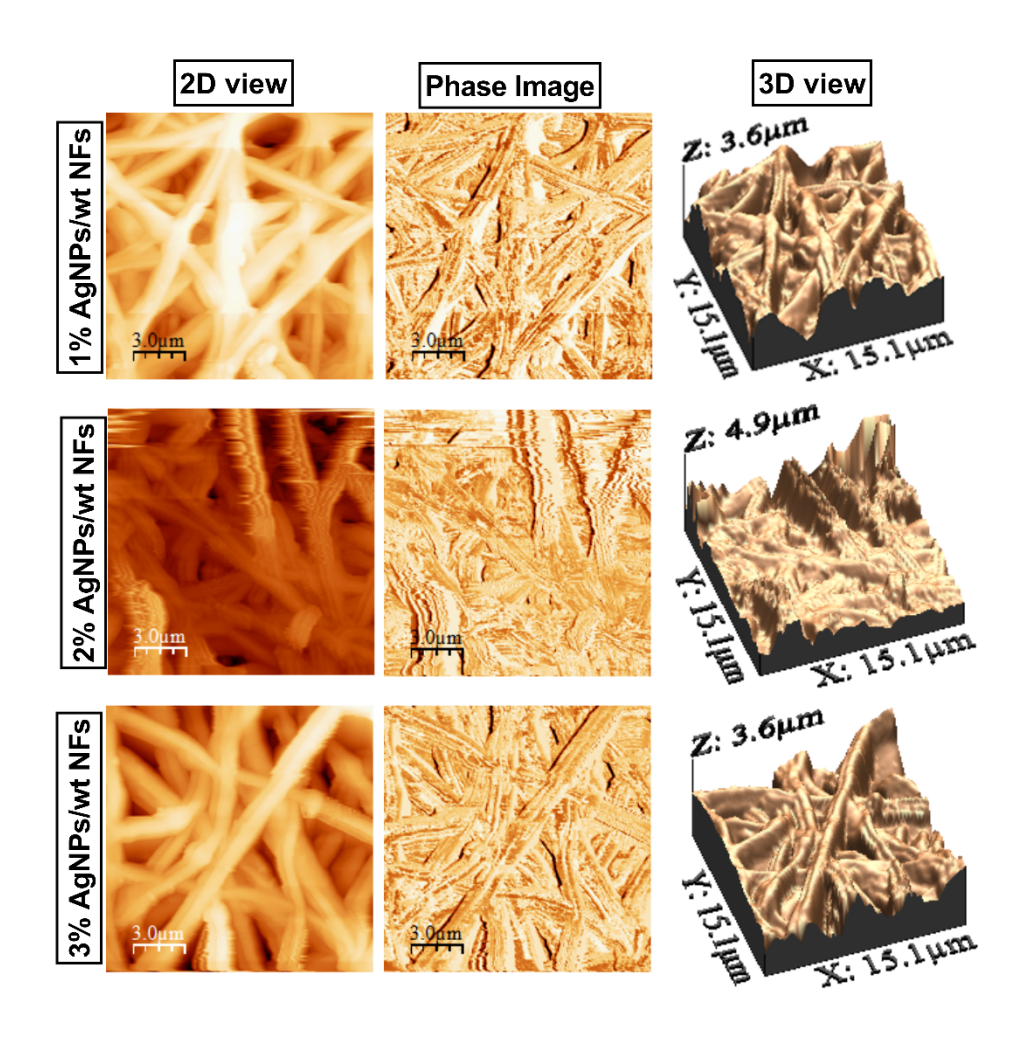


Figure 4.15. Surface roughness analysis using AFM of OBTe-AgNPs-NFs

4.3.2 Ag ion release from nanofibers

In-vitro drug-release profiles were used to examine the sustainability of OBTe-AgNPs in PEG-PCL nanofibers under various physiological circumstances and time periods. The encapsulated OBTe-AgNPs release rate demonstrated a steady, continuous release that followed an initial burst release that lasted for three to twenty-four hours (see Figure 4.16). Approximately half of the encapsulated OBTe-AgNPs were released from the NFs during the course of the 96-h incubation period. Diffusion of OBTe-AgNPs that were adsorbed at the surface of the polymeric NFs may have caused the first burst release of OBTe-AgNPs. Nonetheless, the prolonged release of OBTe-AgNPs in later phases may have resulted from the breakdown of PEG inside the polymeric matrix or from the diffusion of encapsulated OBTe-AgNPs from the polymeric NFs core area.

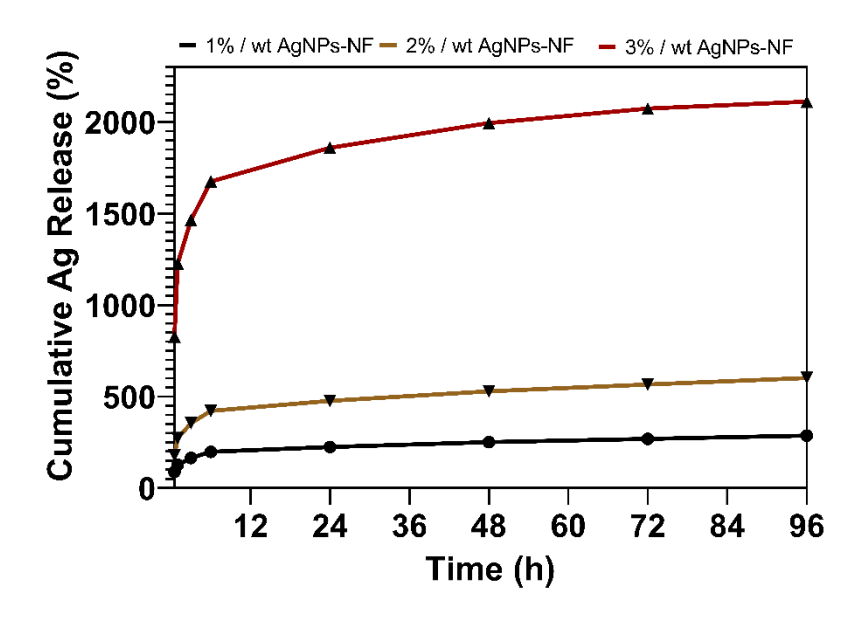


Figure 4.16. Silver ion cumulative release over time from NFs

4.3.3 Application of nanofibers to remove atherosclerosis

In order to observe the practical use of OBTe-AgNPs-NFs in the treatment of atherosclerosis, all different forms of OBTe-AgNPs-NFs were tested on atherosclerosis model HUVEC cells. The cell viability was assessed using the MTT test, as seen in figure 4.17. The findings revealed that the survival rate of HUVEC cells decreased considerably (p < 0.001) as the dose of OBTe-AgNPs in NFs increased, relative to the control group, after 24 and 72 h of exposure. Following a 24-hour exposure to OBTe-AgNPs-NFs, the vitality of HUVEC cells in the dose groups of 1%, 2%, and 3% OBTe-AgNPs-NFs was measured to be 61.64%, 20.03%, and 14.68%, respectively. In contrast, after being exposed to OBTe-AgNPs-NFs after 72 hours, the vitality of HUVEC cells in the dose groups of 1%, 2%, and 3% was 39.91%, 18.46%, and 11.79%, respectively.

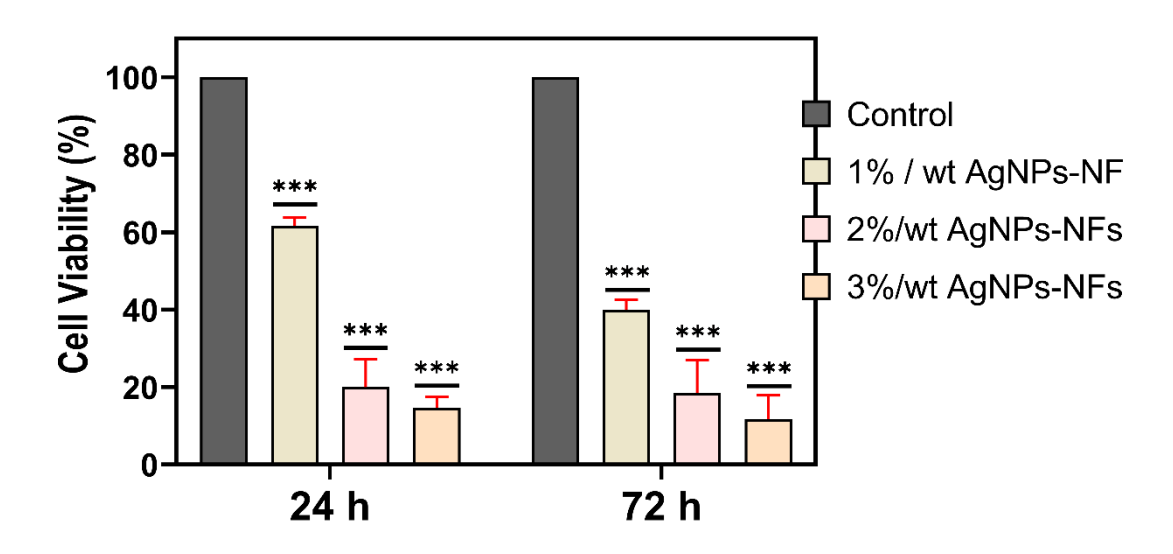


Figure 4.17. HUVEC viability after exposure to various variations of NFs

Chapter 5

Discussion

The synthesis of ecologically sustainable AgNPs is a method that bears major relevance within the field of nanotechnology. Over the past several years, there has been a great emphasis placed on the development of procedures that are friendly to the environment in order to reduce the likelihood of environmental pollution. Several natural resources, including plant extracts, fungus, and bacteria, have been utilized in the production of AgNPs as a result of this rationale-based approach. In addition to acting as capping and reducing agents, the plant extract contains active components such as terpenoids, alkaloids, phenols, tannins, and vitamins. These components are responsible for performing these functions (Qamar & Ahmad, 2021).

Consequently, in the current investigation, we investigated the possible anticancer effects of AgNPs that were produced by employing Bosiljak (O. basilicum) extract, which is a traditional tea from Serbia. The transformation of the hue from dark brown to dark black was the initial stage in the process of determining the fact that OBTe-AgNPs were formed. There is a correlation between the description of our earlier work and the first hint that OBTe-AgNPs are being formed. In the previous study, an extract of O. tenuiflorum was utilized to generate AgNPs for the purpose of eliminating insect pests (Qamar & Ahmad, 2021). As a result of the change in color of the reaction mixture, the creation of AgNPs was clearly visible. It was also observed by Abdelsattar et al. that the change in hue was the early indicator of the synthesis of AgNPs when H. sabdariffa L. was utilized for the manufacture of AgNPs to kill bacteria (Abdelsattar et al., 2022). According to the findings of both of these experiments, the first step toward producing a stable AgNPs product is the alteration in color of the reaction mixture. The ultraviolet-visible spectra of the reaction solution that was supplied inside of on the production of OBTe-AgNPs with a peak at 344 nm in a range of 315-390 nm were analyzed in order to offer additional confirmation of the development of OBTe-AgNPs (see Figure 4.1A). It is possible that the presence of various metabolites in the reaction solution that were formed from the extract of O. basilicum tea extract and that were assessed within the experimental spectrophotometric range is responsible for the wide range of UV-Vis absorption spectra. Analysis of the surface plasmon resonance (SPR) peak is a method that may be utilized to accomplish the identification and characterization of NPs at the nanoscale. A single SPR band may be seen in the absorbance spectrum of a solution that contains NPs that are both spherical and homogeneous in shape. According to the findings of prior research, the number of peaks that are observed is directly proportional to the degree of anisotropy being present (Abdelkhalek et al., 2022). Finally, the OBTe-AgNPs that are biosynthesized always have a spherical shape. In addition, the experiment causes the NPs concentration to rise and the particle size to grow (Motafeghi et al., 2023).

An FTIR analysis was performed on the tea extract of *O. basilicum* with the purpose of identifying prospective biomolecules that may be accountable for the reduction, biocapping, or effective stabilization of Ag⁺ ions to Ag⁰. The application of FTIR spectroscopy to discern numerous peaks falling within the spectral range of 500-4000 cm⁻¹. It is worth mentioning that substantial absorption peaks were observed at 2105 cm⁻¹, 3310 cm⁻¹, and 1636 cm⁻¹, as illustrated in Figure 4.1B. The peak observed at 3310 cm⁻¹ is indicative of phenolic acids, flavanol, and O-H bonded polyphenols.

Conversely, the peak at 1636 cm⁻¹ corresponds to amide I bonds carbonyl stretch (C=O) bonded or proteins formed as a result of the C=O stretch (see Figure 4.2B). The chemical compounds identified in this investigation, in conjunction with prior phytochemical reports on extracts from the leaves, seeds, and flowers of *O. basilicum*, suggest the existence of varying concentrations of reducing biomolecules, secondary metabolites, lipids, carbohydrates, and pigments, carbonyl groups, flavonoids, alkaloids, terpenoids, amines, and pigments (Fouzia et al., 2020). The phenomenon of proteins binding to MNPs via free carboxylate groups is well-established (Ajitha et al., 2014). The carboxylate groups that are found in proteins have the potential to behave as a surfactant, which would enable them to bind to the surface of NPs (Abarca-Cabrera et al., 2021). There is a high probability that these chemicals are accountable for the bio-reduction of Ag⁺ ions. For this reason, it is recommended that more study be conducted in order to shed light on the role of biomolecules that are derived from the tea extract of *O. basilicum*.

At a magnification of one hundred thousand times, a FESEM investigation of OBTe-AgNPs was carried out for the objective of determining their specific dimensions and shapes. Clusters of OBTe-AgNPs were found to exist, according to the findings. In Figure 4.1C, it was observed that oval-shaped OBTe-AgNPs had an average size of 55 nm. As an additional point of interest, the micrographs (see Figure 4.1C) made it abundantly evident that the OBTe-AgNPs possessed a biomolecular covering. In addition, the DLS analysis offered a comprehensive understanding of the size distribution of OBTe-AgNPs. As can be observed in Figure 4.1D, the peaks indicate the existence of two different sizes of OBTe-AgNPs, which range from 50-180 nm. In spite of this, the average size that was determined by calculating zeta potential and PDI was found to be 173 nm. This larger size in the indication from DLS analysis offers insight that smaller OBTe-AgNPs aggregate and form bulk OBTe-AgNPs, which is why agglomeration was detected in FESEM pictures. Additionally, the EDS and TEM analyses provide a distinct viewpoint of the size and structure of the OBTe-AgNPs to be examined. Figure 4.2A shows that the EDS spectra validated the presence of silver in the NPs solution. On the other hand, the transmission electron microscopy (TEM) examination revealed that the OBTe-AgNPs have an oval shape, and the average size of the OBTe-AgNPs is 35 nm (see Figure 4.2B).

It has been demonstrated by Liaqut et al. that the temperature and pH have a significant influence on the synthesis of AgNPs as well as their stability (Liagat et al., 2022). Furthermore, in order to investigate the impact that pH has on the stability of OBTe-AgNPs, we utilized pH values of 2, 4, 8, and 11 in our research. Figure 4.3A illustrates the effect that the pH of the OBTe-AgNPs that were synthesized has. At a pH of 11, the absorption peak at 435 nm indicates the production of particles with a size that is not uniform. On the other hand, the peak represents the synthesis of particles with a size that is uniform at pH 2, 4, and 8. Nevertheless, the OBTe-AgNPs maintained their stability over the whole pH spectrum. In a similar manner, the thermal stability of the synthesized AgNPs was evaluated by exposing the reaction mixture to a range of temperatures (25, 40, 60, 80, and 100 °C) for a period of thirty minutes. At temperatures of 80 and 100 °C, the peak with the highest intensity measuring 340 nm was observed Figure 4.3B). The amount of absorption increased in a manner that was proportionate to the increase in temperature. At a temperature that is considered normal, the rate of OBTe-AgNPs synthesis is increased when the temperature of the combination is raised slightly. However, the OBTe-AgNPs were stable throughout a wide temperature range, including both lower and higher temperatures. As stated by Ahmad et al., the maximum kinetic energy that exists between the AgNPs is the reason why they are able to maintain their stability even when subjected to the greatest temperature (Ahmad et al., 2022). MNPs, such as AgNPs, have a large concentration of unbound electrons, which lead to the absorption of light in the SPR band. SPR was produced as a result of the oscillation of these electrons, which was caused by the resonance of the light waves. At temperatures of 80 and 100 °C, we observed the largest absorption peaks (340 nm) due to the phenomena that occurs among AgNPs.

According to the research that has been conducted, in order for the AgNPs to be able to efficiently destroy cancer cells, they need to have a size that falls within the range of 5 to 100 nm. This will enable them to penetrate the cells and cause damage by entering them (Abbasi et al., 2023; Ivask et al., 2014). The results of our investigation, which included the use of FESEM, DLS, and TEM, demonstrated that the OBTe-AgNPs fall within the range that was determined in a previous study to be more successful in the elimination of cancer cells. As a result, cell viability assays are applied in order to collect data concerning the response of cells to AgNPs. This response encompasses the cells capacity to live, undergo cell death, and participate in metabolic activities. As a result, we subjected the HeLa cells to being exposed to OBTe-AgNPs at a range of concentrations, including 0.5, 1, 5, 10, 20, and 40 µg/ml. It was discovered from the findings that the viability of HeLa cells declined in a manner that was dependent on the dose, and it was discovered to be considerably (p < 0.001) lower at higher concentrations. After 24 hours of treatment, the vitality of the cells was seen to be 55.8%, 59.28%, 46.3%, and 36.73%, respectively, at concentrations of 5, 10, 20, and 40 μg/ml (see Figure 4.4). Furthermore, it was discovered that the IC₅₀ value was 21.78 ± 0.68 μg/ml. A number of studies were conducted to evaluate the toxicity of biosynthesized AgNPs generated from the extract of Salvia officinalis, Citrus hystrix, and Acer oblongifolium. The results of these studies revealed a decrease in cell viability in a dose-dependent manner, with the IC₅₀ value ranging from 3 to 56 µg/ml (Naveed et al., 2022; Okaiyeto et al., 2021; Srimurugan et al., 2022). The effectiveness of AgNPs that were produced from C. hystrix was investigated by Srimurugan and colleagues. Based on the results of their cell viability investigation, it was determined that the AgNPs have shown strong inhibitory activity by reducing the viability of cancer cells in a manner that is dependent on both the dosage and the period of exposure. The value of the IC₅₀, which is the concentration that is necessary to inhibit fifty percent of the cancer cells, was determined to be 56 μg/ml (Srimurugan et al., 2022). In a similar manner, Okaiyeto and colleagues conducted an evaluation to assess the toxic effects of AgNPs on HeLa cells. Their findings revealed that at a concentration of 50 μg/ml, the aqueous extract of S. officinalis and the AgNPs exhibited small toxicity on HeLa cells. According to the comparison, the proportion of viable cells was 84 ± 9 and 92 ± 0.1 , respectively, when compared to the untreated controls. According to previous research, the AgNPs that were produced by certain medicinal plants, such as Nepeta deflersiana (E. S. Al-Sheddi et al., 2018) and Curcuma aromatica had a considerable cytotoxic influence on HeLa cells (Nadhe et al., 2020).

Evidence from earlier research suggests that one mechanism by which AgNPs cause toxicity is through interfering with cellular energy metabolism, specifically by decreasing mitochondrial function and increasing oxidative stress (Carlson et al., 2008). By measuring the quantities of glutathione (GSH), superoxide anion radical $(O_2^{\bullet-})$, and nitrite (NO_2^-) , it is possible to arrive at an evaluation of the levels of oxidative stress

that are present in cells (Gwozdzinski et al., 2021). In order to assess oxidative stress, OBTe-AgNPs were subsequently exposed to HeLa cells. The findings demonstrated a dose-dependent rise in GSH levels (see Figure 4.5A). GSH levels at 20 µg/ml (32.7 µM, p < 0.05) and 40 µg/ml (40.21 µM, p < 0.005) were significantly higher. Our findings make it clear that a cell's attempt to lessen oxidative stress is reflected in its elevated GSH content. It has been shown that AgNPs cause changes in glutathione levels and the generation of ROS (Avalos et al., 2014). The decrease in antioxidants, such as glutathione and protein linked sulfhydryl groups, along with the increase in the activity of various antioxidant enzymes, may be responsible for the oxidative destruction of cell molecules. These findings indicate the occurrence of lipid peroxidation (Kurutas, 2016). The process of intracellular reduced GSH involves the oxidation of ROS generated within cells, resulting in the formation of glutathione disulfide (GSSG). The AgNPs were able to traverse the cell membrane and engage with glutathione (GSH), resulting in a notable decrease in its concentrations mostly through the oxidation of reduced GSH to glutathione (2 GSHGSSG + 2H⁺). There is a potential for the formation of a compound between Ag2⁺ and glutathione subsequent to cellular entry (H. Khan et al., 2011). Alrawi et al. conducted a study to assess the GSH level in HeLa cells following exposure to AgNPs at an IC₅₀ dosage of 3.125 µg/ml. The findings of their study revealed a slight decrease in the quantity of GSH following a 24 h exposure to synthesized AgNPs in comparison to the control group for HeLa cell lines. Nevertheless, no statistically significant variation in the GSH level was seen at the IC₅₀ dose. (ALrawi et al., 2017). Similarly, as the dose of OBTe-AgNPs increased, nitrite and superoxide anion radical concentrations in cells increased as well. At 40µg/ml (185.82 μ M, p < 0.05), the results demonstrated a notable alteration in the level of the super oxide anion radical (see Figure 4.5B). Following 24 h of treatment, the levels of nitrite were found to be considerably higher at 20 μ g/ml (30.58 μ M, p < 0.05) and 40 μ g/ml (38.6 μ M, p < 0.001), as shown in Figure 4.5C. Figure 4.5 shows that nitrite, superoxide anion radical, and GSH levels followed a pattern similar to that of cell death (see Figure 4.4). Reportedly implicated in numerous chemical and biological systems, the superoxide anion radical is a crucial radical species (Hayyan et al., 2016). The production of peroxy nitrites (ONOO⁻) mostly results from its interaction with nitric oxide (NO•) during the operation of the mitochondrial electron transport chain (ETC). Apoptosis and necrosis are two forms of programmed cell death that peroxy nitrites, a very reactive oxidizing chemical, can set in motion. The manganese superoxide dismutase (MnSOD) protein is mostly found in mitochondria and protects cells from nitric oxide by neutralizing superoxide anion (O2 •-) (Indo et al., 2015). In this context, Alsubki et al. showed that the antioxidant efficiency of CS-AgNPs in scavenging free radicals, specifically hydroxyl and superoxide radicals, was proven to be much higher than that of standard ascorbic acid, at varied doses (Alsubki et al., 2021). Another study has shown that AgNPs possess a notable ability to scavenge superoxide anion radicals, hence demonstrating a robust antioxidant activity. Furthermore, these substances have demonstrated significant cytotoxic properties by impeding the viability of Hela cells (Alahmad et al., 2021). In addition, Tosun et al. assessed the generation of ROS in MCF-7, Saos-2, A549, and HT-29 cells when introduced to artificially produced AgNPs derived from the extracts of *Rhizopogon luteolus* (RL) and *Paxina leucomelas* (PL). They noted that the AgNPs induced significantly increased oxidative stress in the examined cells as compared to untreated cells. Moreover, their findings revealed that RL-AgNPs had a greater capacity to enhance oxidative stress compared to PL-AgNPs. Experimental research conducted by the same group of researchers has revealed that the generation of ROS caused by AgNPs has been observed to initiate the intrinsic apoptotic pathway in cancer cells (Kaplan et al., 2022). The cellular formation of reactive oxygen species (ROS) is induced by the conversion of neutral silver (Ag°) to Ag⁺, Ag–S– and Ag–O– (Yu et al., 2020).

There is a correlation between increased amounts of ROS within cells and lipid peroxidation, DNA damage, and protein oxidation, which ultimately leads to the activation of the intrinsic apoptotic cascade in cells (L. J. Su et al., 2019). The intrinsic apoptotic pathway is activated when the level of cellular damage reaches a threshold point. This is accomplished by elevating the production of pro-apoptotic Bcl-2 family members (including Bax, Bok, and Bak) and lowering the levels of anti-apoptotic proteins (such Bcl-2, Bcl-w and Bcl-xL) (Hata et al., 2015). Consequently, a pivotal strategy in cancer treatment is the targeted stimulation of intrinsic apoptotic pathways mediated by ROS (Gökşen Tosun et al., 2022). To explore the likely mechanism of cellular demise resulting from exposure to OBTe-AgNPs via the apoptotic pathway, we performed an examination of the genes implicated in apoptosis, namely Bcl-2, Bax, Cas 3, 8, 9, and β -actin, employing the quantitative reverse transcription polymerase chain reaction (qRT-PCR) methodology. The findings of the study revealed a statistically significant increase (p < 0.005) in the gene expression levels of Cas 3, 8, 9, and Bcl-2 in cells treated with both 5 and 40 µg/ml, as compared to the control group (see Figure 4.6). Nevertheless, the expression of Bax remained unchanged irrespective of the dosage. According to reports, Cas 9 plays a crucial role in causing changes in the structure of mitochondria and producing ROS by breaking down and activating Bid, leading to the creation of tBid. After being activated by Cas 9, Cas 3 assumes a pivotal function in inhibiting the production of ROS and is essential for the efficient execution of apoptosis. Cas 8 and Bcl-2 play a role in both the extrinsic and intrinsic pathways of apoptosis signaling via death receptors, respectively (Hardwick & Soane, 2013). Li et al. observed an increase in the levels of Cas 3, 9, and Bcl-2 when lung adenocarcinoma (A549) cells were exposed to AgNPs at a dose range of 20-160 μg/ml (Li et al., 2021). According to the findings of a study that was carried out by Gurunathan and colleagues, the exposure of human breast cancer (MDA-MB-231) cells to AgNPs results in the activation of numerous signaling pathways, such as p53, p-Erk1/2, and Cas 3, which in turn leads to the initiation of cellular death. At the same time, the expression of Bcl-2 is downregulated (Gurunathan et al., 2015). Upon exposure to AgNPs at a concentration of 12.35 µg/ml, it was confirmed by another study that the initiation of apoptosis takes place in MCF-7 cells. This interaction takes place through the interaction between Cas 3, 8, and 9 (Ullah et al., 2020).

It is to the best of our knowledge that the type of cell death that has been produced in HeLa cells by the treatment with OBTe-AgNPs has not been explored up until this point. Because of this, we carried out an annexin FITC assay, which revealed that there were substantial amounts of both early and late apoptosis, which is evidence that apoptosis was the major mode of cell death (see Figure 4.7A). These results are in conjunction with a high level of expression of initiator *Cas* 8 and executive *Cas* 3 expressions as reported in Figure 4.6.

In light of the findings that we have obtained, we are certain that the plant-based AgNPs that we have developed can serve as an alternative to killing machines for different types of cancer cells, including those that are found in the skin, breast, and lung. However, prior to the transition of these AgNPs into clinical investigations, we would be interested in doing pre-clinical studies and environmental distribution of these AgNPs in order to ensure that they are safe to employ in both of these scenarios.

Furthermore, experts are currently prioritizing the development of a single-step cure for various disorders. In this work, we employed V. myrtillus tea extract, commonly referred to as Borovnica tea, to investigate its potential as an agent to make AgNPs with anti-cancer and anti-atherosclerosis properties. To verify the creation of VMTe-AgNPs, the first stage involved observing a color shift in the mixture from dark brown to dark black, as well as the presence of precipitation, which indicated the synthesis of AgNPs. This finding aligns with our prior investigation, whereby we employed O. basilicum tea and O. tenuiflorum extracts to synthesize AgNPs. These AgNPs were subsequently utilized as anti-cancer agents and nano pesticides, effectively eliminating HeLa cells and insect pests, respectively (Qamar et al., 2021; Qamar et al., 2024). In a comparable manner, Khan et al. found that the creation of AgNPs caused a color change during their synthesis. They investigated the possibility of using AgNPs as anti-diabetic and antibacterial medicines (Z. u. R. Khan et al., 2023). The findings of our study align with those of earlier research. Prior to reaching a conclusion, the mixed sample was subjected to UV-Visible spectroscopy within the wavelength range of 200-800 nm. The investigation conducted in this study has confirmed the presence of a peak at 305 nm in samples containing different quantities of VMTe-AgNPs, as depicted in Figure 4.8A. The reaction solution exhibited a diverse array of metabolites derived from the tea extract of V. myrtillus, which were identified within the experimental spectrophotometric range. This observation sheds light on the broad spectrum of UV-Vis absorption spectra seen. The identification and characterization of AgNPs can be facilitated through the analysis of the SPR peak. The absorbance spectra of a solution containing spherical and homogenous AgNPs exhibit a single SPR band. Prior research indicates that anisotropy has a direct impact on the number of peaks (González-Aguiñaga et al., 2023). Overall, the VMTe-AgNPs produced during biosynthesis have a consistent circular morphology. The experiment additionally induces an increase in the concentration of AgNPs and an enlargement in the size of the particles.

We employed FESEM, TEM, and DLS techniques to validate the dimensions and morphology of VMTe-AgNPs. The FESEM examination conducted at a magnification of 100 kx revealed an oval shape with a size of 52 nm (see Figure 4.8B). Furthermore, the micrographs provided unambiguous evidence of the presence of a biomolecular coating on the VMTe-AgNPs. In the same manner, TEM examination yielded precise measurements of size and shape at a magnification of 100 nm. After analyzing the TEM micrograph, it was seen that the VMTe-AgNPs had an average size of 80 nm and exhibited an oval shape (see Figure 4.8C). After analyzing the DLS data, it was found that the solution primarily consisted of VMTe-AgNPs, with an average cluster size of 196 nm. This can be attributed to the claustration of VMTe-AgNPs, as shown by a zeta potential of -27.9 and a PDI of 0.269. The DLS analysis provided valuable insights into the distribution of VMTe-AgNPs sizes in the reaction mixture. Figure 4.8D demonstrates the presence of VMTe-AgNPs with diameters ranging from 90 to 200 nm, as indicated by the peak. The increased size observed in the DLS investigation indicates that smaller VMTe-AgNPs aggregate to produce larger VMTe-AgNPs, resulting in the observed clumping in the FESEM images.

Additionally, we searched the *V. myrtillus* tea extract using FTIR for biomolecules that would aid in the reduction, bio-capture, or stabilization of Ag⁺ ions to Ag⁰. FTIR spectroscopy revealed several peaks between 400 and 4000 cm⁻¹, the most notable of which were absorption peaks at 3281.13 cm⁻¹, 2916.51 cm⁻¹, 2849.27 cm⁻¹, 1613.56 cm⁻¹, 1318.58 cm⁻¹, 1030.48 cm⁻¹, and 779.13 cm⁻¹ (see Figure 4.8F). From these

peaks, the –OH stretch of phenolic acids, polyphenols, and flavanol is represented by 3281.13 cm⁻¹, the C–H stretch by 2916.51 cm⁻¹ and 2849.27 cm⁻¹, the –C=C stretch by 1613.56 cm⁻¹, the C–O stretch by 1318.58 cm⁻¹ and 1030.48 cm⁻¹, and the aromatic compound of C–H out of plane bending by 779.13 cm⁻¹. The existence of carbonyl groups, terpenoids, polyphenols, flavonoids, alkaloids, carbohydrates, amines, and other reducing secondary metabolites, biomolecules, and proteins is indicated by the observed peaks from this study and earlier investigations (Mosoarca et al., 2022; Traksele & Snitka, 2022). It is commonly recognized that unbound carboxylate groups allow proteins to attach to MNPs (Ajitha et al., 2014). Protein carboxylate groups have the ability to serve as surfactants, which allows them to adhere to MNPs surfaces (Abarca-Cabrera et al., 2021). These compounds most likely control the bio-reduction of Ag⁺ ions.

Studies that have already been published indicate that temperature and pH affect the stability and production of AgNPs (Ahmad et al., 2022; Fernando & Zhou, 2019). Consequently, the stability of VMTe-AgNPs was assessed by subjecting them to variations in temperature and pH. The thermal stability of the VMTe-AgNPs was assessed by subjecting the reaction mixture to varying temperatures for a duration of 45 minutes at 25, 40, 60, 80, and 100 °C (see Figure 4.9A). The data presented in Figure 4.9A demonstrates a positive correlation between temperature and the extent of absorption. Nevertheless, no alteration in the stability of VMTe-AgNPs was detected, suggesting that VMTe-AgNPs exhibit stability throughout a range of temperature conditions. Raising the mixture temperature at room temperature leads to an increase in the synthesis rate of VMTe-AgNPs. However, when exposed to high temperatures, the particles experience polydispersity. Prior research indicates that the stability of AgNPs at the highest temperature is attributed to the maximum kinetic energy between the AgNPs (P. Gupta et al., 2020; Liaqat et al., 2022). In contrast, pH values of 2, 5, 6, 10, and 11 were employed in our study to examine the impact of pH on the stability of VMTe-AgNPs. The pH effect of the VMTe-AgNPs produced is depicted in Figure 4.9B. Particles with non-uniform diameters are shown by the absorption peak at 550 nm for pH 2, 10, and 11. In contrast, the presence of a peak at pH 5 and 6 signifies the occurrence of particles that possess consistent diameters. These finding are in parallel with our previously published study in which AgNPs were prepared from O. basilicum L. tea (Qamar et al., 2024).

Previous research has indicated that in order to effectively eliminate cancer cells through penetration, it is necessary for the size of AgNPs to fall between the range of 10-100 nm. The results obtained from FESEM and TEM examination indicate that VMTe-AgNPs are suitable for effective biological applications within the specified range. Hence, in order to examine and determine the optimal dosage of VMTe-AgNPs as a means to combat cancer and atherosclerosis, the cells were subjected to different concentrations (10, 20, 40, 60 µg/ml) for durations of 24 and 72 h (see Figure 4.10). As the dose of VMTe-AgNPs increases, the viability of MDA-MB-231 and HUVEC cells diminishes, according to the results (see Figure 4.10A-B). The viability of MDA-MB-231 cells at 40 and 60 µg/ml was seen to be 32.41% (p < 0.01) and 25.2% (p < 0.01) after a 24-h period. In the 24-h group, the IC50 value was 29.69 \pm 1.47 µg/ml. However, it was observed that the cell viability in the same dose group had considerably (p < 0.001) decreased to 21.35% and 11.2%, respectively, after 72 h (see Figure 4.10A). In the 72-h group, the IC50 value was 20 \pm 1.30 µg/ml. AgNPs from *Bacillus funiculus* were synthesized by Gurunathan et al., who then evaluated their anti-cancer potential

against MDA-MB-231. They discovered a reduction in cell viability that was dosage dependent and reported an IC₅₀ value of 8.7 μ g/ml (Gurunathan et al., 2013). Xu et al. observed that AgNPs derived from *Allium saralicum* exhibited a comparable decrease in cell viability of MDA-MB-231 cells, with an IC₅₀ value of 250 μ g/ml, which was dependent on the dosage administered (X. Xu et al., 2023). Furthermore, another study documented a comparable result in which AgNPs generated by Adina cordifolia were subjected to MDA-MB-231, resulting in an IC₅₀ value of 64.92 μ g/ml (Koteswara Rao et al., 2021).

The HUVEC cell lines exhibited a similar pattern of cell viability decline that was dosage dependent. The vitality of HUVEC cells was found to be 64.22% (p < 0.05), 32.89% (p < 0.001), 28.5% (p < 0.001) and 16.47% (p < 0.001) in 10, 20, 40 and 60 µg/ml, respectively, after 24 h. There was a substantial decrease in cell viability to 55.32% (p < 0.05), 28.54% (p < 0.01), 22.74% (p < 0.01), and 8.19% (p < 0.001), respectively, after 72 h in the same dosing group (see Figure 4.10B). In the 24 and 72 h group, the IC₅₀ value was determined to be 17.72 \pm 1.25 and 20.38 \pm 1.31 µg/ml, respectively. We saw a dose-dependent decrease in cell viability in both cell lines, which is consistent with other research that has been published and suggests that VMTe-AgNPs may have anti-cancer and anti-atherosclerotic properties. Taking into account the IC₅₀ values and adhering to the American National Cancer Institute (NCI) criteria for cytotoxicity, which state that a substance is considered cytotoxic if the IC₅₀ value is less than 30 µg/ml (Suffness & Pezzuto, 1991), it appears that our VMTe-AgNPs can be classified as significantly cytotoxic.

Previous studies have indicated that AgNPs toxicity can be accounted for in part by their impact on cellular energy metabolism, which reduces mitochondrial function and raises oxidative stress (Carlson et al., 2008). Examining the concentrations of glutathione (GSH), superoxide anion radical (O2°-), and nitrite (NO2-) in the cell environment is one technique to gauge the degree of oxidative stress in cells (Gwozdzinski et al., 2021; Qamar et al., 2024). GSH plays a crucial role in the removal of ROS and reactive nitrogen species (RNS) by either directly interacting with them or acting as a cofactor in the GSH redox cycle. This cycle involves the interaction between GSH peroxidase, GSH S-transferases, and GSH reductase (Conde de la Rosa et al., 2014). Consequently, MDA-MB-231 cells and HUVEC cells were subjected to different concentrations (20, 40, and 60 µg/ml) of VMTe-AgNPs. In the MDA-MB-231 cell line, a dose-dependent elevation in the concentrations of GSH, O₂•-, and NO₂- was observed following a 24-h exposure to VMTe-AgNPs, indicating an adaptive response to oxidative stress. Nevertheless, despite the observed increase in dosage, it was determined that not all dose groups exhibited a statistically significant increase when compared to the control group (see Figure 4.11). These findings suggest that the cells experience oxidative stress and exhibit adaptive responses to mitigate the detrimental effects induced by our VMTe-AgNPs. Nevertheless, although there was no substantial rise in ROS, the damage is significant, leading to reduced cell viability at the highest concentrations of VMTe-AgNPs after 24 h of treatment (refer to figure 4.10A-B). In a similar way, we observed a dose-dependent rise in the concentrations of GSH, O₂•-, and NO₂⁻ in the group treated for 72 h. However, it was only noticed that there were statistically significant increases in the concentration of O₂• at 40 µg/ml (26.63 µM, p < 0.001) and 60 µg/ml (38.74 µM, p < 0.001) when compared to the control group (refer to Figure 4.11B). This finding aligns with the cytotoxicity outcomes depicted in Figure 4.10A. Prior research involving the exposure of MDA-MB-231 cells to AgNPs has documented the generation of ROS, leading to cellular demise through apoptosis. In their study, Gurunathan et al. observed a dose-dependent elevation in ROS levels, which ultimately resulted in the beginning of apoptosis in MDA-MB-231 cells when exposed to silver nanoparticles generated by *B. funiculus* (Gurunathan et al., 2013). Another work involved the synthesis of AgNPs using *Phlomis armeniaca*. The researcher observed the generation of ROS in MDA-MB-231 cells and confirmed that the cells died through apoptosis in a manner that depended on the dosage (Yesilot et al., 2023).

Conversely, HUVEC cells were observed to be more vulnerable to the generation of ROS when exposed to VMTe-AgNPs. A non-significant dose-dependent rise in GSH was seen at concentrations of 20, 40, and 60 µg/ml in the 24-h treatment group. However, during a 72-h treatment period, we found a consistent and dose-dependent rise in GSH concentration across all treatment doses. Although there was a dosedependent increase, it was observed that only the group receiving a dose of 60 µg/ml showed statistical significance (p < 0.01) compared to the control group (see Figure 4.12A). This finding suggests that cells attempt to cope with ROS stress by increasing their production of GSH at higher concentrations. This is supported by the fact that cell viability was also reduced at the same concentration after 72 h of treatment, as depicted in Figure 4.10B. Likewise, a comparable dose-dependent elevation in the concentration of O₂• was seen following a 24-72 h exposure to VMTe-AgNPs. A statistically not significant difference in concentration was detected in 20, 40 and 60 µg/ml dosage group and the control group. In contrast, it was noted that after a duration of 72 h, there were similar statistically not significant increases in the concentration of O₂• across all treatment concentrations as compared to the control group (see Figure 4.12B). Furthermore, both the 24 h and 72 h treatment groups exhibited a comparable increase in nitrite (NO₂⁻) concentration, which was dependent on the dosage. A statistically not significant difference was observed in the concentration of the 20, 40, 60 µg/ml dosage group compared to the control group in the 24-h exposure group. In contrast, we observed statistically significant (p < 0.01) elevations in NO₂⁻ concentration at concentrations of 20, 40, and 60 µg/ml in the group exposed to 72 h of VMTe-AgNPs, as compared to the control group (see Figure 4.12C).

Based on these findings, we have determined that the primary species of ROS is the superoxide anion radical $(O_2^{\bullet -})$, which is responsible for causing cell death. The superoxide anion, a primary oxygen radical, is generated when an oxygen molecule acquires an electron. The initial generation of O₂•- triggers a cascade of ROS, wherein specific species, such as H₂O₂, play a crucial role in cellular signaling, while others, such as HO, have detrimental effects (Andrés et al., 2023). The biological impact of these chemicals will eventually be contingent upon cellular defense mechanisms, the abundance of ROS, and the cellular adaptability (Hancock, 2021). O2^{•-}, which is generated as a byproduct of the mitochondrial respiratory chain, is a prominent ROS that plays a crucial role in inducing oxidative stress in living organisms. The reduced permeability of superoxide across membranes can be attributed to its electric charge. While superoxide is able to pass through anion channels, its effectiveness is limited. As a result, the physiological compartment from where superoxide originates is the primary site of major superoxide reaction (Turrens & Boveris, 1980). Based on the obtained results, a preliminary mechanism of oxidative stress resulting in cellular demise was established (see Figure 5.1).

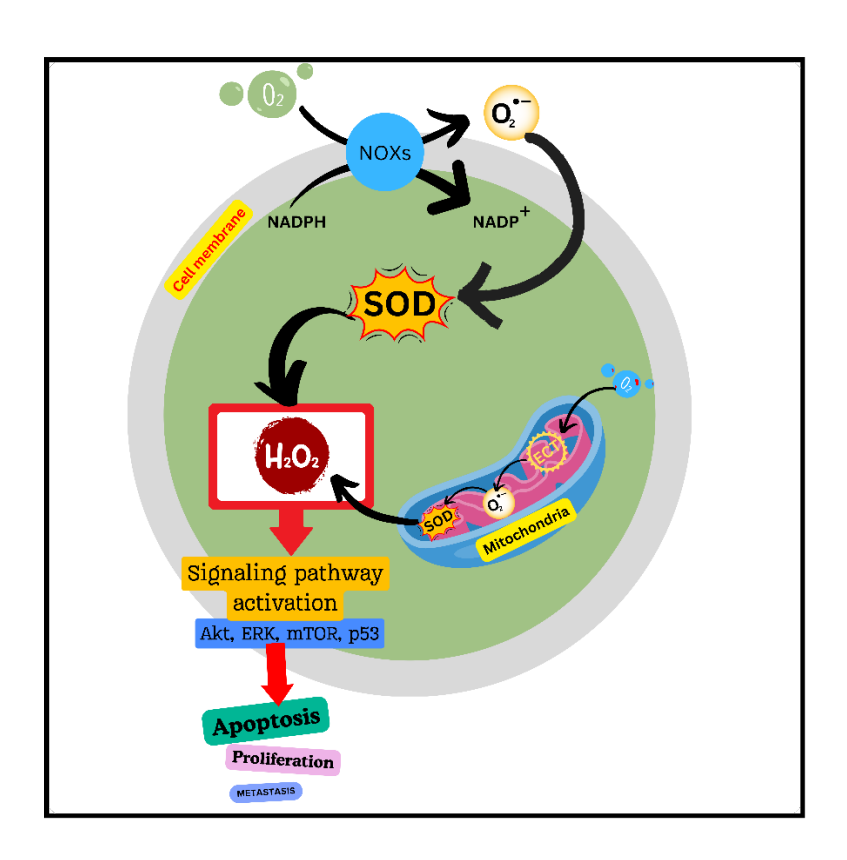


Figure 5.1. Potential mechanisms behind cellular apoptosis

The natural world has had NFs for millions of years, and they have been very important in many biological processes. The extracellular matrix (ECM) NFs, the protein and polysaccharide-based cytoskeletons, and the NFs of silkworms and spiders are all good examples. Electrospun nanofibers are used in a lot of different fields, like biosensors, clothing making, and water filtering (Virijević et al., 2023; Virijević et al., 2024). It is important to note that they are frequently used as scaffolds in tissue engineering. However, our research is focused on the production, properties, and application of AgNPs-incorporated NFs in the DCBs coating membrane for the treatment of atherosclerosis. This was achieved through the utilization of the electrospinning technique, a sophisticated multiphase process that is distinguished by the introduction of an exceptionally powerful electric field (Živanović, 2020) (see Figure 3.2). Synthetic polymers, carbohydrate polymers, and protein-based polymers are the three types of polymers that researchers seem to choose most often. Nylon-66, PCL, PLLA, PEG, and PVA are some of the synthetic plastics that are often used (Adeli et al., 2019; Capuana et al., 2022; X. Liu et al., 2022). Synthetic polymers are popular due to their availability, homogenous monomer dispersion, cost, and solubility. Therefore, to create AgNPs integrated NFs, we used PEG-PCl polymers. Our NFs were characterized by FTIR, SEM, and AFM for changes in OBTe-AgNP encapsulation with polymer, NF membrane size and shape, and surface structure, respectively.

FTIR analysis of OBTe-AgNPs-NFs was conducted to observe the integration of biogenic OBTe-AgNPs into NFs. The spectra of OBTe-AgNPs-NFs exhibited distinct peaks at around 1700 cm⁻¹, indicating the stretching of C=O bonds, and in the region of 1100-1200 cm⁻¹, indicating the stretching vibrations of C-O-C bonds and -COO-bonds, which are specific to NFs. In contrast, the spectra of biogenic OBTe-AgNPs do not exhibit any distinct absorption bands in this region, suggesting the successful formation of AgNPs-NFs as shown in figure 4.13.

In addition, the FESEM was employed to observe the morphological distinctions among all the different forms of OBTe-AgNPs-NFs (as shown in figure 4.14). The mean diameter of OBTe-AgNPs-NFs with concentrations of 1%, 2%, and 3% was observed to be 179.29 ± 18.65 nm, 181.55 ± 12.67 nm, and 194.80 ± 17.80 nm, respectively. The diameter of the fibers in all versions of OBTe-AgNPs-NFs ranged from 168.21 to 216.26 nm. Conversely, NFs without AgNPs had an average diameter of 472.68 ± 51.33 nm, ranging from 406.84 to 572.95 nm. The presence of charge conducting MNPs in NFs could be the source of the difference in diameter between NFs containing OBTe-AgNPs and NFs that do not contain AgNPs.

The surface roughness was examined and assessed using AFM. Two viable ways to describe a surface's roughness parameter are as an average along the surface's centerline or as the distance between the two extremes of the surface's irregularities. The 1%, 2%, and 3% OBTe-AgNPs-NFs had average surface roughness (Ra) values of 72.77, 98.34, and 149.01 nm, respectively, according to our research. Surface roughness increases as the percentage of OBTe-AgNPs incorporated into NFs increases. Figure 4.15 shows that when the fraction of incorporated OBTe-AgNPs increases, more OBTe-AgNPs collect on the surface of NFs. When Dubey et al. synthesized in-vitro AgNPs-NFs for wound healing activities, they observed findings that were comparable to those described above. The surface roughness of AgNPs-NFs was measured to be 305.8 nm, as indicated by their findings (Dubey et al., 2015). According to the findings of another study conducted by Xu and colleagues, the surface roughness increases rely on the chemical that is added to the polymer mixture in order to generate NFs. As a result, roughness has a direct impact on the number of cells that stick to the material (C. Xu et al., 2004). This is the reason we observed an increase in surface roughness of our NFs depended on amount of OBTe-AgNPs added to polymer mixture. Findings from the AFM corroborate those from the SEM pictures and the Ag ion release profile.

It is important for the NFs membrane to break down so that AgNPs can be released from their individual NFs. In the first week of the degradation assay, our earlier study showed that about half of the NFs membrane was broken down (Virijević et al., 2024). Therefore, *in-vitro* Ag-release profiles were used to examine the sustainability of OBTe-AgNPs in PEG-PCL nanofibers under various physiological circumstances and time periods. The encapsulated OBTe-AgNPs release rate demonstrated a steady, continuous release that followed an initial burst release that lasted for three to twentyfour hours (see Figure 4.16). Approximately half of the encapsulated OBTe-AgNPs were released from the NFs during the course of the 96-h incubation period. Diffusion of OBTe-AgNPs that were adsorbed at the surface of the polymeric NFs may have caused the first burst release of OBTe-AgNPs. Nonetheless, the prolonged release of OBTe-AgNPs in later phases may have resulted from the breakdown of PEG inside the polymeric matrix or from the diffusion of encapsulated OBTe-AgNPs from the polymeric NFs core area. The results showed that these NFs have the potential to be useful for the long-term, sustained administration of biogenic AgNPs for biomedical applications, which is consistent with the findings of Wu et al. (Wu et al., 2014) and Dubey et al. (Dubey et al., 2015).

The release profile investigation makes it clear that biogenic OBTe-AgNPs were gradually released from NFs. Using HEVEC cells as an atherosclerosis model, we conducted a cell viability analysis to determine the practical anti-atherosclerosis capability of these OBTe-AgNPs included NFs membranes as DCBs coating material (Medina-Leyte et al., 2020). In order to observe the practical use of OBTe-AgNPs-NFs

in the treatment of atherosclerosis, all different forms of OBTe-AgNPs-NFs were tested on atherosclerosis model HUVEC cells. The cell viability was assessed using the MTT test, as seen in figure 4.17. The findings revealed that the survival rate of HUVEC cells decreased considerably (p < 0.001) as the dose of OBTe-AgNPs in NFs increased, relative to the control group, after 24 and 72 h of exposure. Following a 24-h exposure to OBTe-AgNPs-NFs, the vitality of HUVEC cells in the dose groups of 1%, 2%, and 3% OBTe-AgNPs-NFs was measured to be 61.64%, 20.03%, and 14.68%, respectively. In contrast, after being exposed to OBTe-AgNPs-NFs after 72 h, the vitality of HUVEC cells in the dose groups of 1%, 2%, and 3% was 39.91%, 18.46%, and 11.79%, respectively.

As far as the field of cardiovascular science is concerned, our research is the first to investigate the toxicological implications of biogenic AgNPs combined with NFs as a possible weapon against atherosclerosis. So far, we have not come across any other study that has investigated this specific area of inquiry.

Chapter 6

Conclusion

In conclusion, using Bosiljak extract (which comes from traditional Serbian tea manufactured from *Ocimum basilicum* L.) is an attractive strategy for producing AgNPs in an environmentally conscious and economically viable manner. Nanotechnology and cancer treatment might benefit greatly from this strategy. The unique properties and toxic effects on HeLa cells of the AgNPs produced using this method were exposed by thorough analysis. An inhibitory concentration (IC50) of $21.78 \pm 0.68 \,\mu\text{g/ml}$ was found, indicating that the results show a dosage-dependent decrease in cell viability. Our findings provide more evidence that this medicinal substance may be useful in the fight against cervical cancer. The research also looked at how this cytotoxicity worked, revealing that ROS and the control of apoptotic gene expression were key players. Such results suggest that AgNPs derived from Bosiljak extract may be useful in the treatment of human cervical cancer.

In addition to that, AgNPs synthesized from Borovnica tea extract showed great potential for producing NPs in an eco-friendly and cost-effective manner. The VMTe-AgNPs displayed unique characteristics, such as a surface plasmon resonance observed at 344 nm, an oval shape with an average diameter ranging from 52-80 nm and demonstrated cytotoxic effects on breast adenocarcinoma epithelial cells (MDA-MB-231) and human umbilical vein endothelial cells (HUVEC). The inhibitory concentrations (IC50) for MDA-MB-231 and HUVAC were measured at 30 \pm 1.5 and 18 \pm 1.3 $\mu g/ml$, respectively. In addition, the observed cytotoxicity mediated by ROS indicates promising possibilities for cancer treatment and managing atherosclerosis.

Moreover, the biogenic OBTe-AgNPs were successfully incorporated into the polyethylene glycol-polycaprolactone NFs mats utilizing the blended electrospinning technique. The NFs membranes, including different weight percentages of OBTe-AgNPs (1%, 2%, and 3%), were incorporated into NFs. When assessing the potential of a scaffold for biomedical applications, it is essential to examine the suitability of its structure and the way it releases drugs. Hence, a thorough examination of surface roughness and drug release profile was carried out, and the results were discovered to be remarkably congruent with the previously recorded data for ideal biomedical applications. Research on the prevention of atherosclerosis demonstrated that the suppression of HUVEC cells differed according to the dosage. Nevertheless, it is necessary to carry out animal research in order to ascertain the functionality and safety in model organisms.

These findings highlight the promising potential of OBTe-AgNPs, VMTe-AgNPs and OBTe-AgNPs-NFs for future research in the field of cancer therapy and atherosclerosis treatment. Additional research is needed to investigate their effectiveness, safety, and *in-vivo* mechanisms, which could potentially lead to their application in clinical settings.

References

- Abarca-Cabrera, L., Fraga-García, P., & Berensmeier, S. (2021). Bio-nano interactions: binding proteins, polysaccharides, lipids and nucleic acids onto magnetic nanoparticles. *Biomater Res*, 25(1), 12. doi:10.1186/s40824-021-00212-y
- Abbasi, R., Shineh, G., Mobaraki, M., Doughty, S., & Tayebi, L. (2023). Structural parameters of nanoparticles affecting their toxicity for biomedical applications: a review. *Journal of Nanoparticle Research*, 25(3), 43. doi:10.1007/s11051-023-05690-w
- Abdelkhalek, A., El-Gendi, H., Alotibi, F. O., Al-Askar, A. A., Elbeaino, T., Behiry, S. I., Abd-Elsalam, K. A., & Moawad, H. (2022). Ocimum basilicum-mediated synthesis of silver nanoparticles induces innate immune responses against cucumber mosaic virus in squash. *Plants*, 11(20), 2707.
- Abdelsattar, A. S., Hakim, T. A., Rezk, N., Farouk, W. M., Hassan, Y. Y., Gouda, S. M., & El-Shibiny, A. (2022). Green Synthesis of Silver Nanoparticles Using Ocimum basilicum L. and Hibiscus sabdariffa L. Extracts and Their Antibacterial Activity in Combination with Phage ZCSE6 and Sensing Properties. *Journal of Inorganic and Organometallic Polymers and Materials*, 32(6), 1951-1965. doi:10.1007/s10904-022-02234-y
- Abu-Dief, A. M., Abdel-Rahman, L. H., Abd-El Sayed, M. A., Zikry, M. M., & Nafady, A. (2020). Green Synthesis of AgNPs() Ultilizing Delonix Regia Extract as Anticancer and Antimicrobial Agents**. *ChemistrySelect*, 5(42), 13263-13268. doi:https://doi.org/10.1002/slct.202003218
- Adeli, H., Khorasani, M. T., & Parvazinia, M. (2019). Wound dressing based on electrospun PVA/chitosan/starch nanofibrous mats: Fabrication, antibacterial and cytocompatibility evaluation and in vitro healing assay. *International journal of biological macromolecules*, 122, 238-254.
- Adlakha, S., Sheikh, M., Wu, J., Burket, M. W., Pandya, U., Colyer, W., Eltahawy, E., & Cooper, C. J. (2010). Stent fracture in the coronary and peripheral arteries. *Journal of interventional cardiology*, 23(4), 411-419.
- Ahmad, N., Fozia, Jabeen, M., Haq, Z. U., Ahmad, I., Wahab, A., Islam, Z. U., Ullah, R., Bari, A., Abdel-Daim, M. M., El-Demerdash, F. M., & Khan, M. Y. (2022). Green Fabrication of Silver Nanoparticles using Euphorbia serpens Kunth Aqueous Extract, Their Characterization, and Investigation of Its In Vitro Antioxidative, Antimicrobial, Insecticidal, and Cytotoxic Activities. *BioMed Research International*, 2022, 5562849. doi:10.1155/2022/5562849
- Ahmed, S. F., Mofijur, M., Rafa, N., Chowdhury, A. T., Chowdhury, S., Nahrin, M., Islam, A. B. M. S., & Ong, H. C. (2022). Green approaches in synthesising nanomaterials for environmental nanobioremediation: Technological advancements, applications, benefits and challenges. *Environmental Research*, 204, 111967. doi:https://doi.org/10.1016/j.envres.2021.111967
- Ahn, E.-Y., & Park, Y. (2020). Anticancer prospects of silver nanoparticles greensynthesized by plant extracts. *Materials Science and Engineering: C, 116*, 111253. doi:https://doi.org/10.1016/j.msec.2020.111253
- Ajaykumar, A. P., Mathew, A., Chandni, A. P., Varma, S. R., Jayaraj, K. N., Sabira, O., Rasheed, V. A., Binitha, V. S., Swaminathan, T. R., Basheer, V. S., Giri, S., & Chatterjee, S. (2023). Green Synthesis of Silver Nanoparticles Using the Leaf Extract of the Medicinal Plant, Uvaria narum and Its Antibacterial, Antiangiogenic, Anticancer and Catalytic Properties. *Antibiotics*, 12(3), 564. Retrieved from https://www.mdpi.com/2079-6382/12/3/564

- Ajitha, B., Ashok Kumar Reddy, Y., & Reddy, P. S. (2014). Biogenic nano-scale silver particles by Tephrosia purpurea leaf extract and their inborn antimicrobial activity. *Spectrochimica Acta Part A: Molecular and Biomolecular Spectroscopy*, 121, 164-172. doi:https://doi.org/10.1016/j.saa.2013.10.077
- Al-Dujaili, A. N. G., & Al-Shemeri, M. K. (2016). Effect of Silver Nanoparticles and Rosuvastatin on Endothelin and Obestatin in Rats Induced By High Fat-Diet. *Research Journal of Pharmaceutical Biological and Chemical Sciences*, 7(3), 1022-1030.
- Al-Khalaf, A. A., Hassan, H. M., Alrajhi, A. M., Mohamed, R. A. E. H., & Hozzein, W. N. (2021). Anti-Cancer and Anti-Inflammatory Potential of the Green Synthesized Silver Nanoparticles of the Red Sea Sponge Phyllospongia lamellosa Supported by Metabolomics Analysis and Docking Study. *Antibiotics*, 10(10), 1155. Retrieved from https://www.mdpi.com/2079-6382/10/10/1155
- Al-Sheddi, E. S., Alsohaibani, N., bin Rshoud, N., Al-Oqail, M. M., Al-Massarani, S. M., Farshori, N. N., Malik, T., Al-Khedhairy, A. A., & Siddiqui, M. A. (2023). Anticancer efficacy of green synthesized silver nanoparticles from Artemisia monosperma against human breast cancer cells. South African Journal of Botany, 160, 123-131.
- Al-Sheddi, E. S., Farshori, N. N., Al-Oqail, M. M., Al-Massarani, S. M., Saquib, Q., Wahab, R., Musarrat, J., Al-Khedhairy, A. A., & Siddiqui, M. A. (2018). Anticancer Potential of Green Synthesized Silver Nanoparticles Using Extract of Nepeta deflersiana against Human Cervical Cancer Cells (HeLA). *Bioinorg Chem Appl*, 2018, 9390784. doi:10.1155/2018/9390784
- Alahmad, A., Feldhoff, A., Bigall, N. C., Rusch, P., Scheper, T., & Walter, J.-G. (2021). Hypericum perforatum L.-Mediated Green Synthesis of Silver Nanoparticles Exhibiting Antioxidant and Anticancer Activities. *Nanomaterials*, 11(2), 487. Retrieved from https://www.mdpi.com/2079-4991/11/2/487
- Alotaibi, A. M., Alsaleh, N. B., Aljasham, A. T., Tawfik, E. A., Almutairi, M. M., Assiri, M. A., Alkholief, M., & Almutairi, M. M. (2022). Silver nanoparticle-based combinations with antimicrobial agents against antimicrobial-resistant clinical isolates. *Antibiotics*, 11(9), 1219.
- ALrawi, N. N., Al-Ani, M. Q., Tawfeeq, A. T., & Yaseen, N. Y. (2017). Growth inhibition and apoptosis induction in two types of women cancer cell lines using laser ablated silver nanoparticles in polyvinylpyrrolidone solution. *Iraqi Journal of Cancer and Medical Genetics*, 10(2).
- Alsareii, S. A., Manaa Alamri, A., AlAsmari, M. Y., Bawahab, M. A., Mahnashi, M. H., Shaikh, I. A., Shettar, A. K., Hoskeri, J. H., & Kumbar, V. (2022). Synthesis and characterization of silver nanoparticles from Rhizophora apiculata and studies on their wound healing, antioxidant, anti-inflammatory, and cytotoxic activity. *Molecules*, 27(19), 6306.
- Alsubki, R., Tabassum, H., Abudawood, M., Rabaan, A. A., Alsobaie, S. F., & Ansar, S. (2021). Green synthesis, characterization, enhanced functionality and biological evaluation of silver nanoparticles based on Coriander sativum. *Saudi J Biol Sci*, 28(4), 2102-2108. doi:10.1016/j.sjbs.2020.12.055
- Altammar, K. A. (2023). A review on nanoparticles: characteristics, synthesis, applications, and challenges. *Front Microbiol*, 14, 1155622. doi:10.3389/fmicb.2023.1155622
- Amooaghaie, R., Saeri, M. R., & Azizi, M. (2015). Synthesis, characterization and biocompatibility of silver nanoparticles synthesized from Nigella sativa leaf

- extract in comparison with chemical silver nanoparticles. *Ecotoxicology and Environmental Safety*, 120, 400-408.
- Andrés, C. M. C., Pérez de la Lastra, J. M., Andrés Juan, C., Plou, F. J., & Pérez-Lebeña, E. (2023). Superoxide Anion Chemistry-Its Role at the Core of the Innate Immunity. *Int J Mol Sci*, 24(3). doi:10.3390/ijms24031841
- Ašćerić, R. R., Dimković, N. B., Trajković, G. Ž., Ristić, B. S., Janković, A. N., Durić, P. S., & Ilijevski, N. S. (2019). Prevalence, clinical characteristics, and predictors of peripheral arterial disease in hemodialysis patients: a cross-sectional study. *BMC Nephrology*, 20(1), 281. doi:10.1186/s12882-019-1468-x
- Asgary, V., Shoari, A., Baghbani-Arani, F., Sadat Shandiz, S. A., Khosravy, M. S., Janani, A., Bigdeli, R., Bashar, R., & Cohan, R. A. (2016). Green synthesis and evaluation of silver nanoparticles as adjuvant in rabies veterinary vaccine. *International journal of nanomedicine*, 11(null), 3597-3605. doi:10.2147/IJN.S109098
- Avalos, A., Haza, A. I., Mateo, D., & Morales, P. (2014). Cytotoxicity and ROS production of manufactured silver nanoparticles of different sizes in hepatoma and leukemia cells. *Journal of Applied Toxicology*, 34(4), 413-423.
- Axel, D. I., Kunert, W., Göggelmann, C., Oberhoff, M., Herdeg, C., Küttner, A., Wild, D. H., Brehm, B. R., Riessen, R., & Köveker, G. (1997). Paclitaxel inhibits arterial smooth muscle cell proliferation and migration in vitro and in vivo using local drug delivery. *Circulation*, *96*(2), 636-645.
- Bailey, A. G. (1984). Electrostatic spraying of liquids. *Physics Bulletin*, 35(4), 146.
- Baskar, R., Dai, J., Wenlong, N., Yeo, R., & Yeoh, K. W. (2014). Biological response of cancer cells to radiation treatment. *Front Mol Biosci, 1*, 24. doi:10.3389/fmolb.2014.00024
- Beebe-Dimmer, J. L., Pfeifer, J. R., Engle, J. S., & Schottenfeld, D. (2005). The epidemiology of chronic venous insufficiency and varicose veins. *Annals of epidemiology*, 15(3), 175-184.
- Begicevic, R. R., & Falasca, M. (2017). ABC Transporters in Cancer Stem Cells: Beyond Chemoresistance. *Int J Mol Sci*, 18(11). doi:10.3390/ijms18112362
- Benyettou, F., Rezgui, R., Ravaux, F., Jaber, T., Blumer, K., Jouiad, M., Motte, L., Olsen, J.-C., Platas-Iglesias, C., & Magzoub, M. (2015). Synthesis of silver nanoparticles for the dual delivery of doxorubicin and alendronate to cancer cells. *Journal of Materials Chemistry B*, 3(36), 7237-7245.
- Bray, F., Laversanne, M., Weiderpass, E., & Soerjomataram, I. (2021). The everincreasing importance of cancer as a leading cause of premature death worldwide. *Cancer*, 127(16), 3029-3030. doi:https://doi.org/10.1002/cncr.33587
- Cao, Z., Li, J., Fang, Z., Feierkaiti, Y., Zheng, X., & Jiang, X. (2022). The factors influencing the efficiency of drug-coated balloons. *Frontiers in Cardiovascular Medicine*, 9.
- Capuana, E., Lopresti, F., Ceraulo, M., & La Carrubba, V. (2022). Poly-1-lactic acid (PLLA)-based biomaterials for regenerative medicine: a review on processing and applications. *Polymers*, 14(6), 1153.
- Carlson, C., Hussain, S. M., Schrand, A. M., K. Braydich-Stolle, L., Hess, K. L., Jones, R. L., & Schlager, J. J. (2008). Unique Cellular Interaction of Silver Nanoparticles: Size-Dependent Generation of Reactive Oxygen Species. *The Journal of Physical Chemistry B*, 112(43), 13608-13619. doi:10.1021/jp712087m

- Chang, C.-H., Lin, J.-W., Hsu, J., Wu, L.-C., & Lai, M.-S. (2016). Stent revascularization versus bypass surgery for peripheral artery disease in type 2 diabetic patients—an instrumental variable analysis. *Scientific Reports*, 6(1), 37177.
- Chorny, M., Fishbein, I., Yellen, B. B., Alferiev, I. S., Bakay, M., Ganta, S., Adamo, R., Amiji, M., Friedman, G., & Levy, R. J. (2010). Targeting stents with local delivery of paclitaxel-loaded magnetic nanoparticles using uniform fields. *Proceedings of the National Academy of Sciences*, 107(18), 8346-8351.
- Chouke, P. B., Shrirame, T., Potbhare, A. K., Mondal, A., Chaudhary, A. R., Mondal, S., Thakare, S. R., Nepovimova, E., Valis, M., Kuca, K., Sharma, R., & Chaudhary, R. G. (2022). Bioinspired metal/metal oxide nanoparticles: A road map to potential applications. *Materials Today Advances*, 16, 100314. doi:https://doi.org/10.1016/j.mtadv.2022.100314
- Conde de la Rosa, L., García-Ruiz, C., & Fernández-Checa, J. C. (2014). Glutathione in Mammalian Biology. In I. Laher (Ed.), *Systems Biology of Free Radicals and Antioxidants* (pp. 617-644). Berlin, Heidelberg: Springer Berlin Heidelberg.
- Cornejo Del Río, V., Mostaza, J., Lahoz, C., Sánchez-Arroyo, V., Sabín, C., López, S., Patrón, P., Fernández-García, P., Fernández-Puntero, B., Vicent, D., Montesano-Sánchez, L., García-Iglesias, F., González-Alegre, T., Estirado, E., Laguna, F., de Burgos-Lunar, C., Gómez-Campelo, P., Abanades-Herranz, J. C., de Miguel-Yanes, J. M., & Salinero-Fort, M. A. (2017). Prevalence of peripheral artery disease (PAD) and factors associated: An epidemiological analysis from the population-based Screening PRE-diabetes and type 2 DIAbetes (SPREDIA-2) study. *PloS one*, *12*(10), e0186220. doi:10.1371/journal.pone.0186220
- Crawford, S. (2013). Is it time for a new paradigm for systemic cancer treatment? Lessons from a century of cancer chemotherapy. *Frontiers in Pharmacology*, 4, 68
- Creager, M. A. (2020). A Bon VOYAGER for peripheral artery disease. In (Vol. 382, pp. 2047-2048): Mass Medical Soc.
- Danenberg, H. D., Golomb, G., Groothuis, A., Gao, J., Epstein, H., Swaminathan, R. V., Seifert, P., & Edelman, E. R. (2003). Liposomal alendronate inhibits systemic innate immunity and reduces in-stent neointimal hyperplasia in rabbits. *Circulation*, 108(22), 2798-2804. doi:10.1161/01.Cir.0000097002.69209.Cd
- Dangas, G. D., Serruys, P. W., Kereiakes, D. J., Hermiller, J., Rizvi, A., Newman, W., Sudhir, K., Smith, R. S., Cao, S., & Theodoropoulos, K. (2013). Meta-analysis of everolimus-eluting versus paclitaxel-eluting stents in coronary artery disease: final 3-year results of the SPIRIT clinical trials program (Clinical Evaluation of the Xience V Everolimus Eluting Coronary Stent System in the Treatment of Patients With De Novo Native Coronary Artery Lesions). *JACC: Cardiovascular Interventions*, 6(9), 914-922.
- Deb, P. K., Kokaz, S. F., Abed, S. N., Paradkar, A., & Tekade, R. K. (2019). Chapter 6 Pharmaceutical and Biomedical Applications of Polymers. In R. K. Tekade (Ed.), *Basic Fundamentals of Drug Delivery* (pp. 203-267): Academic Press.
- DeVierno Kreuder, A., House-Knight, T., Whitford, J., Ponnusamy, E., Miller, P., Jesse, N., Rodenborn, R., Sayag, S., Gebel, M., Aped, I., Sharfstein, I., Manaster, E., Ergaz, I., Harris, A., & Nelowet Grice, L. (2017). A Method for Assessing Greener Alternatives between Chemical Products Following the 12 Principles of Green Chemistry. *ACS Sustainable Chemistry & Engineering*, 5(4), 2927-2935. doi:10.1021/acssuschemeng.6b02399

- Dinparvar, S., Bagirova, M., Allahverdiyev, A. M., Abamor, E. S., Safarov, T., Aydogdu, M., & Aktas, D. (2020). A nanotechnology-based new approach in the treatment of breast cancer: Biosynthesized silver nanoparticles using Cuminum cyminum L. seed extract. *Journal of Photochemistry and Photobiology B: Biology, 208*, 111902. doi:https://doi.org/10.1016/j.jphotobiol.2020.111902
- dos Santos, M. A., Paterno, L. G., Moreira, S. G. C., & Sales, M. J. A. (2019). Original photochemical synthesis of Ag nanoparticles mediated by potato starch. *SN Applied Sciences*, 1, 1-13.
- Dubey, P., Bhushan, B., Sachdev, A., Matai, I., Uday Kumar, S., & Gopinath, P. (2015). Silver-nanoparticle-Incorporated composite nanofibers for potential wound-dressing applications. *Journal of Applied Polymer Science*, 132(35). doi:https://doi.org/10.1002/app.42473
- Duft, D., Achtzehn, T., Müller, R., Huber, B. A., & Leisner, T. (2003). Rayleigh jets from levitated microdroplets. *Nature*, 421(6919), 128-128.
- Dutt, Y., Pandey, R. P., Dutt, M., Gupta, A., Vibhuti, A., Raj, V. S., Chang, C.-M., & Priyadarshini, A. (2023). Silver nanoparticles phytofabricated through Azadirachta indica: Anticancer, apoptotic, and wound-healing properties. *Antibiotics*, 12(1), 121.
- Dys, K., Drelichowska-Durawa, J., Dołega-Kozierowski, B., Lis, M., Sokratous, K., Iwanowski, W., Drelichowski, S., & Witkiewicz, W. (2013). Mechanical thrombectomy using Rotarex system and stent-in-stent placement for treatment of distal femoral artery occlusion secondary to stent fracture—a case report and literature review. *Polish Journal of Radiology*, 78(3), 74.
- Edelman, E. R., Adams, D. H., & Karnovsky, M. J. (1990). Effect of controlled adventitial heparin delivery on smooth muscle cell proliferation following endothelial injury. *Proceedings of the National Academy of Sciences*, 87(10), 3773-3777.
- Elemike, E. E., Onwudiwe, D. C., Fayemi, O. E., & Botha, T. L. (2019). Green synthesis and electrochemistry of Ag, Au, and Ag–Au bimetallic nanoparticles using golden rod (Solidago canadensis) leaf extract. *Applied Physics A*, 125, 1-12.
- Fahimirad, S., Ajalloueian, F., & Ghorbanpour, M. (2019). Synthesis and therapeutic potential of silver nanomaterials derived from plant extracts. *Ecotoxicology and environmental safety*, *168*, 260-278.
- Faisal, S., Ullah, R., Alotaibi, A., Zafar, S., Rizwan, M., & Tariq, M. H. (2023). Biofabrication of silver nanoparticles employing biomolecules of Paraclostridium benzoelyticum strain: Its characterization and their in-vitro antibacterial, anti-aging, anti-cancer and other biomedical applications. *Microscopy Research and Technique*, 86(7), 846-861. doi:https://doi.org/10.1002/jemt.24362
- Felimban, A. I., Alharbi, N. S., & Alsubhi, N. S. (2022). Optimization, Characterization, and Anticancer Potential of Silver Nanoparticles Biosynthesized Using Olea europaea. *Int J Biomater*, 2022, 6859637. doi:10.1155/2022/6859637
- Fernando, I., & Zhou, Y. (2019). Impact of pH on the stability, dissolution and aggregation kinetics of silver nanoparticles. *Chemosphere*, 216, 297-305. doi:https://doi.org/10.1016/j.chemosphere.2018.10.122
- Fletcher, J. I., Haber, M., Henderson, M. J., & Norris, M. D. (2010). ABC transporters in cancer: more than just drug efflux pumps. *Nature Reviews Cancer*, 10(2), 147-156.

- Fouzia, A. T., Khalilullah, A., & Uddin, I. (2020). Synthesis of Silver Nanoparticles by Ocimum basilicum Seed Extract and its Application in H2O2 Sensing. *Microbiology*, *3*, 17-22.
- Fowkes, F. G., Rudan, D., Rudan, I., Aboyans, V., Denenberg, J. O., McDermott, M. M., Norman, P. E., Sampson, U. K., Williams, L. J., Mensah, G. A., & Criqui, M. H. (2013). Comparison of global estimates of prevalence and risk factors for peripheral artery disease in 2000 and 2010: a systematic review and analysis. *Lancet*, 382(9901), 1329-1340. doi:10.1016/s0140-6736(13)61249-0
- Fowkes, F. G. R., Aboyans, V., Fowkes, F. J. I., McDermott, M. M., Sampson, U. K. A., & Criqui, M. H. (2017). Peripheral artery disease: epidemiology and global perspectives. *Nature Reviews Cardiology*, 14(3), 156-170. doi:10.1038/nrcardio.2016.179
- Gajbhiye, S., & Sakharwade, S. (2016). Silver nanoparticles in cosmetics. *Journal of Cosmetics, Dermatological Sciences and Applications*, 6(1), 48-53.
- Gao, Q., Feng, J., Liu, W., Wen, C., Wu, Y., Liao, Q., Zou, L., Sui, X., Xie, T., Zhang, J., & Hu, Y. (2022). Opportunities and challenges for co-delivery nanomedicines based on combination of phytochemicals with chemotherapeutic drugs in cancer treatment. *Advanced Drug Delivery Reviews*, 188, 114445. doi:https://doi.org/10.1016/j.addr.2022.114445
- Gholamali, I., Asnaashariisfahani, M., & Alipour, E. (2020). Silver Nanoparticles Incorporated in pH-Sensitive Nanocomposite Hydrogels Based on Carboxymethyl Chitosan-Poly (Vinyl Alcohol) for Use in a Drug Delivery System. *Regenerative Engineering and Translational Medicine*, 6(2), 138-153. doi:10.1007/s40883-019-00120-7
- Gilbert, W. (1956). De magnete, magneticisque corporibus, et de magno magnete tellure: Short.
- Gökşen Tosun, N., Kaplan, Ö., Imamoğlu, R., Türkekul, İ., Gökçe, İ., & Özgür, A. (2022). Green synthesized silver nanoparticles with mushroom extracts of Paxina leucomelas and Rhizopogon luteolus induce ROS-Induced intrinsic apoptotic pathway in cancer cells. *Inorganic and Nano-Metal Chemistry*, 1-10. doi:10.1080/24701556.2022.2081200
- Goldman, B., Blanke, H., & Wolinsky, H. (1987). Influence of pressure on permeability of normal and diseased muscular arteries to horseradish peroxidase: a new catheter approach. *Atherosclerosis*, 65(3), 215-225.
- Gomes, H. I. O., Martins, C. S. M., & Prior, J. A. V. (2021). Silver Nanoparticles as Carriers of Anticancer Drugs for Efficient Target Treatment of Cancer Cells. *Nanomaterials (Basel)*, 11(4). doi:10.3390/nano11040964
- González-Aguiñaga, E., Cardoso-Ávila, P. E., Patakfalvi, R., & Pedro-Garcia, F. (2023). The morphology-dependent catalytic activity of anisotropic silver nanoparticles. *Materials Letters*, *342*, 134334.
- González-Pedroza, M. G., Benítez, A. R. T., Navarro-Marchal, S. A., Martínez-Martínez, E., Marchal, J. A., Boulaiz, H., & Morales-Luckie, R. A. (2023). Biogeneration of silver nanoparticles from Cuphea procumbens for biomedical and environmental applications. *Scientific Reports*, 13(1), 790.
- Gosselin, B., Retout, M., Dutour, R., Troian-Gautier, L., Bevernaegie, R., Herens, S., Lefèvre, P., Denis, O., Bruylants, G., & Jabin, I. (2022). Ultrastable silver nanoparticles for rapid serology detection of anti-SARS-CoV-2 immunoglobulins G. *Analytical chemistry*, 94(20), 7383-7390.

- Gray, S. (1731). II. A letter concerning the electricity of water, from Mr. Stephen Gray to Cromwell Mortimer, MD Secr. R. S. *Philosophical Transactions of the Royal Society of London*, 37(422), 227-260.
- Greaves, M., & Maley, C. C. (2012). Clonal evolution in cancer. *Nature*, 481(7381), 306-313.
- Gul, A. R., Shaheen, F., Rafique, R., Bal, J., Waseem, S., & Park, T. J. (2021). Grass-mediated biogenic synthesis of silver nanoparticles and their drug delivery evaluation: A biocompatible anti-cancer therapy. *Chemical Engineering Journal*, 407, 127202. doi:https://doi.org/10.1016/j.cej.2020.127202
- Gupta, M., & Seema, K. (2021). Living Nano-factories: An Eco-friendly Approach Towards Medicine and Environment. In K. Pal (Ed.), *Bio-manufactured Nanomaterials: Perspectives and Promotion* (pp. 95-124). Cham: Springer International Publishing.
- Gupta, P., Verma, R., Verma, A. K., & Chattopadhyay, P. C. (2020). A versatile tool in controlling aggregation and Ag nanoparticles assisted in vitro folding of thermally denatured zDHFR. *Biochemistry and Biophysics Reports*, *24*, 100856. doi:https://doi.org/10.1016/j.bbrep.2020.100856
- Gurunathan, S., Han, J. W., Eppakayala, V., Jeyaraj, M., & Kim, J.-H. (2013). Cytotoxicity of Biologically Synthesized Silver Nanoparticles in MDA-MB-231 Human Breast Cancer Cells. *BioMed Research International*, 2013, 535796. doi:10.1155/2013/535796
- Gurunathan, S., Lee, K.-J., Kalishwaralal, K., Sheikpranbabu, S., Vaidyanathan, R., & Eom, S. H. (2009). Antiangiogenic properties of silver nanoparticles. *Biomaterials*, 30(31), 6341-6350.
- Gurunathan, S., Park, J. H., Han, J. W., & Kim, J.-H. (2015). Comparative assessment of the apoptotic potential of silver nanoparticles synthesized by Bacillus tequilensis and Calocybe indica in MDA-MB-231 human breast cancer cells: targeting p53 for anticancer therapy. *International journal of nanomedicine*, 4203-4223.
- Guzman, M., Dille, J., & Godet, S. (2008). Synthesis of Silver Nanoparticles by Chemical Reduction Method and Their Antibacterial Activity. World Academy of Science, Engineering and Technology, International Journal of Chemical, Molecular, Nuclear, Materials and Metallurgical Engineering, 2, 91-98.
- Gwozdzinski, K., Pieniazek, A., & Gwozdzinski, L. (2021). Reactive Oxygen Species and Their Involvement in Red Blood Cell Damage in Chronic Kidney Disease. *Oxid Med Cell Longev*, 2021, 6639199. doi:10.1155/2021/6639199
- Ha, W., Yang, J.-L., & Shi, Y.-P. (2023). Tannic Acid-Modified Silver Nanoparticles for Antibacterial and Anticancer Applications. *ACS Applied Nano Materials*.
- Hajtuch, J., Iwicka, E., Szczoczarz, A., Flis, D., Megiel, E., Cieciórski, P., Radomski, M. W., Santos-Martinez, M. J., & Inkielewicz-Stepniak, I. (2022). The pharmacological effects of silver nanoparticles functionalized with eptifibatide on platelets and endothelial cells. *International journal of nanomedicine*, 17, 4383.
- Hajtuch, J., Santos-Martinez, M. J., Wojcik, M., Tomczyk, E., Jaskiewicz, M., Kamysz,
 W., Narajczyk, M., & Inkielewicz-Stepniak, I. (2022). Lipoic Acid-Coated
 Silver Nanoparticles: Biosafety Potential on the Vascular Microenvironment
 and Antibacterial Properties. Frontiers in Pharmacology, 12.
 doi:10.3389/fphar.2021.733743

- Hamburg, N. M., & Balady, G. J. (2011). Exercise rehabilitation in peripheral artery disease: functional impact and mechanisms of benefits. *Circulation*, 123(1), 87-97.
- Hanahan, D. (2022). Hallmarks of Cancer: New Dimensions. *Cancer Discovery*, 12(1), 31-46. doi:10.1158/2159-8290.Cd-21-1059
- Hancock, J. T. (2021). Oxygen is instrumental for biological signaling: An overview. *Oxygen*, *I*(1), 3-15.
- Hardwick, J. M., & Soane, L. (2013). Multiple functions of BCL-2 family proteins. Cold Spring Harb Perspect Biol, 5(2). doi:10.1101/cshperspect.a008722
- Harris, S. K., Roos, M. G., & Landry, G. J. (2016). Statin use in patients with peripheral arterial disease. *Journal of vascular surgery*, 64(6), 1881-1888.
- Hata, A. N., Engelman, J. A., & Faber, A. C. (2015). The BCL2 Family: Key Mediators of the Apoptotic Response to Targeted Anticancer Therapeutics. *Cancer Discovery*, 5(5), 475-487. doi:10.1158/2159-8290.Cd-15-0011
- Hayyan, M., Hashim, M. A., & AlNashef, I. M. (2016). Superoxide Ion: Generation and Chemical Implications. *Chemical Reviews*, 116(5), 3029-3085. doi:10.1021/acs.chemrev.5b00407
- Heisnam, P., Moirangthem, A., Singh, Y. D., Dutta, P., Devi, C. V., & Hazarika, B. (2022). Exploitation of Silver Nanoparticles in Bioremediation. In *Bioremediation: Green Approaches for a Clean and Sustainable Environment* (pp. 143-155): CRC Press.
- Henson, L. A., Maddocks, M., Evans, C., Davidson, M., Hicks, S., & Higginson, I. J. (2020). Palliative care and the management of common distressing symptoms in advanced cancer: pain, breathlessness, nausea and vomiting, and fatigue. *Journal of clinical oncology*, 38(9), 905.
- Horcas, I., Fernández, R., Gomez-Rodriguez, J., Colchero, J., Gómez-Herrero, J., & Baro, A. M. (2007). WSXM: A software for scanning probe microscopy and a tool for nanotechnology. *Review of scientific instruments*, 78(1).
- Hussein, H. A., & Abdullah, M. A. (2022). Novel drug delivery systems based on silver nanoparticles, hyaluronic acid, lipid nanoparticles and liposomes for cancer treatment. *Applied Nanoscience*, 12(11), 3071-3096.
- Indo, H. P., Yen, H. C., Nakanishi, I., Matsumoto, K., Tamura, M., Nagano, Y., Matsui, H., Gusev, O., Cornette, R., Okuda, T., Minamiyama, Y., Ichikawa, H., Suenaga, S., Oki, M., Sato, T., Ozawa, T., Clair, D. K., & Majima, H. J. (2015). A mitochondrial superoxide theory for oxidative stress diseases and aging. *J Clin Biochem Nutr*, 56(1), 1-7. doi:10.3164/jcbn.14-42
- Ivask, A., Kurvet, I., Kasemets, K., Blinova, I., Aruoja, V., Suppi, S., Vija, H., Käkinen, A., Titma, T., & Heinlaan, M. (2014). Size-dependent toxicity of silver nanoparticles to bacteria, yeast, algae, crustaceans and mammalian cells in vitro. *PloS one*, *9*(7), e102108.
- Jazayeri, S. D., Ideris, A., Zakaria, Z., Shameli, K., Moeini, H., & Omar, A. R. (2012). Cytotoxicity and immunological responses following oral vaccination of nanoencapsulated avian influenza virus H5 DNA vaccine with green synthesis silver nanoparticles. *Journal of Controlled Release*, 161(1), 116-123. doi:https://doi.org/10.1016/j.jconrel.2012.04.015
- Jeremias, A., & Kirtane, A. (2008). Balancing efficacy and safety of drug-eluting stents in patients undergoing percutaneous coronary intervention. *Annals of internal medicine*, 148(3), 234-238.
- Johnson, B., Toland, B., Chokshi, R., Mochalin, V., Koutzaki, S., & Polyak, B. (2010). Magnetically responsive paclitaxel-loaded biodegradable nanoparticles for

- treatment of vascular disease: preparation, characterization and in vitro evaluation of anti-proliferative potential. *Current drug delivery*, 7(4), 263-273.
- Joner, M., Morimoto, K., Kasukawa, H., Steigerwald, K., Merl, S., Nakazawa, G., John, M. C., Finn, A. V., Acampado, E., & Kolodgie, F. D. (2008). Site-specific targeting of nanoparticle prednisolone reduces in-stent restenosis in a rabbit model of established atheroma. *Arteriosclerosis, thrombosis, and vascular biology*, 28(11), 1960-1966.
- Joudeh, N., & Linke, D. (2022). Nanoparticle classification, physicochemical properties, characterization, and applications: a comprehensive review for biologists. *Journal of Nanobiotechnology*, 20(1), 262.
- Kah, G., Chandran, R., & Abrahamse, H. (2023). Biogenic Silver Nanoparticles for Targeted Cancer Therapy and Enhancing Photodynamic Therapy. *Cells*, *12*(15). doi:10.3390/cells12152012
- Kalaiarasi, K., Raja, B., Saranya, D., & Dhakshinamoorthi, R. (2022). Actions of Caffeic Acid Loaded-Silver Nanoparticles on Blood Pressure, Oxidative Stress, and Antioxidants in Nitric Oxide Deficient Hypertensive Rats. *International Journal of Nutrition, Pharmacology, Neurological Diseases, 12*(4), 275-281. doi:10.4103/ijnpnd.ijnpnd_41_22
- Kaplan, Ö., Gökşen Tosun, N., İmamoğlu, R., Türkekul, İ., Gökçe, İ., & Özgür, A. (2022). Biosynthesis and characterization of silver nanoparticles from Tricholoma ustale and Agaricus arvensis extracts and investigation of their antimicrobial, cytotoxic, and apoptotic potentials. *Journal of Drug Delivery Science* and Technology, 69, 103178. doi:https://doi.org/10.1016/j.jddst.2022.103178
- Khan, H., Khan, M. F., Asim ur, R., Jan, S. U., & Ullah, N. (2011). The protective role of glutathione in silver induced toxicity in blood components. *Pak J Pharm Sci*, 24(2), 123-128.
- Khan, Y., Numan, M., Ali, M., Khali, A., Ali, T., Abbas, N., & Shinwari, Z. (2017). Bio-synthesized silver nanoparticles using different plant extracts as anti-cancer agent. *Journal of Nanomedine Biotherapeutic Discovery*, 7(154), 2.
- Khan, Z. u. R., Assad, N., Naeem-ul-Hassan, M., Sher, M., Alatawi, F. S., Alatawi, M. S., Omran, A. M., Jame, R. M., Adnan, M., & Khan, M. N. (2023). Aconitum lycoctonum L.(Ranunculaceae) mediated biogenic synthesis of silver nanoparticles as potential antioxidant, anti-inflammatory, antimicrobial and antidiabetic agents. *BMC chemistry*, 17(1), 128.
- Kim, M. S., Hwang, J., Yon, D. K., Lee, S. W., Jung, S. Y., Park, S., & al, e. (2023). Global burden of peripheral artery disease and its risk factors, 1990-2019: a systematic analysis for the Global Burden of Disease Study 2019. *Lancet Glob Health*, 11(10), e1553-e1565. doi:10.1016/s2214-109x(23)00355-8
- King III, S. B., & Meier, B. (2000). Interventional treatment of coronary heart disease and peripheral vascular disease. *Circulation*, 102(suppl 4), Iv-81-Iv-86.
- Kolodgie, F. D., John, M., Khurana, C., Farb, A., Wilson, P. S., Acampado, E., Desai, N., Soon-Shiong, P., & Virmani, R. (2002). Sustained reduction of in-stent neointimal growth with the use of a novel systemic nanoparticle paclitaxel. *Circulation*, 106(10), 1195-1198.
- Koteswara Rao, P., Srinivasulu, S., Ravindra nadh, M., Vikram Babu, B., Reddi, M. S., & Rama Krishna, A. (2021). Anticancer and antibacterial activity of green synthesized silver nanoparticles using Adina cordifolia. *Materials Today: Proceedings*, 43, 1700-1706. doi:https://doi.org/10.1016/j.matpr.2020.10.043

- Kovács, D., Igaz, N., Gopisetty, M. K., & Kiricsi, M. (2022). Cancer Therapy by Silver Nanoparticles: Fiction or Reality? *International Journal of Molecular Sciences*, 23(2), 839. Retrieved from https://www.mdpi.com/1422-0067/23/2/839
- Kovács, D., Igaz, N., Gopisetty, M. K., & Kiricsi, M. (2022). Cancer Therapy by Silver Nanoparticles: Fiction or Reality? *Int J Mol Sci*, 23(2). doi:10.3390/ijms23020839
- Kumari, S., Kumari, P., Panda, P. K., Patel, P., Jha, E., Mallick, M. A., & Verma, S. K. (2020). Biocompatible biogenic silver nanoparticles interact with caspases on an atomic level to elicit apoptosis. *Nanomedicine*, 15(22), 2119-2132.
- Kurutas, E. B. (2016). The importance of antioxidants which play the role in cellular response against oxidative/nitrosative stress: current state. *Nutr J*, 15(1), 71. doi:10.1186/s12937-016-0186-5
- Lange, A., Sawosz, E., Wierzbicki, M., Kutwin, M., Daniluk, K., Strojny, B., Ostrowska, A., Wójcik, B., Łojkowski, M., & Gołębiewski, M. (2022). Nanocomposites of graphene oxide—silver nanoparticles for enhanced antibacterial activity: mechanism of action and medical textiles coating. *Materials*, 15(9), 3122.
- Le, T. T. H., Ngo, T. H., Nguyen, T. H., Hoang, V. H., Nguyen, V. H., & Nguyen, P. H. (2023). Anti-cancer activity of green synthesized silver nanoparticles using Ardisia gigantifolia leaf extract against gastric cancer cells. *Biochemical and Biophysical Research Communications*, 661, 99-107. doi:https://doi.org/10.1016/j.bbrc.2023.04.037
- Lemos, P. A., Farooq, V., Takimura, C. K., Gutierrez, P. S., Virmani, R., Kolodgie, F., Christians, U., Kharlamov, A., Doshi, M., & Sojitra, P. (2013). Emerging technologies: polymer-free phospholipid encapsulated sirolimus nanocarriers for the controlled release of drug from a stent-plus-balloon or a stand-alone balloon catheter. *EuroIntervention*, *9*(1), 148-156.
- Li, J., Chang, X., Shang, M., Niu, S., Zhang, W., Zhang, B., Huang, W., Wu, T., Zhang, T., Tang, M., & Xue, Y. (2021). Mitophagy–lysosomal pathway is involved in silver nanoparticle-induced apoptosis in A549 cells. *Ecotoxicology and Environmental*Safety, 208, 111463. doi:https://doi.org/10.1016/j.ecoenv.2020.111463
- Liao, Y., Loh, C.-H., Tian, M., Wang, R., & Fane, A. G. (2018). Progress in electrospun polymeric nanofibrous membranes for water treatment: Fabrication, modification and applications. *Progress in Polymer Science*, 77, 69-94.
- Liaqat, N., Jahan, N., Khalil Ur, R., Anwar, T., & Qureshi, H. (2022). Green synthesized silver nanoparticles: Optimization, characterization, antimicrobial activity, and cytotoxicity study by hemolysis assay. *Front Chem*, 10, 952006. doi:10.3389/fchem.2022.952006
- Liu, T., Zeng, Z., Liu, Y., Wang, J., Maitz, M. F., Wang, Y., Liu, S., Chen, J., & Huang, N. (2014). Surface modification with dopamine and heparin/poly-L-lysine nanoparticles provides a favorable release behavior for the healing of vascular stent lesions. *ACS Applied Materials & Interfaces*, 6(11), 8729-8743.
- Liu, X., Wang, C., Cai, Z., Hu, Z., & Zhu, P. (2022). Fabrication and characterization of polyacrylonitrile and polyethylene glycol composite nanofibers by electrospinning. *Journal of Energy Storage*, 53, 105171.
- Londhe, S., Haque, S., & Patra, C. R. (2023). Silver and gold nanoparticles: Potential cancer theranostic applications, recent development, challenges, and future perspectives. In *Gold and Silver Nanoparticles* (pp. 247-290): Elsevier.

- Long, Y.-Z., Yan, X., Wang, X.-X., Zhang, J., & Yu, M. (2019). Chapter 2 Electrospinning: The Setup and Procedure. In B. Ding, X. Wang, & J. Yu (Eds.), *Electrospinning: Nanofabrication and Applications* (pp. 21-52): William Andrew Publishing.
- Lu, J. T., & Creager, M. A. (2004). The relationship of cigarette smoking to peripheral arterial disease. *Reviews in cardiovascular medicine*, *5*(4), 189-193.
- Madkour, L. H. (2018). Biogenic-biosynthesis metallic nanoparticles (MNPs) for pharmacological, biomedical and environmental nanobiotechnological applications. *Chron. Pharm. Sci. J.* 2(1), 384-444.
- Marassi, V., Di Cristo, L., Smith, S. G., Ortelli, S., Blosi, M., Costa, A. L., Reschiglian, P., Volkov, Y., & Prina-Mello, A. (2018). Silver nanoparticles as a medical device in healthcare settings: A five-step approach for candidate screening of coating agents. *Royal Society open science*, 5(1), 171113.
- Matic, M., Matic, A., Djuran, V., Gajinov, Z., Prcic, S., & Golusin, Z. (2016). Frequency of Peripheral Arterial Disease in Patients With Chronic Venous Insufficiency. *Iran Red Crescent Med J, 18*(1), e20781. doi:10.5812/ircmj.20781
- McWilliams, A. (2018a). *Nanocomposites, Nanoparticles, Nanoclays and Nanotubes: Global Markets to 2022*. Retrieved from https://www.bccresearch.com/market-research/nanotechnology/nanocomposites-nanoparticles-nanoclays-and-nanotubes-global-markets.html
- McWilliams, A. (2018b). *Nanodevices and nanomachines: the global market*. Retrieved from https://www.bccresearch.com/market-research/nanotechnology/nanodevices-and-nanomachines-market-report.html
- Medina-Leyte, D. J., Domínguez-Pérez, M., Mercado, I., Villarreal-Molina, M. T., & Jacobo-Albavera, L. (2020). Use of Human Umbilical Vein Endothelial Cells (HUVEC) as a Model to Study Cardiovascular Disease: A Review. *Applied Sciences*, 10(3), 938. Retrieved from https://www.mdpi.com/2076-3417/10/3/938
- Miller, K. D., Nogueira, L., Devasia, T., Mariotto, A. B., Yabroff, K. R., Jemal, A., Kramer, J., & Siegel, R. L. (2022). Cancer treatment and survivorship statistics, 2022. *CA: A Cancer Journal for Clinicians*, 72(5), 409-436. doi:https://doi.org/10.3322/caac.21731
- Mohamed, N. (2020). Synthesis of Hybrid Chitosan Silver Nanoparticles Loaded with Doxorubicin with Promising Anti-cancer Activity. *BioNanoScience*, 10(3), 758-765. doi:10.1007/s12668-020-00760-y
- Mosoarca, G., Vancea, C., Popa, S., Dan, M., & Boran, S. (2022). The Use of Bilberry Leaves (Vaccinium myrtillus L.) as an Efficient Adsorbent for Cationic Dye Removal from Aqueous Solutions. *Polymers*, 14(5), 978. Retrieved from https://www.mdpi.com/2073-4360/14/5/978
- Motafeghi, F., Gerami, M., Mortazavi, P., Khayambashi, B., Ghassemi-Barghi, N., & Shokrzadeh, M. (2023). Green synthesis of silver nanoparticles, graphene, and silver-graphene nanocomposite using Melissa officinalis ethanolic extract: Anticancer effect on MCF-7 cell line. *Iranian Journal of Basic Medical Sciences*, 26(1), 57.
- Muhammad, N., Zhao, H., Song, W., Gu, M., Li, Q., Liu, Y., Li, C., Wang, J., & Zhan, H. (2020). Silver nanoparticles functionalized Paclitaxel nanocrystals enhance overall anti-cancer effect on human cancer cells. *Nanotechnology*, 32(8), 085105.

- Mukherjee, S., & Patra, C. R. (2017). Biologically synthesized metal nanoparticles: Recent advancement and future perspectives in cancer theranostics. In (Vol. 3, pp. FSO203): Future Science.
- Mulvihill, M. J., Beach, E. S., Zimmerman, J. B., & Anastas, P. T. (2011). Green chemistry and green engineering: a framework for sustainable technology development. *Annual review of environment and resources*, *36*, 271-293.
- Murugesan, A. K., Pannerselvam, B., Javee, A., Rajenderan, M., & Thiyagarajan, D. (2021). Facile green synthesis and characterization of Gloriosa superba L. tuber extract-capped silver nanoparticles (GST-AgNPs) and its potential antibacterial and anticancer activities against A549 human cancer cells. *Environmental Nanotechnology, Monitoring & Management, 15*, 100460. doi:https://doi.org/10.1016/j.enmm.2021.100460
- Nadaf, S. J., Jadhav, N. R., Naikwadi, H. S., Savekar, P. L., Sapkal, I. D., Kambli, M. M., & Desai, I. A. (2022). Green synthesis of gold and silver nanoparticles: Updates on research, patents, and future prospects. *OpenNano*, 100076.
- Nadhe, S. B., Tawre, M. S., Agrawal, S., Chopade, B. A., Sarkar, D., & Pardesi, K. (2020). Anticancer potential of AgNPs synthesized using Acinetobacter sp. and Curcuma aromatica against HeLa cell lines: A comparative study. *Journal of Trace Elements in Medicine and Biology*, 62, 126630. doi:https://doi.org/10.1016/j.jtemb.2020.126630
- Nakanishi, T., & Ross, D. D. (2012). Breast cancer resistance protein (BCRP/ABCG2): its role in multidrug resistance and regulation of its gene expression. *Chin J Cancer*, 31(2), 73-99. doi:10.5732/cjc.011.10320
- Nakhlband, A., Eskandani, M., Omidi, Y., Saeedi, N., Ghaffari, S., Barar, J., & Garjani, A. (2018). Combating atherosclerosis with targeted nanomedicines: recent advances and future prospective. *Bioimpacts*, 8(1), 59-75. doi:10.15171/bi.2018.08
- Natarajan, K., Xie, Y., Baer, M. R., & Ross, D. D. (2012). Role of breast cancer resistance protein (BCRP/ABCG2) in cancer drug resistance. *Biochem Pharmacol*, 83(8), 1084-1103. doi:10.1016/j.bcp.2012.01.002
- Naveed, M., Bukhari, B., Aziz, T., Zaib, S., Mansoor, M. A., Khan, A. A., Shahzad, M., Dablool, A. S., Alruways, M. W., Almalki, A. A., Alamri, A. S., & Alhomrani, M. (2022). Green Synthesis of Silver Nanoparticles Using the Plant Extract of Acer oblongifolium and Study of Its Antibacterial and Antiproliferative Activity via Mathematical Approaches. *Molecules*, 27(13), 4226. Retrieved from https://www.mdpi.com/1420-3049/27/13/4226
- Nečas, D., & Klapetek, P. (2012). Gwyddion: an open-source software for SPM data analysis. *Open Physics*, 10(1), 181-188.
- Nikolova, S., Milusheva, M., Gledacheva, V., Feizi-Dehnayebi, M., Kaynarova, L., Georgieva, D., Delchev, V., Stefanova, I., Tumbarski, Y., Mihaylova, R., Cherneva, E., Stoencheva, S., & Todorova, M. (2023). Drug-Delivery Silver Nanoparticles: A New Perspective for Phenindione as an Anticoagulant. *Biomedicines*, 11(8), 2201. Retrieved from https://www.mdpi.com/2227-9059/11/8/2201
- Nollet, J. A. (1748). X. Part of a letter from Abbè Nollet, of the Royal Academy of Science at Paris, and FRS to Martin Folkes Esq; President of the same, concerning electricity. *Philosophical Transactions of the Royal Society of London*, 45(486), 187-194.
- Noorbazargan, H., Amintehrani, S., Dolatabadi, A., Mashayekhi, A., Khayam, N., Moulavi, P., Naghizadeh, M., Mirzaie, A., Mirzaei rad, F., & Kavousi, M.

- (2021). Anti-cancer & anti-metastasis properties of bioorganic-capped silver nanoparticles fabricated from Juniperus chinensis extract against lung cancer cells. *AMB Express*, 11(1), 61. doi:10.1186/s13568-021-01216-6
- Noukeu, L. C., Wolf, J., Yuan, B., Banerjee, S., & Nguyen, K. T. (2018). Nanoparticles for Detection and Treatment of Peripheral Arterial Disease. *Small*, 14(32), 1800644. doi:https://doi.org/10.1002/smll.201800644
- Okaiyeto, K., Hoppe, H., & Okoh, A. I. (2021). Plant-Based Synthesis of Silver Nanoparticles Using Aqueous Leaf Extract of Salvia officinalis: Characterization and its Antiplasmodial Activity. *Journal of Cluster Science*, 32(1), 101-109. doi:10.1007/s10876-020-01766-y
- Omidian, H., Babanejad, N., & Cubeddu, L. X. (2023). Nanosystems in Cardiovascular Medicine: Advancements, Applications, and Future Perspectives. *Pharmaceutics*, 15(7). doi:10.3390/pharmaceutics15071935
- Panda, P. K., Kumari, P., Patel, P., Samal, S. K., Mishra, S., Tambuwala, M. M., Dutt, A., Hilscherová, K., Mishra, Y. K., & Varma, R. S. (2022). Molecular nanoinformatics approach assessing the biocompatibility of biogenic silver nanoparticles with channelized intrinsic steatosis and apoptosis. *Green Chemistry*, 24(3), 1190-1210.
- Pannerselvam, B., Thiyagarajan, D., Pazhani, A., Thangavelu, K. P., Kim, H. J., & Rangarajulu, S. K. (2021). Copperpod Plant Synthesized AgNPs Enhance Cytotoxic and Apoptotic Effect in Cancer Cell Lines. *Processes*, *9*(5), 888. Retrieved from https://www.mdpi.com/2227-9717/9/5/888
- Patra, S., Mukherjee, S., Barui, A. K., Ganguly, A., Sreedhar, B., & Patra, C. R. (2015). Green synthesis, characterization of gold and silver nanoparticles and their potential application for cancer therapeutics. *Materials Science and Engineering: C*, 53, 298-309.
- Pauksch, L., Hartmann, S., Rohnke, M., Szalay, G., Alt, V., Schnettler, R., & Lips, K. S. (2014). Biocompatibility of silver nanoparticles and silver ions in primary human mesenchymal stem cells and osteoblasts. *Acta biomaterialia*, 10(1), 439-449.
- Pauzi, N., Zain, N. M., & Yusof, N. A. A. (2019). Microwave-assisted synthesis of ZnO nanoparticles stabilized with gum arabic: Effect of microwave irradiation time on ZnO nanoparticles size and morphology. *Bulletin of Chemical Reaction Engineering & Catalysis*, 14(1), 182-188.
- Payne, M. M. (2001). Charles Theodore Dotter: the father of intervention. *Texas Heart Institute Journal*, 28(1), 28.
- Pei, J., Fu, B., Jiang, L., & Sun, T. (2019). Biosynthesis, characterization, and anticancer effect of plant-mediated silver nanoparticles using Coptis chinensis. *International journal of nanomedicine, 14*(null), 1969-1978. doi:10.2147/IJN.S188235
- Pizzoli, S. F. M., Renzi, C., Arnaboldi, P., Russell-Edu, W., & Pravettoni, G. (2019). From life-threatening to chronic disease: Is this the case of cancers? A systematic review. *Cogent Psychology*, 6(1), 1577593.
- Poudel, B. K., Soe, Z. C., Ruttala, H. B., Gupta, B., Ramasamy, T., Thapa, R. K., Gautam, M., Ou, W., Nguyen, H. T., & Jeong, J.-H. (2018). In situ fabrication of mesoporous silica-coated silver-gold hollow nanoshell for remotely controllable chemo-photothermal therapy via phase-change molecule as gatekeepers. *International journal of pharmaceutics*, 548(1), 92-103.
- Prasher, P., Sharma, M., Mudila, H., Gupta, G., Sharma, A. K., Kumar, D., Bakshi, H. A., Negi, P., Kapoor, D. N., & Chellappan, D. K. (2020). Emerging trends in

- clinical implications of bio-conjugated silver nanoparticles in drug delivery. *Colloid and Interface Science Communications*, *35*, 100244.
- Qamar, S. U. R. (2021). Nanocomposites: Potential therapeutic agents for the diagnosis and treatment of infectious diseases and cancer. *Colloid and Interface Science Communications*, 43, 100463. doi:https://doi.org/10.1016/j.colcom.2021.100463
- Qamar, S. U. R., & Ahmad, J. N. (2021). Nanoparticles: Mechanism of biosynthesis using plant extracts, bacteria, fungi, and their applications. *Journal of Molecular Liquids*, 334, 116040. doi:https://doi.org/10.1016/j.molliq.2021.116040
- Qamar, S. U. R., Spahić, L., Benolić, L., Zivanovic, M., & Filipović, N. (2023). Treatment of Peripheral Artery Disease Using Injectable Biomaterials and Drug-Coated Balloons: Safety and Efficacy Perspective. *Pharmaceutics*, 15(7), 1813. Retrieved from https://www.mdpi.com/1999-4923/15/7/1813
- Qamar, S. U. R., Tanwir, S., Khan, W. A., Altaf, J., & Ahmad, J. N. (2021). Biosynthesis of silver nanoparticles using Ocimum tenuiflorum extract and its efficacy assessment against Helicoverpa armigera. *International Journal of Pest Management*, 1-9. doi:10.1080/09670874.2021.1980244
- Qamar, S. U. R., Virijević, K., Arsenijević, D., Avdović, E., Živanović, M., Filipović, N., Ćirić, A., & Petrović, I. (2024). Silver nanoparticles from Ocimum basilicum L. tea: A green route with potent anticancer efficacy. *Colloid and Interface Science Communications*, 59, 100771. doi:https://doi.org/10.1016/j.colcom.2024.100771
- Raaijmakers, M. H. G. P., de Grouw, E. P. L. M., Heuver, L. H. H., van der Reijden, B. A., Jansen, J. H., Scheper, R. J., Scheffer, G. L., de Witte, T. J. M., & Raymakers, R. A. P. (2005). Breast Cancer Resistance Protein in Drug Resistance of Primitive CD34+38– Cells in Acute Myeloid Leukemia. *Clinical Cancer Research*, 11(6), 2436-2444. doi:10.1158/1078-0432.Ccr-04-0212
- Rafique, M., Rafique, M. S., Kalsoom, U., Afzal, A., Butt, S. H., & Usman, A. (2019). Laser ablation synthesis of silver nanoparticles in water and dependence on laser nature. *Optical and Ouantum Electronics*, 51, 1-11.
- Ramchandani, M., Kumari, P., & Goyal, A. K. (2023). Aptamers as Theranostics in Cardiovascular Diseases. *Journal of Nanotheranostics*, *4*(3), 408-428. Retrieved from https://www.mdpi.com/2624-845X/4/3/18
- Ramzan, U., Majeed, W., Hussain, A. A., Qurashi, F., Qamar, S. U. R., Naeem, M., Uddin, J., Khan, A., Al-Harrasi, A., Razak, S. I. A., & Lee, T. Y. (2022). New Insights for Exploring the Risks of Bioaccumulation, Molecular Mechanisms, and Cellular Toxicities of AgNPs in Aquatic Ecosystem. *Water*, *14*(14), 2192. Retrieved from https://www.mdpi.com/2073-4441/14/14/2192
- Rayleigh, L. (1882). XX. On the equilibrium of liquid conducting masses charged with electricity. *The London, Edinburgh, and Dublin Philosophical Magazine and Journal of Science, 14*(87), 184-186.
- Reneker, D. H., & Yarin, A. L. (2008). Electrospinning jets and polymer nanofibers. *Polymer*, 49(10), 2387-2425.
- Rodríguez-Félix, F., Graciano-Verdugo, A. Z., Moreno-Vásquez, M. J., Lagarda-Díaz, I., Barreras-Urbina, C. G., Armenta-Villegas, L., Olguín-Moreno, A., & Tapia-Hernández, J. A. (2022). Trends in sustainable green synthesis of silver nanoparticles using agri-food waste extracts and their applications in health. *Journal of Nanomaterials*, 2022, 1-37.
- Rowinsky, E. K., & Donehower, R. C. (1995). Paclitaxel (taxol). *New England Journal of Medicine*, 332(15), 1004-1014.

- Rozalen, M., Sánchez-Polo, M., Fernández-Perales, M., Widmann, T. J., & Rivera-Utrilla, J. (2020). Synthesis of controlled-size silver nanoparticles for the administration of methotrexate drug and its activity in colon and lung cancer cells. *RSC Advances*, 10(18), 10646-10660. doi:10.1039/C9RA08657A
- Sanchez-Guzman, D., Le Guen, P., Villeret, B., Sola, N., Le Borgne, R., Guyard, A., Kemmel, A., Crestani, B., Sallenave, J.-M., & Garcia-Verdugo, I. (2019). Silver nanoparticle-adjuvanted vaccine protects against lethal influenza infection through inducing BALT and IgA-mediated mucosal immunity. *Biomaterials*, 217, 119308. doi:https://doi.org/10.1016/j.biomaterials.2019.119308
- Scheller, B., Speck, U., Abramjuk, C., Bernhardt, U., Böhm, M., & Nickenig, G. (2004). Paclitaxel balloon coating, a novel method for prevention and therapy of restenosis. *Circulation*, 110(7), 810-814.
- Scheller, B., Speck, U., Schmitt, A., Clauss, W., Sovak, M., Böhm, M., & Stoll, H.-P. (2002). Acute cardiac tolerance of current contrast media and the new taxane protaxel using iopromide as carrier during porcine coronary angiography and stenting. *Investigative radiology*, 37(1), 29-34.
- Shafique, R., Rani, M., Munawar, A., & Arshad, M. (2023). Impacts of Nanotechnology. In *Modeling and Simulation of Functional Nanomaterials for Forensic Investigation* (pp. 10-27): IGI Global.
- Shaikh, W. A., Chakraborty, S., Owens, G., & Islam, R. U. (2021). A review of the phytochemical mediated synthesis of AgNP (silver nanoparticle): the wonder particle of the past decade. *Applied Nanoscience*, 11(11), 2625-2660. doi:10.1007/s13204-021-02135-5
- Shammas, N. W., Shammas, G. A., Helou, T. J., Voelliger, C. M., Mrad, L., & Jerin, M. (2012). Safety and 1-year revascularization outcome of SilverHawk atherectomy in treating in-stent restenosis of femoropopliteal arteries: a retrospective review from a single center. *Cardiovascular Revascularization Medicine*, 13(4), 224-227.
- Sharma, A. K., Kaith, B. S., Shanker, U., & Gupta, B. (2020). γ-radiation induced synthesis of antibacterial silver nanocomposite scaffolds derived from natural gum Boswellia serrata. *Journal of Drug Delivery Science and Technology*, 56, 101550.
- Shi, J., Ren, Y., Ma, J., Luo, X., Li, J., Wu, Y., Gu, H., Fu, C., Cao, Z., & Zhang, J. (2021). Novel CD44-targeting and pH/redox-dual-stimuli-responsive core—shell nanoparticles loading triptolide combats breast cancer growth and lung metastasis. *Journal of nanobiotechnology*, 19(1), 188.
- Shi, J., Sun, X., Lin, Y., Zou, X., Li, Z., Liao, Y., Du, M., & Zhang, H. (2014). Endothelial cell injury and dysfunction induced by silver nanoparticles through oxidative stress via IKK/NF-κB pathways. *Biomaterials*, *35*(24), 6657-6666. doi:https://doi.org/10.1016/j.biomaterials.2014.04.093
- Siakavella, I. K., Lamari, F., Papoulis, D., Orkoula, M., Gkolfi, P., Lykouras, M., Avgoustakis, K., & Hatziantoniou, S. (2020). Effect of Plant Extracts on the Characteristics of Silver Nanoparticles for Topical Application. *Pharmaceutics*, *12*(12). doi:10.3390/pharmaceutics12121244
- Siegel, R. L., Miller, K. D., Fuchs, H. E., & Jemal, A. (2022). Cancer statistics, 2022. *CA: A Cancer Journal for Clinicians,* 72(1), 7-33. doi:https://doi.org/10.3322/caac.21708
- Simon, S., Sibuyi, N. R. S., Fadaka, A. O., Meyer, S., Josephs, J., Onani, M. O., Meyer, M., & Madiehe, A. M. (2022). Biomedical applications of plant extract-synthesized silver nanoparticles. *Biomedicines*, 10(11), 2792.

- Song, P., Rudan, D., Zhu, Y., Fowkes, F. J., Rahimi, K., Fowkes, F. G. R., & Rudan, I. (2019). Global, regional, and national prevalence and risk factors for peripheral artery disease in 2015: an updated systematic review and analysis. *The Lancet Global Health*, 7(8), e1020-e1030.
- Srimurugan, S., Ravi, A. K., Arumugam, V. A., & Muthukrishnan, S. (2022). Biosynthesis of silver nanoparticles using Citrus hystrix leaf extract and evaluation of its anticancer efficacy against HeLa cell line. *Drug Development and Industrial Pharmacy*, 48(9), 480-490. doi:10.1080/03639045.2022.2130352
- Steckiewicz, K. P., Cieciórski, P., Barcińska, E., Jaśkiewicz, M., Narajczyk, M., Bauer, M., Kamysz, W., Megiel, E., & Inkielewicz-Stepniak, I. (2022). Silver nanoparticles as chlorhexidine and metronidazole drug delivery platforms: their potential use in treating periodontitis. *International journal of nanomedicine*, 495-517.
- Su, L. J., Zhang, J. H., Gomez, H., Murugan, R., Hong, X., Xu, D., Jiang, F., & Peng, Z. Y. (2019). Reactive Oxygen Species-Induced Lipid Peroxidation in Apoptosis, Autophagy, and Ferroptosis. Oxid Med Cell Longev, 2019, 5080843. doi:10.1155/2019/5080843
- Su, Y., Cockerill, I., Wang, Y., Qin, Y.-X., Chang, L., Zheng, Y., & Zhu, D. (2019). Zinc-based biomaterials for regeneration and therapy. *Trends in biotechnology*, 37(4), 428-441.
- Suffness, M., & Pezzuto, J. M. (1991). Methods in Plant Biochemistry: Assays for Bioactivity. Methods in Plant Biochemistry. In: Hostettmann, 6th Edition. London: Academic Press.
- Sun, X., Qiang, Q., Yin, Z., Wang, Z., Ma, Y., & Zhao, C. (2019). Monodispersed silver-palladium nanoparticles for ethanol oxidation reaction achieved by controllable electrochemical synthesis from ionic liquid microemulsions. *Journal of colloid and interface science*, 557, 450-457.
- Taha, I. M., Zaghlool, A., Nasr, A., Nagib, A., El Azab, I. H., Mersal, G. A., Ibrahim,
 M. M., & Fahmy, A. (2022). Impact of starch coating embedded with silver nanoparticles on strawberry storage time. *Polymers*, 14(7), 1439.
- Tekade, R. K., Maheshwari, R., Soni, N., Tekade, M., & Chougule, M. B. (2017). Nanotechnology for the development of nanomedicine. In *Nanotechnology-based approaches for targeting and delivery of drugs and genes* (pp. 3-61): Elsevier.
- Thangavel, P., Muthukumar, S., Karthekeyan, B. R., Vakamudi, M., & Nayagam, H. (2014). Anaesthetic challenges in cardiac interventional procedures.
- Thipe, V. C., Karikachery, A. R., Çakılkaya, P., Farooq, U., Genedy, H. H., Kaeokhamloed, N., Phan, D.-H., Rezwan, R., Tezcan, G., Roger, E., & Katti, K. V. (2022). Green nanotechnology—An innovative pathway towards biocompatible and medically relevant gold nanoparticles. *Journal of Drug Delivery Science and Technology*, 70, 103256. doi:https://doi.org/10.1016/j.jddst.2022.103256
- Tian, S., Saravanan, K., Mothana, R. A., Ramachandran, G., Rajivgandhi, G., & Manoharan, N. (2020). Anti-cancer activity of biosynthesized silver nanoparticles using Avicennia marina against A549 lung cancer cells through ROS/mitochondrial damages. *Saudi Journal of Biological Sciences*, 27(11), 3018-3024. doi:https://doi.org/10.1016/j.sjbs.2020.08.029

- Tilsed, C. M., Fisher, S. A., Nowak, A. K., Lake, R. A., & Lesterhuis, W. J. (2022). Cancer chemotherapy: insights into cellular and tumor microenvironmental mechanisms of action. *Frontiers in Oncology*, 12, 960317.
- Traksele, L., & Snitka, V. (2022). Surface-enhanced Raman spectroscopy for the characterization of Vaccinium myrtillus L. bilberries of the Baltic–Nordic regions. *European Food Research and Technology*, 248(2), 427-435. doi:10.1007/s00217-021-03887-8
- Tsukie, N., Nakano, K., Matoba, T., Masuda, S., Iwata, E., Miyagawa, M., Zhao, G., Meng, W., Kishimoto, J., & Sunagawa, K. (2013). Pitavastatin-incorporated nanoparticle-eluting stents attenuate in-stent stenosis without delayed endothelial healing effects in a porcine coronary artery model. *Journal of atherosclerosis and thrombosis*, 20(1), 32-45.
- Turrens, J. F., & Boveris, A. (1980). Generation of superoxide anion by the NADH dehydrogenase of bovine heart mitochondria. *Biochemical journal*, 191(2), 421-427.
- Ullah, I., Khalil, A. T., Ali, M., Iqbal, J., Ali, W., Alarifi, S., & Shinwari, Z. K. (2020). Green-Synthesized Silver Nanoparticles Induced Apoptotic Cell Death in MCF-7 Breast Cancer Cells by Generating Reactive Oxygen Species and Activating Caspase 3 and 9 Enzyme Activities. *Oxid Med Cell Longev*, 2020, 1215395. doi:10.1155/2020/1215395
- Vaduganathan, M., Mensah, G. A., Turco, J. V., Fuster, V., & Roth, G. A. (2022). The global burden of cardiovascular diseases and risk: a compass for future health. In (Vol. 80, pp. 2361-2371): American College of Cardiology Foundation Washington DC.
- Venkatadri, B., Shanparvish, E., Rameshkumar, M. R., Arasu, M. V., Al-Dhabi, N. A., Ponnusamy, V. K., & Agastian, P. (2020). Green synthesis of silver nanoparticles using aqueous rhizome extract of Zingiber officinale and Curcuma longa: In-vitro anti-cancer potential on human colon carcinoma HT-29 cells. *Saudi Journal of Biological Sciences*, 27(11), 2980-2986. doi:https://doi.org/10.1016/j.sjbs.2020.09.021
- Venmani, S., Palsamy Kesavan, M., Ayyanaar, S., & Muniyappan, N. (2023). Cymodocea serrulata capped silver nanoparticles for battling human lung cancer, breast cancer, hepatic cancer: Optimization by full factorial design and in vitro cytotoxicity evaluation. *Heliyon*, 9(9). doi:10.1016/j.heliyon.2023.e20039
- Verma, A., Gautam, S. P., Bansal, K. K., Prabhakar, N., & Rosenholm, J. M. (2019). Green Nanotechnology: Advancement in Phytoformulation Research. *Medicines (Basel)*, 6(1). doi:10.3390/medicines6010039
- Virijević, K., Marković, B., Grujić, J., Jovanović, M., Kastratović, N., Živanović, M., Nikolić, D., & Filipović, N. (2023). Electrospun Poly(Lactic Acid)-Chitosan Nanofibers for Wound Healing Application. *Engineering Proceedings*, 31(1), 24. Retrieved from https://www.mdpi.com/2673-4591/31/1/24
- Virijević, K., Živanović, M. N., Nikolić, D., Milivojević, N., Pavić, J., Morić, I., Šenerović, L., Dragačević, L., Thurner, P. J., Rufin, M., Andriotis, O. G., Ljujić, B., Miletić Kovačević, M., Papić, M., & Filipović, N. (2024). AI-Driven Optimization of PCL/PEG Electrospun Scaffolds for Enhanced In Vivo Wound Healing. *ACS Applied Materials & Interfaces*, 16(18), 22989-23002. doi:10.1021/acsami.4c03266
- Vlajinac, H. D., Marinković, J. M., Maksimović, M. Z., Radak, D. J., Arsić, R. B., & Jorga, J. B. (2019). The prevalence of polyvascular disease in patients with

- carotid artery disease and peripheral artery disease. *Kardiologia Polska (Polish Heart Journal)*, 77(10), 926-934. doi:{}
- Wang, J., An, Q., Li, D., Wu, T., Chen, W., Sun, B., Ei-Hamshary, H., Al-Deyab, S. S., Zhu, W., & Mo, X. (2015). Heparin and vascular endothelial growth factor loaded poly (L-lactide-co-caprolactone) nanofiber covered stent-graft for aneurysm treatment. *Journal of Biomedical Nanotechnology*, 11(11), 1947-1960.
- Wang, Y., Zhang, X., Bai, Y., Li, W., Li, X., Xing, X., Wang, C., Gao, L., Yogi, M., & Swamy, M. K. (2020). Anticancer and Antibacterial Activities of Silver Nanoparticles (AgNPs) Synthesized from Cucumis melo L. *Journal of Nanoscience and Nanotechnology*, 20(7), 4143-4151.
- Ward, R. A., Fawell, S., Floc'h, N., Flemington, V., McKerrecher, D., & Smith, P. D. (2020). Challenges and opportunities in cancer drug resistance. *Chemical Reviews*, 121(6), 3297-3351.
- WHO. (2020). Global health estimates 2020: deaths by cause, age, sex, by country and by region, 2000–2019. In: WHO Geneva, Switzerland.
- Wu, J., Zheng, Y., Song, W., Luan, J., Wen, X., Wu, Z., Chen, X., Wang, Q., & Guo, S. (2014). In situ synthesis of silver-nanoparticles/bacterial cellulose composites for slow-released antimicrobial wound dressing. *Carbohydrate polymers*, 102, 762-771.
- Xie, Z., Chu, Y., Zhang, W., Lang, D., & Zhang, X. (2019). Bacillus pumilus alleviates drought stress and increases metabolite accumulation in Glycyrrhiza uralensis Fisch. *Environmental and Experimental Botany*, 158, 99-106.
- Xu, C., Yang, F., Wang, S., & Ramakrishna, S. (2004). In vitro study of human vascular endothelial cell function on materials with various surface roughness. *Journal of biomedical materials research Part A*, 71A(1), 154-161. doi:https://doi.org/10.1002/jbm.a.30143
- Xu, X., Amraii, S. A., Toushmalani, R., & Almasi, M. (2023). Formulation of a modern anti-human breast cancer drug from silver nanoparticles green-synthesized using Allium saralicum. *Journal of Engineering Research*, 11(4), 288-292. doi:https://doi.org/10.1016/j.jer.2023.100136
- Xue, J., Wu, T., Dai, Y., & Xia, Y. (2019). Electrospinning and Electrospun Nanofibers: Methods, Materials, and Applications. *Chemical Reviews*, 119(8), 5298-5415. doi:10.1021/acs.chemrev.8b00593
- Yesilot, S., Bayram, D., Özgöçmen, M., & Toğay, V. A. (2023). Apoptotic effects of Phlomis armeniaca mediated biosynthesized silver nanoparticles in monolayer (2D) and spheroid (3D) cultures of human breast cancer cell lines. *3 Biotech*, 13(1), 4. doi:10.1007/s13205-022-03417-7
- Younas, W., Khan, F. U., Zaman, M., Lin, D., Zuberi, A., & Wang, Y. (2022). Toxicity of synthesized silver nanoparticles in a widespread fish: A comparison between green and chemical. *Science of The Total Environment*, 845, 157366.
- Yu, Z., Li, Q., Wang, J., Yu, Y., Wang, Y., Zhou, Q., & Li, P. (2020). Reactive Oxygen Species-Related Nanoparticle Toxicity in the Biomedical Field. *Nanoscale Res Lett*, 15(1), 115. doi:10.1186/s11671-020-03344-7
- Yu, Z., Pestell, T. G., Lisanti, M. P., & Pestell, R. G. (2012). Cancer stem cells. *Int J Biochem Cell Biol*, 44(12), 2144-2151. doi:10.1016/j.biocel.2012.08.022
- Yusuf, A., Almotairy, A. R. Z., Henidi, H., Alshehri, O. Y., & Aldughaim, M. S. (2023). Nanoparticles as Drug Delivery Systems: A Review of the implication of nanoparticles' physicochemical properties on responses in biological systems. *Polymers*, 15(7), 1596.

- Yusuf, S., Reddy, S., Ôunpuu, S., & Anand, S. (2001). Global burden of cardiovascular diseases: part I: general considerations, the epidemiologic transition, risk factors, and impact of urbanization. *Circulation*, 104(22), 2746-2753.
- Zilla, P., Bezuidenhout, D., & Human, P. (2007). Prosthetic vascular grafts: wrong models, wrong questions and no healing. *Biomaterials*, 28(34), 5009-5027.
- Živanović, M. N. (2020). Use of Electrospinning to Enhance the Versatility of Drug Delivery. In W.-F. Lai (Ed.), *Systemic Delivery Technologies in Anti-Aging Medicine: Methods and Applications* (pp. 347-364). Cham: Springer International Publishing.

Biography of Author

Safi Ur Rehman Qamar was born in Faisalabad, Pakistan, where he grew up with a strong interest in science and technology. His educational journey began in Faisalabad, a city known for its educational institutions and vibrant academic environment. Qamar's passion for biology and chemistry led him to pursue a Bachelor of Science (BS) in Zoology at Government College University Faisalabad (GCUF), where he enrolled in September 2013. GCUF, one of the oldest and most prestigious institutions in Pakistan, provided Qamar with a robust foundation in the life sciences. In addition to his major in Zoology, Qamar pursued a Bachelor of Education (B.Ed) from Allama Iqbal Open University (AIOU), Islamabad, from September 2017 to September 2020. This degree equipped him with the pedagogical skills necessary for teaching and research, allowing him to communicate complex scientific concepts effectively.

Qamar's academic journey took a significant leap when he was awarded a scholarship by the Government of Thailand to pursue a Master of Science (MSc) in Applied Biological Sciences: Environmental Health at Chulabhorn Graduate Institute (CGI), Bangkok. From June 2019 to August 2021, Qamar worked on his master's thesis titled "Study of the Nanocomposites as an Alternative Therapeutic Approach for Nosocomial Infections." His research was innovative, exploring the potential of nanocomposites as therapeutic agents against hospital-acquired infections, which are a major challenge in healthcare settings globally.

Building on his master's research, Qamar was awarded a prestigious fellowship under the European Union's Horizon 2020 research and innovation program, specifically the Marie Skłodowska-Curie grant agreement No. 956470 (DECODE ITN). This fellowship allowed him to embark on a Doctor of Philosophy (Ph.D.) in Bioengineering at the University of Kragujevac, Serbia, beginning in April 2022. At the University of Kragujevac, Qamar's research focuses on the "Biomedical Application of Green Synthesized Nanoparticles as Anti-Cancer Agents and Nanoparticle Incorporated Nanofibers as Potential Coating for Drug-Coated Balloons." Qamar's Ph.D. research is at the cutting edge of biomedical engineering, combining the principles of nanotechnology with green chemistry to develop innovative solutions for cancer treatment and drug delivery systems. His work has the potential to revolutionize the way we approach the treatment of cancer and other serious diseases, making significant contributions to the field of nanomedicine.

Email: surqamar@gmail.com

Website: https://sites.google.com/view/surqamar

AUTHOR'S STATEMENT ON THE ORIGINALITY OF THE DOCTORAL DISSERTATION

I declare that the doctoral dissertation entitled:

"Biomedical application of green synthesized nanoparticles as anti-cancer agents and nanoparticle incorporated nanofibers as potential coating for drug coated balloons"

represents an original author's work created as a result of own research work.

With this Declaration, I also confirm:

- that I am the sole author of the aforementioned doctoral dissertation,
- that I have not infringed the copyright or other intellectual property rights of other persons in the aforementioned doctoral dissertation,

In Kragujevac, 2024 year,

Safi Ur

Rehman

Qamar

Digitaly signed by Saf Ur Rehman

Qamar

Dis-C-OS. OU-Faculty of Engineering,
O-Librershy of Posspience, Chi-Safi

Rehman

Qamar

Discount of Engineering Chi-Safi

Responsion in the author of this

document of the Safi

Localized Registers. Seria

Localized Registers. Seria

Localized Registers. Seria

Localized Registers. Seria

Discount of the Safi Viz. 420-42000

Registers of Tyz. 420-42000

Seria Registers of Tyz. 420-42000

Registers of Tyz. 420-42000

Registers of Tyz. 420-42000

Registers of Tyz. 420-42000

Registers of Tyz. 420-42000

Registers of Tyz. 420-42000

Registers of Tyz. 420-42000

Registers of Tyz. 420-42000

Registers of Tyz. 420-42000

Registers of Tyz. 420-42000

Registers of Tyz. 420-42000

Registers of Tyz. 420-42000

Registers of Tyz. 420-42000

Registers of Tyz. 420-42000

Registers of Tyz. 420-42000

Registers of Tyz. 420-42000

Registers of Tyz. 420-42000

Registers of Tyz. 420-42000

Registers of Tyz. 420-42000

Registers of Tyz. 420-42000

Registers of Tyz. 420-42000

Registers of Tyz. 420-42000

Registers of Tyz. 420-42000

Registers of Tyz. 420-42000

Registers of Tyz. 420-42000

Registers of Tyz. 420-42000

Registers of Tyz. 420-42000

Registers of Tyz. 420-42000

Registers of Tyz. 420-42000

Registers of Tyz. 420-42000

Registers of Tyz. 420-42000

Registers of Tyz. 420-42000

Registers of Tyz. 420-42000

Registers of Tyz. 420-42000

Registers of Tyz. 420-42000

Registers of Tyz. 420-42000

Registers of Tyz. 420-42000

Registers of Tyz. 420-42000

Registers of Tyz. 420-42000

Registers of Tyz. 420-42000

Registers of Tyz. 420-42000

Registers of Tyz. 420-42000

Registers of Tyz. 420-42000

Registers of Tyz. 420-42000

Registers of Tyz. 420-42000

Registers of Tyz. 420-42000

Registers of Tyz. 420-42000

Registers of Tyz. 420-42000

Registers of Tyz. 420-42000

Registers of Tyz. 420-42000

Registers of Tyz. 420-42000

Registers of Tyz. 420-42000

Registers of Tyz. 420-42000

Registers of Tyz. 420-42000

Registers of Tyz. 420-42000

Registers of Tyz. 420-4

signature of the author

AUTHOR'S STATEMENT ON THE IDENTITY OF THE PRINTED AND ELECTRONIC VERSIONS OF THE DOCTORAL DISSERTATION

I declare that the printed and electronic version of the doctoral dissertation under the title:

"Biomedical application of green synthesized nanoparticles as anti-cancer agents and nanoparticle incorporated nanofibers as potential coating for drug coated balloons"

and are identical.

In Kragujevac, 2024 year,

Safi Ur Digitally signed by Safi Ur Presence of the Community of Engineering, Outbreaker of Engineerin

signature of the author

AUTHOR'S STATEMENT ON THE USE OF THE DOCTORAL DISSERTATION
I, Safi-Ur-Rehman Qamar,
X I allow
I don't allow it
to the University Library in Kragujevac to make two permanent duplicate copies in electronic form of the doctoral dissertation under the title:
"Biomedical application of green synthesized nanoparticles as anti-cancer
agents and nanoparticle incorporated nanofibers as potential coating for drug
coated balloons"
in its entirety, as well as to make one copy of the duplicated doctoral dissertation permanently available to the public through the digital repository of the University of Kragujevac and the central repository of the competent ministry, so that members of the public can make permanent duplicate copies in electronic form of the said doctoral dissertation by download. This statement also
X I allow
I don't allow it
members of the public to use the doctoral dissertation thus available under the conditions established by one of the following Creative Commons licenses:
1) Authorship
2) Authorship - share under the same conditions
3) Authorship - no processing
4) Authorship - non-commercial
5) Authorship - non-commercial - share under the same conditions
6) Authorship - non-commercial - no processing
In Kragujevac, 2024 year, Safi Ur Rehman Rehman Qamar Digitally, signed by Safi Ur Rehman Resurrant@unic Chi-Safi Ur herman Readon, I am the author of this Signature of the author